NASA Contractor Report 172184

C18

DEVELOPMENT OF A MULTILEVEL OPTIMIZATION APPROACH TO THE DESIGN OF MODERN ENGINEERING SYSTEMS

(NASA-CR-172184) DEVELOPMENT OF A MULTILEVEL OPTIMIZATION APPROACH TO THE DESIGN OF MODERN ENGINEERING SYSTEMS Ph.D. Thesis (Virginia Polytechnic Inst. and State Univ.) 238 p HC A11/MF A01 CSCL 01C G3/05

N83-32796

Unclas
36013

Jean-Francois Marie Barthelemy

VIRGINIA POLYTECHNIC INSTITUTE AND STATE UNIVERSITY
Blacksburg, Virginia

Grant NAG1-145
August 1983

National Aeronautics and
Space Administration

Langley Research Center
Hampton, Virginia 23665

DEVELOPMENT OF A MULTILEVEL OPTIMIZATION APPROACH TO THE DESIGN OF MODERN ENGINEERING SYSTEMS

by

Jean-Francois Marie Barthelemy

(ABSTRACT)

This work describes an optimization approach to the design of complex engineering systems. The approach assumes a decomposition of the original problem (design of the system) into smaller subproblems (design of subsystems) organized in a multilevel hierarchy. As one goes down the levels, the details of the system become more precisely defined; furthermore, each subproblem may control the design of lower level subproblems.

A general algorithm is proposed which carries out the design process iteratively, starting at the top of the hierarchy and proceeding downward. Each subproblem is optimized separately for fixed controls from higher level subproblems. An optimum sensitivity analysis is then performed which determines the sensitivity of the subproblem

design to changes in higher level subproblem controls. The resulting sensitivity derivatives are used to construct constraints which force the controlling subproblems into chosing their own designs so as to improve the lower level subproblem designs while satisfying their own constraints.

The applicability of the proposed algorithm is demonstrated by devising a four-level hierarchy to perform the simultaneous aerodynamic and structural design of a high-performance sailplane wing for maximum cross-country speed. The levels are devoted successively to selecting global performance parameters, determining the wing aerodynamic shape, defining the spanwise distributions of global structural characteristics, and, performing the detailed design of wing substructures.

Finally, the concepts discussed are applied to the two-level minimum weight structural design of the sailplane wing. The numerical experiments show that discontinuities in the sensitivity derivatives may delay convergence, but that the algorithm is robust enough to overcome these discontinuities and produce low-weight feasible designs, regardless of whether the optimization is started from the feasible space or the infeasible one.

TABLE OF CONTENTS

LIST OF TABLES

LIST OF FIGURES

Chapter I

INTRODUCTION

The design of modern engineering systems is a procedure which often integrates different disciplines and always involves a large number of variables. While optimization techniques provide an attractive formal tool for carrying out the design process, a weakness of these techniques remains in their inability to handle truly large multidisciplinary design problems. To overcome that weakness, designers must resort to some sort of decomposition method. The original design problem is broken down into smaller subproblems which are then optimized separately. However, these subproblems are generally coupled so that an iterative scheme must be devised which coordinates their optimization in order that the resulting design is, to some extent, optimum with respect to the original problem.

1.1 OVERVIEW OF EXISTING LITERATURE

Several studies have been devoted to decomposition of large optimization problems. These studies pertain to all the areas of engineering as well as economics and management. The following overview focuses mainly on structural

optimization. For the sake of the discussion, two classes of decomposition methods are defined: formal methods and intuitive methods. In formal methods, the mathematical structure of the problem is exploited to arrive at a rigid decomposition scheme. Consequently, a rigorous framework exists within which the mathematical properties of the method may be assessed. In intuitive methods, understanding of the behavior of the physical system considered is apparently the prime factor directing the decomposition. These methods are sometimes referred to as rational methods and their mathematical characteristics can seldom be studied in great detail. An intuitive approach provides, of course, the only option for decomposing those problems which do not possess the structure for which a formal decomposition method exists. This division into formal and intuitive methods is somewhat arbitrary as a given approach may very well be shown to belong to both classes; however,it facilitates the discussion.

1.1.1 Formal Decomposition Methods

A very extensive body of work exists on decomposition in linear programming (LP). The existence of truly large problems in the fields of economics and operations research has stimulated efforts aiming at exploiting the special

structures of the constraint matrix. The major initial step in that area seems to have been the introduction of the Dantzig-Wolfe decomposition principle in 1960. By 1970 the developments in this active field were so numerous as to warrant the publication of a textbook by Lasdon (Ref. 1). In the area of structural design, problems involving collapse design of trusses and frames were solved successfully using the LP decomposition techniques (Refs. 2-5).

Dynamic programming (DP) was discussed by Bellman as early as 1957 (Ref. 6). It is a decomposition method suitable for nonlinear problems. The problems must be serial, that is, of the form such that any change in the design of one subproblem affects only those subproblems that are "downstream" in the decision-making process. Furthermore, the problem objective function must be additive. However, DP cannot easily handle constraints that involve more than one subproblem. Also, it becomes very expensive if there are large amounts of data transmitted between successive subproblems. Among the advantages of the DP method are its capability to generate global optimum designs and to handle discrete variables and discontinuous functions. In structural design, dynamic programming seems to find use in optimization of "one-dimensional" structures,

that is, beams, one-bay multistory or one-story multibay frames, and transmission towers (see Ref. 7 Chap. XI or Ref. 8).

Optimization algorithms were devised for separable nonlinear problems using coordination techniques developed in the context of multilevel decision-making processes. Once a problem has been decomposed into smaller subproblems, the main task is to coordinate the design of the different subproblems. Essentially, the subproblems are grouped on the lower level of a hierarchy and an additional higher level subproblem is added whose role is to select the values of coordinating variables so as to force the other subproblems into choosing designs corresponding to improved overall problem performance. The coordinating subproblem is itself cast in the form of an optimization problem. As the evaluation of the objective function of the coordinating subproblem requires complete optimization of all lower level subproblems, this type of algorithm may turn out to be very expensive. A study of coordination in hierarchical systems is given in the 1970 monograph by Mesarovic and coauthors (Ref. 9). Kirsch and coworkers have used both the model coordination technique and the goal coordination technique to solve various structural design problems (Ref. 7 Chap. X and Refs. 10-12)

1.1.2 Intuitive Decomposition Methods

The first attempts at developing intuitive decomposition schemes for large structural design problems were extensions of the fully stressed design method. In these approaches the structure is seen as a combination of elements (substructures). Given an initial design for all the elements, an analysis of the structure is made to determine inter-element forces. Then, each element is optimized separately on the assumption that changes in that element design do not change inter-element forces. Once all the elements have been designed, the structure is analyzed again and the process repeated until convergence is achieved. Giles (Ref. 13) and Sobieski (Ref. 14) performed the design of airplane wings under constraints on stresses and element stability using that approach. Kirsch and coworkers (Ref. 15) designed frameworks using a similar approach but reanalyzing the structure after each substructure optimization, in order to account better for load redistribution.

When optimizing a structure one substructure at a time, it is difficult to handle global constraints, that is, those constraints affected by variables belonging to more than one substructure. In Ref. 16, Sobieski and Loendorf designed airplane fuselages under local constraints on stresses and

local instabilities and global constraints on fuselage elastic displacements. The optimization was first carried out with the local constraints, as described above. If necessary, the resulting design was subsequently modified to satisfy the displacement constraints using a unit load method to determine the impact that changes in element design have on the violated displacements. Another example of treatment of global constraints is given by Hughes and coworkers (Ref. 17) who designed ship compartments for minimum cost under constraints on stresses.

A generalized fully stressed design approach to large problems is certainly economically appealing. However, it presents two difficulties. As pointed out in Ref. 14 "...minimization of the individual component masses does not guarantee minimization of the total mass . This situation is caused by the inability to control the load path on the assembled structure level... ." As mentioned earlier also, it makes it difficult to handle global constraints. In Refs. 18 and 19 Schmit and coworkers used a two-level approach to design trusses and aircraft wings. At the global level, the distributions of stiffnesses, the global level variables, were chosen so as to minimize the total structural weight, while satisfying global displacement constraints and also some local constraints on stresses and

structural element buckling. For known stiffnesses, the end forces on the various structural elements were calculated. At the local level, these structural elements were optimized separately with respect to their detail design, the local level variables, so that the changes in element stiffnesses were minimized, while the local constraints were still satisfied. The process was repeated until convergence was achieved. In this decomposition, the introduction of the global level problem was a key factor in overcoming both difficulties attributed to the generalized fully stressed design approach. By placing the minimization of the weight at the global level, the opportunity was kept to trade structural mass between the elements in order to improve the load paths while reducing the total weight. Also, the provision was left to explicitly handle global constraints.

1.1.3 General Approach to Engineering System Design

The intuitive decomposition methods discussed to this point are very specific and cannot easily be extended to different classes of problems. In particular, they are not suited for multidisciplinary problems. In Ref. 20, Sobieski proposed a general approach to the design of large engineering systems, and in Ref. 21, he proceeded to demonstrate the proposed concepts by applying them to the two-level minimum weight

design of a portal framework under local constraints on stresses and local buckling and global constraints on displacement. At the global level, the weight of the framework is minimized with respect to the cross-sectional area and bending moment of inertia of the different beams, while satisfying constraints on displacements. Once a global design is obtained, the framework is analyzed to obtain the end loads on the beams. At the local level, each beam is designed separately. Its detailed dimensions are proportioned so as achieve the values of cross-sectional area and bending moment of inertia chosen at the global level while satisfying constraints on stresses and local buckling. This is done by minimizing a measure of the violation of the subproblem constraints. An optimum sensitivity analysis (Ref. 22) is then performed in order to obtain a linear approximation to the constraint violation of each local level subproblem in terms of the global level variables. The whole optimization is repeated, but, at the global level, it is required that the (linearized) local level constraint violations be reduced. This iterative process is pursued until all the local and global level constraints are satisfied and the framework weight cannot be reduced further. Although the proposed scheme is applied to a structural synthesis problem, it is applicable to any type

of engineering design. Furthermore, it may be used with decompositions involving more than two levels. Some of the key features of the approach are discussed below.

The method postulates a multilevel decomposition of the problem, that is, a decomposition where the different subproblems are grouped on the levels of a hierarchy. The subproblem at the top level is concerned with the optimization of the overall system objective in terms of design variables describing that system in very global terms. As one proceeds down the hierarchy, the subproblems are dealing with subsystems described in deeper and deeper levels of detail. The choice of the specifics of the decomposition for a given application still remains largely a matter of physical insight and convenience.

Below the highest level, each subproblem is concerned with finding a set of design variables which satisfy its own constraints for fixed values of higher level variables. It turns out that this amounts to finding a design vector which satisfies a set of equality constraints and a set of inequality constraints. Such a mathematical problem may not have a solution. It may be transformed into a mathematical programming problem which maximizes a measure of "how well" the design satisfies the sets of constraints. The subproblem formulation of Ref. 21 uses the equality

constraints to eliminate dependent variables and forms a penalty function with the inequality constraints. That penalty function is a measure of constraint violation which is then minimized with respect to the independent variables to find that design which best meets the constraints.

Once designs are obtained for all the subproblems on a given level, sensitivity analyses are performed to determine the effect changes in higher level variables have on lower level constraint violations. The resulting sensitivity derivatives are used to construct linear approximations to the lower subproblem constraint violations in terms of the higher level design variables. These approximations are added as constraints for the next optimization of the higher level subproblems. This enables the optimization of the higher level subproblems to be conducted so as to improve the design of the lower level subproblems which have violated constraints or so as to reduce the margin of satisfaction for those subproblems for which all constraints are amply satisfied. In essence, this makes the trade-offs between the different subproblems visible and allows them to be resolved in a rational fashion.

The task of the highest level subproblem remains the optimization of the system performance index with respect to its own global variables which are required not only to

satisfy its own constraints but also to reduce the constraint violation for the lower level subproblems.

1.2 OUTLINE

The purpose of this work has been to investigate the applicability of Sobieski's method to the design of complex, multidisciplinary engineering systems. It was elected to focus the effort on a specific example: the simultaneous aerodynamic and structural design of a high-performance sailplane wing for maximum cross-country speed. It was determined that this design problem could be carried out by means of a four-level decomposition. An algorithm was developed to solve the problem and it was tested on the two lower levels of the decomposition.

In Chapter II, we discuss the optimum sensitivity analysis technique. We show that the stationary conditions satisfied at a local constrained optimum may be used to determine the sensitivity of optimum objective functions and design variables to changes in those parameters that were kept fixed during the optimization.

Chapter III is devoted to a detailed description of the proposed algorithm. It is constructed along the same lines as that described in Ref. 20. The main difference resides with the specifics of the mathematical formulation for the

individual subproblems. The present algorithm treats equality constraints in a general numerical fashion. Furthermore, it is designed as a constrained programming problem rather than as a penalty function minimization problem. Particular attention is paid to the potential difficulties associated with decompositions that involve more than two levels.

In Chapter IV, the decomposition proposed for the example problem is detailed. It is a four-level decomposition. The highest level subproblem entails selection of global performance parameters which include weight and aerodynamic characteristics. Then follows an aerodynamic subproblem where the shape of the wing is defined so as to obtain the aerodynamic characteristics specified in the performance subproblem and control the initiation of stall. On the third level of the decomposition is a global structural subproblem where the wing spanwise distributions of weight and stiffnesses are selected for fixed total weight and so as to limit the wing bending response and torsional divergence speed. Finally, at the lowest level, the wing is modeled by a series of spanwise elements each of which is designed separately for fixed weight and stiffnesses under stress and local buckling constraints.

In Chapter V, the algorithm introduced in Chap. III is applied to the two lower levels of the hierarchy described in Chap. IV. The problem solved is the minimum weight design of a straight composite wing. Results are given for designs started from both the feasible space and the infeasible space.

Finally, Chapter VI is devoted to synthesizing the experience gained with this work and making recommendations for continued investigation.

Chapter II

SUMMARY OF PERTINENT RESULTS FROM OPTIMUM SENSITIVITY ANALYSIS

Optimum sensitivity analysis is a technique which permits one to investigate the sensitivity of the solution of an optimization problem to variations in the parameters of the problem. It yields derivatives of the optimum values of the design variables and objective function with respect to the parameters, derivatives which may then be used to perform trade-off analyses. These derivatives are called sensitivity derivatives to distinguish them from the derivatives of objective function and constraints with respect to the design variables which are termed behavior derivatives. This technique was recently introduced by Sobieski and coauthors (Ref. 22) as a tool for structural synthesis. It has been specialized by Schmit and Chang (Ref. 23) to a formulation of the problem of structural sizing for mimimum weight based on approximation concepts and dual methods, and has been used by Haftka (Ref. 24) in the optimization of damage tolerant structures. The elements of the technique required for the remainder of this work are discussed in this chapter; the reader interested in a more general discussion should consult Ref. 22.

2.1 STATEMENT OF THE PROBLEM

Assume that we start from the following nonlinear mathematical programming problem

$$\min_{X} F(X,P)$$

$$\text{so that } g(X,P) \leq 0 \qquad (2.1)$$

where vector X contains the n design variables of the problem, while vector P contains k parameters that are kept fixed during the optimization process. The constraint g is vector-valued, in general; it is assumed here to have m components. The optimum solution is functionally dependent on the parameters, hence, using $(^*)$ to denote optimum quantities

$$X^* = X^*(P)$$

$$F^* = F^*(P) \qquad (2.2)$$

At the constrained minimum, the following stationary (Kuhn-Tucker) conditions hold true.

$$F_X^* + g_X^{a*T} \lambda^* = 0$$

$$g^{a*} = 0$$

$$\lambda^* > 0 \qquad (2.3)$$

In these equations, subscript x indicates partial derivatives with respect to the design variables; superscript a refers to the constraints exactly satisfied (active) at the local minimum (there are m_a such constraints and g^a is a subvector of g); finally, λ is the vector of Lagrange multipliers (dual variables). The object of optimum sensitivity analysis is to find the rates of change of F^* and X^* with respect to P. We define these rates of changes as follows

$$X' = \frac{dX^*}{dP} \qquad \text{(matrix, nxk components)}$$

$$F' = \frac{dF^*}{dP} \qquad \text{(vector, k components)} \tag{2.4}$$

If F' and X' are known, we may construct linear approximations to the solution of Problem (2.1),

$$F^*(P+\Delta P) \simeq F^*(P)+F'^T\Delta P$$

$$X^*(P+\Delta P) \simeq X^*(P)+X'^T\Delta P \tag{2.5}$$

The two following sections are devoted to calculating F' and X'.

2.2 SENSITIVITY DERIVATIVES OF THE OBJECTIVE FUNCTION

The optimum sensitivity derivative of the objective function is obtained by the chain rule of differentiation as

$$F' = F_p^*+X'^TF_x^* \tag{2.6}$$

where subscript p indicates partial derivatives with respect to vector P. Now, we can show that F' may be found without actually calculating X'. We require that the optimum point for P+ΔP remain at the intersection of the constraints determining the optimum point for P. Hence, the second of Eqs. 2.3 is stationary with respect to P,

$$\frac{d}{dP}(g^{a*}) = g_p^{a*}+g_x^{a*}X' = 0 \tag{2.7}$$

Combining Eq. 2.7 transposed and postmultiplied by λ^* and the first of Eqs. 2.3 premultiplied by X'^T, we obtain

$$X'^T F_x^* = g_p^{a*T}\lambda^* \tag{2.8}$$

or

$$F' = F_p^*+g_p^{a*T}\lambda^* \tag{2.9}$$

The Lagrange multipliers λ^* may be available as by-products of the optimization scheme; otherwise, they may be obtained by QR decomposition or from the more classical least-squares solution to the first of Eqs. 2.3,

$$\lambda^* = -[g_x^{a*}g_x^{a*T}]^{-1}g_x^{a*}F_x \tag{2.10}$$

Then, Eq. 2.9 yields F' directly. An alternate solution exists because Eq. 2.7 is the only condition that X' must

meet in order for Eq. 2.8 to be satisfied. Therefore, if for some matrix Y (nxk)

$$g_p^{a*} + g_x^{a*} Y = 0 \tag{2.11}$$

then

$$X'^T F_x^* = g_p^{a*T} \lambda^* = Y^T F_x^*$$

and

$$F' = F_p^* + Y^T F_x^* \tag{2.12}$$

Equation 2.11 represents k sets of m_a linear equations in n unknowns, with $m_a \leq n$. We may therefore give arbitrary values to $n-m_a$ components of each column of Y and deduce the remaining m_a components from Eq. 2.11. In general, Y differs from the true sensitivity derivatives of the variables X', unless $n = m_a$. Assume that, in the space of the design variables X, an infinitesimal perturbation of parameter P results in a move from the initial point in the direction specified by Y. Then, the resulting design is still at the intersection of the originally active constraints because condition 2.7 is enforced; however, it may not be optimum because the first of Eqs. 2.3 may not be satisfied any more.

2.3 SENSITIVITY DERIVATIVES OF THE DESIGN VARIABLES

The first two of Eqs. 2.3 must remain satisfied at $P+\Delta P$. Defining the sensitivity derivative of the Lagrange multipliers

$$\lambda' = \frac{d\lambda^*}{dP} \tag{2.13}$$

we have

$$\frac{d}{dP}(g^{a*}) = g_p^{a*}+g_x^{a*}X' = 0$$

and

$$\frac{d}{dP}(F_x^*+g_x^{a*T}\lambda^*)$$

$$= F_{xp}^*+F_{xx}^*X'+\lambda^{*T}g_{xp}^{a*}+\lambda^{*T}g_{xx}^{a*}X'+g_x^{a*T}\lambda' = 0$$

This yields the sensitivity equations, k systems of $n+m_a$ linear equations in $n+m_a$ unknowns. In matrix form, we have

$$\begin{bmatrix} F_{xx}^*+\lambda^{*T}g_{xx}^{a*} & g_x^{a*} \\ g_x^{a*T} & 0 \end{bmatrix} \begin{Bmatrix} X' \\ \lambda' \end{Bmatrix} = - \begin{Bmatrix} F_{xp}^*+\lambda^{*T}g_{xp}^{a*} \\ g_p^{a*} \end{Bmatrix} \tag{2.14}$$

Once Eq. 2.14 is solved for X', Eq. 2.6 gives F' directly. Reference 22 discusses in detail the solvability of the sensitivity equations.

The approach of Sec. 2.2 yields the exact value of F' at considerably lower cost than that of Sec. 2.3 since it involves only first-order partial derivatives of F and g^a with respect to the design variables and parameters of the problem. However, it does not usually permit one to obtain X' (unless $n = m_a$). The choice between the two types of analysis is very much dependent on the application considered and the nature of the optimization problem at hand. It must be guided by a comparison between the cost of calculating second-order partial derivatives of F and g^a on the one hand, and the benefit of knowing the sensitivity derivatives of the variables on the other hand.

It must be noted that higher order sensitivity derivatives may be obtained for X^*, F^* and λ^* by setting higher order total derivatives of the two first stationary conditions (Eqs. 2.3) to zero. In particular, Ref. 25 shows how little additional calculation is required to find F", once X' has been obtained.

2.4 ADDITIONAL COMMENTS

After solving a mathematical programming problem and before performing sensitivity analysis, it is necessary to find the set of the active constraints. These constraints must satisfy Eqs. 2.3; furthermore, their gradients must be

linearly independent, if one wants to obtain the Lagrange multipliers from Eq. 2.10. The algorithm described below was used with success.

i) Select an initial set S^a of nearly satisfied constraints by retaining those constraints whose value is above a small negative tolerance.

ii) Identify S'^a, the subset of S^a which contains the maximum number of constraints with independent gradients. To achieve that, the constraint gradients are taken as the columns of a rectangular matrix and a Gaussian elimination with row and column interchanges is performed to identify the independent columns.

iii) Use Eq. 2.10 to find the Lagrange multipliers corresponding to set S'^a. Note that the fact that the constraints of set S'^a have independent gradients is a guarantee that Eq. 2.10 has a solution.

iv) Find the smallest Lagrange multiplier λ_i.

v) If λ_i is negative (less than a small positive tolerance), eliminate constraint i from set S^a and restart the process in ii). If λ_i is positive, terminate the process since S'^a is the desired set.

Note that steps ii) and iii) would not be required if QR decomposition were used. In step v), only the constraints with strictly positive Lagrange multipliers are kept, even though active constraints may have Lagrange multipliers that are zero. This is because constraints with zero Lagrange multipliers are redundant; hence, their gradients are linearly dependent on other constraint gradients.

In this work, the sensitivity derivatives are used to extend optimization information over a range of variation for the parameters of the design problems considered. This is achieved by means of the linear extrapolations given in Eq. 2.5. The implicit relationships 2.2 are expected to be nonlinear, in general. Hence, the extrapolations being first-order Taylor series expansions, they are valid only for limited ΔP. Furthermore, the calculation of the sensitivity derivatives is based on the assumption that the set of constraints active at the initial optimum will remain unchanged as the parameter P is changed to $P+\Delta P$. Perturbations of the parameters cause moves of the constraint boundaries with respect to each other and, therefore, may very well result in changes in the active constraint set. These changes then imply reduced accuracy of the extrapolated optima. The question arises of whether it is possible to estimate the magnitude of the parameter

perturbations which cause changes in the active constraint set. It was proposed in Ref. 22 that the perturbation of parameter p (element of vector P) which results in constraint i changing from active status to inactive status may be obtained to the first order by stating that λ_i is reduced to zero when constraint i leaves the active set,

$$\lambda_i^*(p+\Delta p_i) = \lambda_i^*(p)+\lambda_i'(p)\Delta p_i = 0$$

or

$$\Delta p_i = -\lambda_i^*(p)/\lambda_i'(p) \qquad (2.15)$$

Reference 22 likewise suggested that the perturbation of parameter p causing constraint i to change from inactive status to active status could be found as that value Δp_i for which $g_i^*(p+\Delta p_i)$ becomes zero.

$$g_i^*(p+\Delta p_i) = g_i^*(p)+[g_{ix}^{*T}(p)X'(p)]\Delta p_i = 0$$

then

$$\Delta p_i = -g_i^*(p)/[g_{ix}^{*T}(p)X'(p)] \qquad (2.16)$$

It was observed in Ref. 26 that Eqs. 2.15 and 2.16 could be unreliable. These estimates were used to determine with a specific design problem example what parameter perturbations cause changes in the status of the different constraints

involved, attempting ,so to speak, to construct an history of the active constraint set as p varies. This may not be an appropriate approach. Indeed, Eqs. 2.15 and 2.16 may be used to estimate a Δp_i for each of the problem constraints, indicating when the status of a particular constraint is supposed to change. However, only the smallest (in absolute value) negative and positive of these Δp_i (Δp_- and Δp_+) should be taken into consideration. The extrapolations based on sensitivity derivatives obtained at p should be adequate for $p+\Delta p_- \leq p+\Delta p \leq p+\Delta p_+$. But any prediction beyond that range (in particular prediction of change in the active constraint set) should not be relied upon since it would have been obtained with derivatives corresponding to an inappropriate active constraint set. In essence, as suggested in Ref. 23, the Δp_i of Eqs. 2.15 and 2.16 must be regarded as bounds on Δp. Barring excessive nonlinearity, the range of Δp defined by the intersection of these bounds is that within which the extrapolations based on sensitivity derivatives calculated at p should be reliable. In the absence of changes in the active constraint set, the accuracy of Eq. 2.5 is limited only by the inherent nonlinearity of the specific design problem considered.

Experiments conducted with various structural design problems showed (Ref. 22) that linear-extrapolation-based

estimates of optimum objective functions and design variables fell within a few percent of actual optimization result, for parameter variations of up to twenty percent; the predictions often were better for the objective function than for the design variables.

Chapter III

PRESENTATION OF THE ALGORITHM

This chapter is devoted to discussing an algorithm proposed for the design of complex engineering systems. The method is based on multilevel decomposition of the corresponding design problems into subproblems which are solved separately. The algorithm is discussed in general terms. This is done so as to avoid focusing on a particular problem. The following chapter will be devoted to investigating the applicability of the approach described here to a specific problem. The abstract concepts introduced here can be more easily put in a physical context if this chapter and the following one are read simultaneously. The presentation begins with a definition of the type of multilevel decomposition considered and of the components of that decomposition. Then, the discussion centers on the formulation and solution of the subproblems. Finally, the organization of the overall optimization is discussed. The developments follow those by Sobieski in Ref. 20.

3.1 DEFINITIONS

The starting point of this discussion is the task of designing a system by finding a set of variables which optimize a performance index while satisfying a number of constraints. This will be referred to as the overall problem. Assume that, for convenience, the overall problem is decomposed into a number of subproblems, each of which corresponds to the design of a subsystem, and has its own sets of variables and constraints. The subproblems are organized in a hierarchy as shown on Fig. 1. The subproblem at the top of the hierarchy is the design of the whole system, in very general terms. The next level deals with major subsystems, the third one with subsystems of the major subsystems, and so on. As one goes down the levels, the details of the system become more and more precisely defined. The subproblems are identified by two numbers ij which define (i) the level of the subproblem, and (j) its position on that level. The level numbers increase downward, and the subproblem numbers increase, say, from left to right. The hierarchy is assumed to have l levels; there are n_i subproblems on level i.

The whole design process is conducted iteratively, starting at the highest level and going down. Each subsystem is designed separately. The object of the algorithm is to coordinate the design of the different

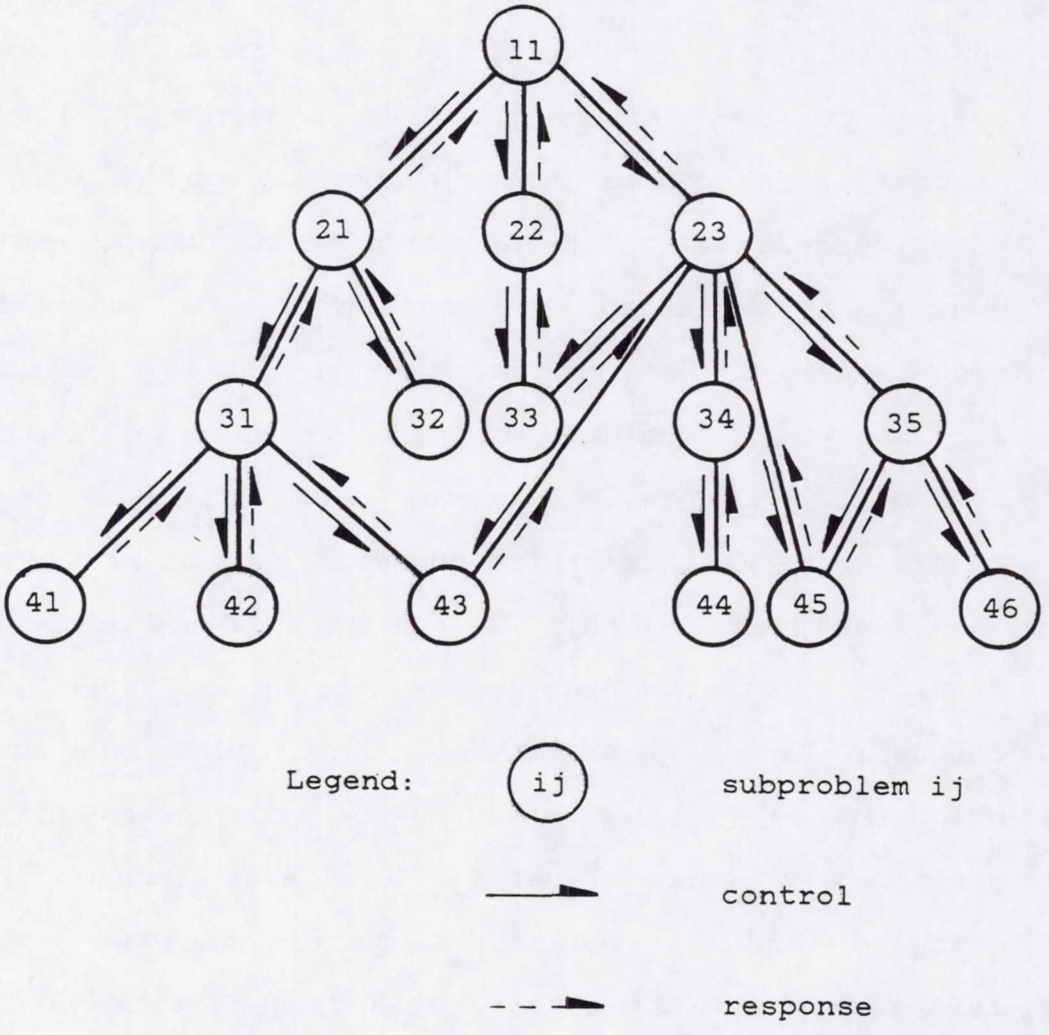

Figure 1: Example of four-level hierarchy.

subsystems so as to obtain optimum system performance by resolving the trade-offs between the subsystems in a rational fashion. This is achieved by manipulating two types of interactions between the subproblems: the controls and the responses. A control is a quantity selected in a subproblem to influence another subproblem in the hierarchy. A response is a quantity that reflects the effect the design of one subproblem has on that of another subproblem. In this work, we assume that the controls flow exclusively downward in the hierarchy, while the responses flow exclusively upward. This excludes situations where a subproblem controls another subproblem on the same level (lateral control) or on a higher level (reverse control).[1] As represented symbolically on Fig. 2, each subproblem is assumed to receive controls from higher level subproblems through vector CI_{ij} (control inputs in subproblem ij), and to receive responses from lower level subproblems through vector RI_{ij} (response inputs in subproblem ij). Also, each subproblem is assumed to control lower level subproblems with vector CO_{ij} (control outputs from subproblem ij), and

[1] In Ref. 20, the controls are named interaction quantities. The interested reader should refer to that source for indications as to how to handle reverse and lateral controls.

c) Highest level subproblem.

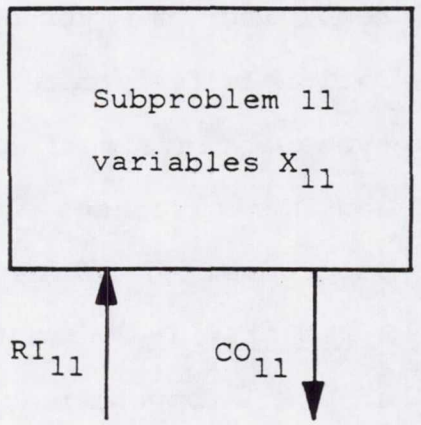

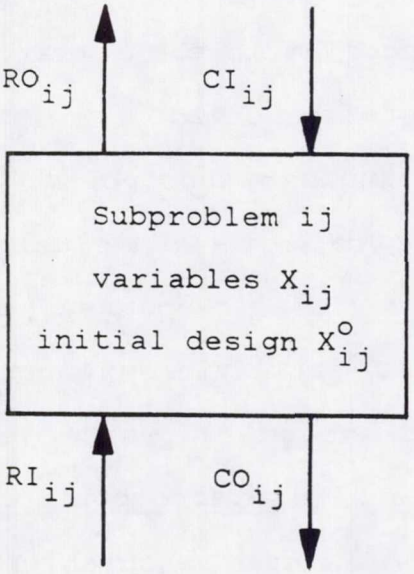

b) Intermediate level subproblem.

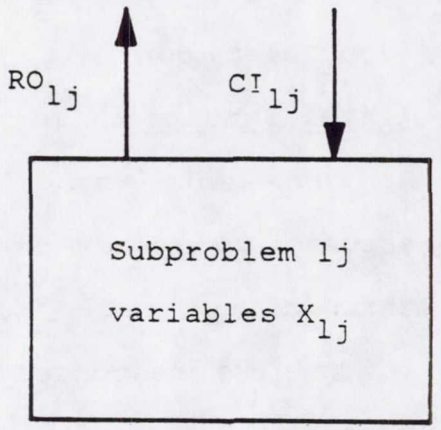

a) Lowest level subproblem.

Figure 2: Symbolic representation of the different types of subproblems.

to respond to higher level subproblems with vector RO_{ij} (response outputs from subproblem ij). This discussion does not make any assumption on the specific form of the controls, except that the control outputs from a subproblem depend on the variables of that subproblem; they may be the variables themselves or functions of these variables ($CO_{ij} = CO_{ij}(X_{ij})$). Likewise, the controls imposed on subproblem ij (CI_{ij}) are not specified , except that they are assumed known once all the control outputs from higher level subproblems ($CO_{\alpha\beta}$, $\alpha<i$) are known. The response outputs from a subproblem (RO_{ij}) will be defined in this chapter. Furthermore, it will be shown that the response inputs into a subproblem (RI_{ij}) are entirely known once the response outputs from the lower level subproblems ($RO_{\alpha\beta}$, $\alpha>i$) are known.

For each iteration of the overall system, each subproblem is concerned with finding a design which satisfies its own constraints for the controls specified by the higher level subproblems (CI_{ij}). In addition, the subproblem manipulates its own controls (CO_{ij}) so as to improve the responses from the lower level subproblems (RI_{ij}). Mathematically, this implies finding a design vector that satisfies a set of

equality constraints and a set of inequality constraints. This problem may be solved by transforming it into a nonlinear mathematical programming problem where a measure of constraint violation is minimized with respect to the design vector. The subproblem's own response (RO_{ij}) is then constituted of the minimum measure of constraint violation as well as derivatives indicating the sensitivity of that minimum measure to changes in the controls imposed on the subproblem.

The subproblem on the highest level of the hierarchy drives the whole design process. It selects its own design variables so as to optimize the overall problem performance index and satisfy its own constraints. It adjusts its controls (CO_{11}) to improve the responses from the lower levels (RI_{11}), that is, reduce the constraint violation in the lower level subproblems.

3.2 LOWEST LEVEL SUBPROBLEM

Figure 2 a) describes symbolically subproblem lj, a subproblem on the lowest level of the hierarchy. The vector of design variables is X_{lj}, the subproblem design is influenced by the controls collected in vector CI_{lj} and the subproblem response is vector RO_{lj}. The subproblem statement is as follows.

find X_{lj} so that

$$g_{lj}(X_{lj}, CI_{lj}) \leq 0 \qquad (3.1.a)$$

$$e_{lj}(X_{lj}, CI_{lj}) = 0 \qquad (3.1.b)$$

$$X^{l}_{lj} \leq X_{lj} \leq X^{u}_{lj} \qquad (3.1.c)$$

The functions g_{lj} and e_{lj} are vector-valued. The subproblem design is subject to a set of inequality constraints (Eq. 3.1.a). These are the constraints set on the corresponding subsystem in the statement of the overall non-decomposed problem. The design is also subject to a set of equality constraints (Eq. 3.1.b). Some of these may come from the formulation of the overall non-decomposed problem; some are imposed on the subproblem during decomposition. The multilevel decomposition consists of different models of the system being designed, the models becoming more refined as one progresses down the hierarchy. The equality constraints arise from the necessity of requiring consistency between the models at different levels. Also, some upper and lower bounds may be set on the variables (Eq. 3.1.c). As stated in the previous section, the subproblem is assumed to be controlled by each subproblem on the higher levels. As a result, the vector of controls CI_{lj} is functionally dependent on the optimum designs of all the subproblems above the lowest level.

$$CI_{lj} = CI_{lj}(X^*_{11},\ldots,X^*_{l-1,n_{l-1}}) \tag{3.2}$$

Problem 3.1[2] may have from zero to an infinity of solutions, depending on the controls CI_{lj}. We transform it into a nonlinear mathematical programming problem by introducing two new variables ε_{lj} and η_{lj} which are used to relax inequality and equality constraints. These new variables are combined into a composite function which is a global measure of constraint violation and which is minimized to identify the "best" design. The transformed problem is

find $X_{lj},\varepsilon_{lj},\eta_{lj}$ so that

$$e^{-\varepsilon_{lj}+b\eta_{lj}} \text{ is minimum} \tag{3.3.a}$$

$$g_{lj}(X_{lj},CI_{lj})+\varepsilon_{lj} \leq 0 \tag{3.3.b}$$

$$-\eta_{lj} \leq e_{lj}(X_{lj},CI_{lj}) \leq \eta_{lj} \tag{3.3.c}$$

$$X^l_{lj} \leq X_{lj} \leq X^u_{lj} \tag{3.3.d}$$

$$-\eta_{lj} \leq 0 \tag{3.3.e}$$

---

[2] In the remainder of this dissertation, references are made to "Problem 3.j", meaning the mathematical problem described by Eqs. 3.j.

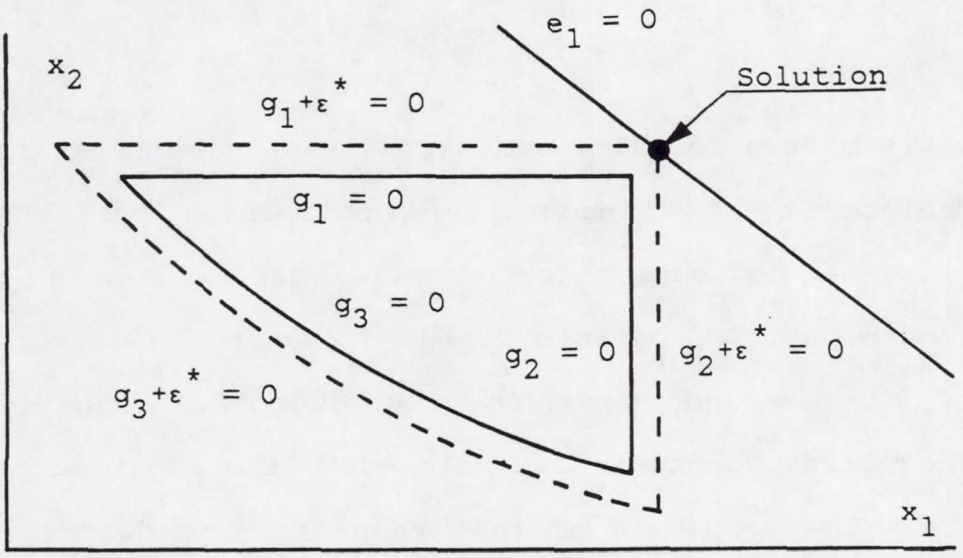

b) Initial problem has no feasible solution ($\varepsilon^* < 0$).

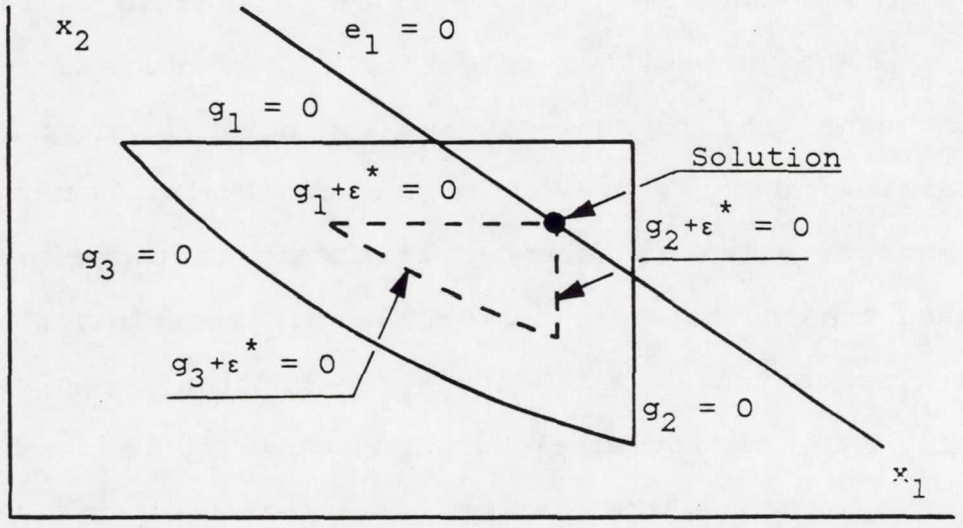

a) Initial problem has feasible solutions ($\varepsilon^* \geq 0$).

Figure 3: Illustration of the principle of inequality constraint relaxation.

where b is a positive constant. Each equality constraint is replaced by two inequality constraints (Eq. 3.3.c). The distance between these constraints ($2\eta_{1j}$) is forced to remain positive because of Eq. 3.3.e and to decrease because of the second term in the objective function. Each inequality constraint is relaxed by the addition of variable ε_{1j}. The mechanism of that relaxation is described in Fig. 3, for a simple two-dimensional problem with one equality and three inequality constraints, assuming that the equality constraint is identically satisfied. The first term in the objective function (Eq. 3.3.a) is defined so as to increase ε_{1j}. A high positive value for ε_{1j} is quite acceptable as it means that the selected design point is deep inside the feasible domain, away from the constraint boundaries, and that decreases the chances of obtaining infeasible designs when the controls are perturbed. If the solution of Problem 3.3 is so that $\varepsilon_{1j} \geq 0$ and $\eta_{1j} = 0$, then it solves Problem 3.1. If, on the other hand, we have $\varepsilon_{1j} < 0$ or $\eta_{1j} \neq 0$, then the resulting design is infeasible with respect to Problem 3.1.

Constant b is added to the definition of the objective function to control the importance attributed to violating

the different constraints. A high value for b results in a heavy penalty paid for violating equality constraints; conversely, a low value for b makes the penalty for violating inequality constraints more important, in relative terms. In addition to adjusting b, it may prove appropriate to scale variables ε_{lj} and η_{lj} in order to make all components of the constraint gradients of the same order of magnitude.

Any nonlinear programming algorithm may be used to solve Problem 3.3. This yields X^*_{lj}, as well as a measure of inequality constraint violation ε^*_{lj} and a measure of equality constraint violation η^*_{lj}. These are functionally dependent on the controls CI_{lj} and, therefore, as indicated by Eq. 3.2, on the optimum design variables of subproblems on higher levels. Optimum sensitivity analysis may be used to study the effect changes in higher level subproblem variables have on the constraint violations for subproblem lj. Considering ε^*_{lj}, if all higher level subproblem designs are perturbed, we have

$$\varepsilon^*_{lj}[CI_{lj}(X^*_{11}+\Delta X_{11},\ldots,X^*_{l-1,n_{l-1}}+\Delta X_{l-1,n_{l-1}})]$$

$$\simeq \sum_{\alpha=1}^{l-1}\sum_{\beta=1}^{n_\alpha} \varepsilon^*_{lj\alpha\beta}(\Delta X_{\alpha\beta}) \qquad (3.4.a)$$

where

$$\varepsilon^*_{1j\alpha\beta}(\Delta X_{\alpha\beta}) = \Psi_{1j\alpha\beta}\varepsilon^*_{1j}[CI_{1j}(X^*_{11},\ldots,X^*_{1-1,n_{1-1}})]$$

$$+ \frac{\partial \varepsilon^*_{1j}}{\partial CI_{1j}} \frac{\partial CI_{1j}}{\partial X_{\alpha\beta}} \Delta X_{\alpha\beta} \qquad (3.4.b)$$

and

$$0 \leq \Psi_{1j\alpha\beta} \leq 1 \qquad (3.4.c)$$

$$\sum_{\alpha=1}^{1-1} \sum_{\beta=1}^{n_\alpha} \Psi_{1j\alpha\beta} = 1 \qquad (3.4.d)$$

Equation 3.4 is a first order Taylor series expansion of the type discussed in Chap. 2. It indicates the sensitivity of the design of subproblem 1j to changes in higher level subproblem designs. It is written as a superposition of responses to each of these subproblems. Equation 3.4.b gives the response to subproblem αβ. Several subproblems may control subproblem 1j. Hence, each one is given the task of reducing a fraction of ε^*_{1j}. The first term in Eq. 3.4.b determines the fraction of constraint violation in subproblem 1j that must be reduced by appropriate choice of the controls of subproblem αβ. The coefficient $\Psi_{1j\alpha\beta}$ may be defined as the coefficient of participation of subproblem αβ in the design of subproblem 1j. It must be chosen on the basis of experience with the type of system considered. Because of Eq. 3.4.d, ε^*_{1j} is entirely divided among all

subproblems controlling subproblem lj. The second term in Eq. 3.4.b indicates how changes in the design of subproblem $\alpha\beta$ will affect the design of subproblem lj. The same linearization may be conducted for η^*_{lj}, providing comparable information for the measure of violation of equality constraints.

The vector of response outputs from subproblem lj is defined as

$$RO^T_{lj} = \left\{ \varepsilon^*_{lj}, \frac{\partial \varepsilon^*_{lj}}{\partial CI_{lj}}, \eta^*_{lj}, \frac{\partial \eta^*_{lj}}{\partial CI_{lj}} \right\} \tag{3.5}$$

This information will be used to construct the response inputs into higher level subproblems ($RI_{\alpha\beta}$, $\alpha<1$).

3.3 INTERMEDIATE LEVEL SUBPROBLEM

Figure 2 b) depicts symbolically a subproblem on any intermediate level of the hierarchy. The design variables are arranged in vector X_{ij}. At the beginning of the present iteration, the initial value of X_{ij} is X^o_{ij}, the optimum design obtained during the previous iteration. The design of the subproblem is influenced by the controls CI_{ij} and the responses RI_{ij}. The subproblem influences the lower level subproblems with its own controls CO_{ij}; its response to the higher level subproblem controls is RO_{ij}. The controls CI_{ij}

are issued from all the higher level subproblems. We have the following functional relationship

$$CI_{ij} = CI_{ij}(X^*_{11},\ldots,X^*_{i-1,n_{i-1}}) \tag{3.6}$$

The definition of RI_{ij} will be discussed at the end of this section. The statement of the subproblem is

find X_{ij} so that

$$g_{ij}(X_{ij},CI_{ij}) \le 0 \tag{3.7.a}$$

$$e_{ij}(X_{ij},CI_{ij}) = 0 \tag{3.7.b}$$

$$-\varepsilon^*_{\mu\nu ij}(\Delta X_{ij}) = -\varepsilon^*_{\mu\nu ij}(X_{ij}-X^o_{ij}) \le 0 \tag{3.7.c}$$

$$\eta^*_{\mu\nu ij}(\Delta X_{ij}) = \eta^*_{\mu\nu ij}(X_{ij}-X^o_{ij}) = 0 \tag{3.7.d}$$

$$\mu = i+1,\ldots,l; \quad \nu = 1,\ldots,n_\mu$$

$$X^l_{ij} \le X_{ij} \le X^u_{ij} \tag{3.7.e}$$

$$(1-\delta)X^o_{ij} \le X_{ij} \le (1+\delta)X^o_{ij} \tag{3.7.f}$$

This statement contains three types of constraints which were not included in the formulation of the lowest level subproblem. Constraints 3.7.c and d are linear extrapolations of the type of Eq. 3.4.b, their coefficients being available from the responses RI_{ij}. They require satisfaction of equality and inequality constraints in lower

level subproblems. Equation 3.4.b gives $\varepsilon_{\mu\nu ij}$ for $\mu = 1$; a more general expression is given at the end of this section. The increment ΔX_{ij} corresponds to the change of X_{ij} with respect to the previous optimum design, or, the current initial design, hence $\Delta X_{ij} = X_{ij} - X_{ij}^{o}$. Constraints 3.7.f are called move limits; they limit the changes in the variables X_{ij} to a fixed fraction δ of the initial values of these variables. This is done to preserve the validity of the sensitivity-analysis-based linear extrapolations of Eqs. 3.7.c and d (see Sec. 2.4).

The solution proposed for this problem is very similar to that used for Problem 3.1, namely:

find $X_{ij}, \varepsilon_{ij}, \eta_{ij}$ so that

$$e^{-\varepsilon_{ij}} + b\eta_{ij} \text{ is minimum} \tag{3.8.a}$$

$$g_{ij}(X_{ij}, CI_{ij}) + \varepsilon_{ij} \leq 0 \tag{3.8.b}$$

$$-\eta_{ij} \leq e_{ij}(X_{ij}, CI_{ij}) \leq \eta_{ij} \tag{3.8.c}$$

$$-\varepsilon^{*}_{\mu\nu ij}(X_{ij} - X_{ij}^{o}) + \varepsilon_{ij} \leq 0 \tag{3.8.d}$$

$$-\eta_{ij} \leq \eta^{*}_{\mu\nu ij}(X_{ij} - X_{ij}^{o}) \leq \eta_{ij} \tag{3.8.e}$$

$$\mu = i+1, \ldots, l; \quad \nu = 1, \ldots, n_{\mu}$$

$$-\eta_{ij} \leq 0 \tag{3.8.f}$$

$$X_{ij}^{l} \leq X_{ij} \leq X_{ij}^{u} \tag{3.8.g}$$

$$(1-\delta)X_{ij}^{o} \leq X_{ij} \leq (1+\delta)X_{ij}^{o} \qquad (3.8.h)$$

The comments relative to Problem 3.3 apply to Problem 3.8 as well. Solution of Problem 3.8 using any nonlinear programming algorithm yields an optimum design X_{ij}^{*}, an optimum measure of inequality constraint violation ε_{ij}^{*}, and an optimum measure of equality constraint violation η_{ij}^{*}. These are now functionally dependent on the controls CI_{ij}, the responses RI_{ij}, and the initial design X_{ij}^{o}. Taking, for example, the measure of violation of inequality constraints, we have

$$\varepsilon_{ij}^{*} = \varepsilon_{ij}^{*}[CI_{ij}(X_{11}^{*},\ldots,X_{i-1,n_{i-1}}^{*}),RI_{ij},X_{ij}^{o}] \qquad (3.9)$$

Again, we may resort to optimum sensitivity analysis to investigate the effect that changes in higher level subproblem designs have on the design of subproblem ij. However, we must also account for the changes in the lower level subproblem responses and in the initial design for subproblem ij.

$$\varepsilon_{ij}^{*}[CI_{ij}(X_{11}^{*}+\Delta X_{11}\ldots),\ldots,X_{ij}^{o}+\Delta X_{ij}^{o}]$$

$$\simeq \sum_{\alpha=1}^{i-1}\sum_{\beta=1}^{n_{\alpha}} \varepsilon_{ij\alpha\beta}^{*}(\Delta X_{\alpha\beta}) \qquad (3.10.a)$$

where

$$\varepsilon^{*}_{ij\alpha\beta}(\Delta X_{\alpha\beta}) = \Psi_{ij\alpha\beta}\left(\varepsilon^{*}_{ij}[CI_{ij}(X^{*}_{11},\ldots),\ldots,X^{o}_{ij}] + \frac{\partial\varepsilon^{*}_{ij}}{\partial RI_{ij}}\Delta RI_{ij} + \frac{\partial\varepsilon^{*}_{ij}}{\partial X^{o}_{ij}}\Delta X^{o}_{ij}\right) + \frac{\partial\varepsilon^{*}_{ij}}{\partial CI_{ij}}\frac{\partial CI_{ij}}{\partial X_{\alpha\beta}}\Delta X_{\alpha\beta} \qquad (3.10.b)$$

and

$$0 \le \Psi_{ij\alpha\beta} \le 1 \qquad (3.10.c)$$

$$\sum_{\alpha=1}^{i-1}\sum_{\beta=1}^{n_{\alpha}} \Psi_{ij\alpha\beta} = 1 \qquad (3.10.d)$$

This equation corresponds to that developed for a lowest level subproblem (Eq. 3.4). The only difference resides in the addition of terms accounting for perturbations in response inputs (ΔRI_{ij}) and in initial design (ΔX^{o}_{ij}). A similar expression may be developed for η^{*}_{ij}.

The vector of response outputs from subproblem ij is defined as

$$RO^{T}_{ij} = \left\{\varepsilon^{*}_{ij}, \frac{\partial\varepsilon^{*}_{ij}}{\partial CI_{ij}}, \frac{\partial\varepsilon^{*}_{ij}}{\partial RI_{ij}}, \frac{\partial\varepsilon^{*}_{ij}}{\partial X^{o}_{ij}}, \eta^{*}_{ij}, \frac{\partial\eta^{*}_{ij}}{\partial CI_{ij}}, \frac{\partial\eta^{*}_{ij}}{\partial RI_{ij}}, \frac{\partial\eta^{*}_{ij}}{\partial X^{o}_{ij}}\right\} \qquad 1 < i < l \qquad (3.11)$$

The vector of response inputs to subproblem ij contains

the information necessary to construct the linear approximations of Eqs. 3.7.c and d.

$$RI_{ij}^T = \left\{ \{\varepsilon^*_{i+1,1ij}\}^T, \ldots, \{\varepsilon^*_{ln_1 ij}\}^T, \{\eta^*_{i+1,1ij}\}^T, \ldots, \{\eta^*_{ln_1 ij}\}^T \right\}$$

$$\{\varepsilon^*_{\mu\nu ij}\}^T = \left\{ \Psi_{\mu\nu ij} \left(\varepsilon^*_{\mu\nu} + \frac{\partial \varepsilon^*_{\mu\nu}}{\partial RI_{\mu\nu}} \Delta RI_{\mu\nu} + \frac{\partial \varepsilon^*_{\mu\nu}}{\partial X^o_{\mu\nu}} \Delta X^o_{\mu\nu} \right) , \right.$$

$$\left. \frac{\partial \varepsilon^*_{\mu\nu}}{\partial CI_{\mu\nu}} \frac{\partial CI_{\mu\nu}}{\partial X_{ij}} \right\} \qquad 1 \le i < l; \quad i < \mu \qquad (3.12)$$

$\{\eta^*_{\mu\nu ij}\}$ is defined similarly. There are two subvectors for each lower level subproblem $\mu\nu$. Their components are obtained recursively from Eq. 3.10.b, redefining ij as $\mu\nu$, and $\alpha\beta$ as ij. To calculate the response inputs into subproblem ij, we need to know, for each lower level subproblem $\mu\nu$, the response outputs ($RO_{\mu\nu}$), the changes in response inputs ($\Delta RI_{\mu\nu}$), the changes in initial design ($\Delta X^o_{\mu\nu}$), and the specific form of the relationship between the control inputs in subproblem $\mu\nu$ and the variables of subproblem ij ($CI_{\mu\nu}(X_{ij})$). The contributions of a subproblem on the lowest level ($\{\varepsilon_{l\nu ij}\}, \{\eta_{l\nu ij}\}$) do not involve terms in $\Delta RI_{l\nu}$ and $\Delta X^o_{l\nu}$, as there are no response inputs nor move limits for a lowest level subproblem (see Problem 3.3).

3.4 HIGHEST LEVEL SUBPROBLEM

The highest level subproblem is depicted in Fig. 2 c). Its task is to select the variables X_{11} which optimize the overall problem objective while satisfying a set of inequality constraints. In addition, the controls C_{11} must be manipulated according to RI_{11} (Eq. 3.12) so as to improve the lower level subproblem constraint violations. Assuming that the overall problem objective is to minimize $F(X_{11})$, the subproblem statement is as follows.

find X_{11} so that

$$F(X_{11}) \text{ is minimum} \tag{3.13.a}$$

$$g_{11}(X_{11}) \leq 0 \tag{3.13.b}$$

$$-\varepsilon^{*}_{\mu\nu 11}(X_{11}-X^{o}_{11}) \leq 0 \tag{3.13.c}$$

$$\eta^{*}_{\mu\nu 11}(X_{11}-X^{o}_{11}) = 0 \tag{3.13.d}$$

$$\mu = 2,\ldots,1; \quad \nu = 1,\ldots,n_{\mu}$$

$$X^{l}_{11} \leq X_{11} \leq X^{u}_{11} \tag{3.13.e}$$

$$(1-\delta)X^{o}_{11} \leq X_{11} \leq (1+\delta)X^{o}_{11} \tag{3.13.f}$$

The corresponding transformed subproblem is now

find $X_{11}, \varepsilon_{11}, \eta_{11}$ so that

$$F(X_{11})-c\varepsilon_{11}+d\eta_{11} \text{ is minimum} \tag{3.14.a}$$

$$g_{11}(X_{11})+\varepsilon_{11} \leq 0 \tag{3.14.b}$$

$$-\varepsilon^{*}_{\mu\nu 11}(X_{11}-X^{o}_{11})+\varepsilon_{11} \leq 0 \tag{3.14.c}$$

$$-\eta_{11} \leq \eta^{*}_{\mu\nu 11}(X_{11}-X^{o}_{11}) \leq \eta_{11} \tag{3.14.d}$$

$$\mu = 2,\ldots,l; \quad \nu = 1,\ldots,n_{\mu}$$

$$X^{l}_{11} \leq X_{11} \leq X^{u}_{11} \tag{3.14.e}$$

$$(1-\delta)X^{o}_{11} \leq X_{11} \leq (1+\delta)X^{o}_{11} \tag{3.14.f}$$

$$\varepsilon_{11} \leq \varepsilon_{11max} \tag{3.14.g}$$

$$-\eta_{11} \leq 0 \tag{3.14.h}$$

The transformation of this subproblem is almost identical to that of the two previously discussed subproblems. The only difference is that even though ε_{11} is still forced to increase, it is limited to a small positive value ε_{11max}. This avoids overdesigning, that is, producing designs with excessive margin with respect to the constraints. If ε_{11} were allowed to become large and positive, the measures of inequality constraint violation $\varepsilon^{*}_{\mu\nu ij}$ would become large and negative, an unnecessary requirement. The additional variables ε_{11} and η_{11} are both driven to zero by addition of a penalty term to the objective function. The exponential is not required for ε_{11} any more as it is constrained to

remain negative or, at best, slightly positive. The positive constants c and d may be adjusted, if necessary, to force ε_{11} and η_{11} within prescribed tolerances.

3.5 ORGANIZATION OF THE ALGORITHM

This section presents the organization of the algorithm. Within a given iteration, the general progression is top-down. The first iteration must be conducted without responses from lower level subproblems. The process terminates when: 1) all constraints of Problems 3.1, 3.7 and 3.13 are satisfied, and 2) the objective function $F(X_{11})$ is stationary.

i) Iteration r=1: for i from 1 to 1, for j from 1 to n_i.

- Read initial design X^o_{ij}.
- For i>1, calculate control inputs CI_{ij} from control outputs $CO_{\alpha\beta}$, $\alpha<i$.
- Optimize subproblem ij, obtain X^*_{ij}, ε^*_{ij}, η^*_{ij}.
  - If i=1, solve Problem 3.14, without Eqs. 3.14.c and d.
  - If 1<i<1, solve Problem 3.8, without Eqs. 3.8.d and e.
  - If i=1, solve Problem 3.3.
- For i<1, calculate control outputs CO_{ij} from X^*_{ij}.

ii) Calculate responses: for i from 1-1 to 1, for j from 1 to n_i.

- For i>1, perform sensitivity analysis, obtain RO_{ij} (Eq. 3.11 if 1<i<1, Eq. 3.5 if i=1).
- Calculate response inputs RI_{ij} from response outputs $RO_{\alpha\beta}$, $\alpha>i$ (Eq. 3.12).

iii) Iteration r=r+1: for i from 1 to 1, for j from 1 to n_i.

- Define new initial point as previous optimum design: $X^{o}_{ij}=X^{*}_{ij}$.
- For i>1, calculate control inputs CI_{ij} from control outputs $CO_{\alpha\beta}$, $\alpha<i$.
- Optimize subproblem ij, obtain X^{*}_{ij}, ε^{*}_{ij}, η^{*}_{ij}.
  - If i=1, solve Problem 3.14.
  - If 1<i<1, solve Problem 3.8.
  - If i=1, solve Problem 3.3.
- For i<1, calculate control outputs CO_{ij} from X^{*}_{ij}.

iv) Check convergence: if converged, exit; otherwise, return to ii).

This organization specifies that the algorithm progresses top-down rather than bottom-up as suggested in Ref. 20. The disadvantage of conducting the optimization as proposed here is that the first iteration must be done without responses from lower level subproblems. Therefore, that iteration may be considered wasted as the first subproblem designs will not have been obtained with full consideration for the requirements from those lower level subproblems. However, this negative effect will be somewhat tempered if the move limits (Eqs. 3.8.h and 3.14.f) are kept for the subproblems above the lowest level. The argument for proceeding top-down is the need for accounting for changes in lower level subproblem response inputs while optimizing a subproblem on a given level (see term in $\Delta RI_{\mu\nu}$ in Eq. 3.12). If optimization were conducted bottom-up, the sensitivity derivatives making up a subproblem $RO_{\mu\nu}$ would be calculated for a given $RI_{\mu\nu}$ but would be used in a higher level subproblem in the same iteration before new $RI_{\mu\nu}$ values were generated, therefore making it impossible to calculate $\Delta RI_{\mu\nu}$.

If the decomposition involves only two levels, the objection to conducting the optimization bottom-up disappears as there is no $\Delta RI_{\mu\nu}$ term to calculate. But then, there is little difference between top-down and

bottom-up optimization. It is only a matter of deciding whether optimization will start at the top or at the bottom; from that point, the optimizations of the different levels follow always in the same sequence.

3.6 MOVE LIMIT SELECTION

The move limits of Problems 3.8 and 3.14 may be chosen on the basis of experience, or, using the bound estimates of Sec. 2.4. When optimization is conducted with fixed move limits, it is observed that the design first progresses steadily towards the optimum solution but does not settle; rather, it oscillates about that solution. During these oscillations, an excessive number of switches in the active constraint set occur, thereby preventing the process from converging. This situation is similar to that observed when solving a nonlinear mathematical programming problem as a sequence of linearized problems. When that type of method is used, similar oscillations are encountered if the optimum of the initial problem does not lie at a vertex of the feasible domain; the solutions of successive linear problems oscillate between adjacent vertices of that domain. As discussed by Pope (Ref. 27), an approach to overcome that difficulty is to reduce the move limits as the oscillating behavior appears. This approach was successfully followed in this study.

3.7 FINAL COMMENTS

This chapter discusses an approach for optimizing decomposed design problems. It must be emphasized that no firm rule is established for devising a decomposition method. For a specific problem, the decomposition must be made on the basis of practical experience. As pointed out by Sobieski (Ref. 20) the large design problems for which this type of approach is conceived have always been treated in decomposed form. For major projects, the design process is carried out by the design office of a company (or even several companies). That office is itself divided into specialty groups and subgroups each of which handles the design of a particular type of subsystem using its own codes and analytic tools. The team managing the design is then concerned with resolving the trade-offs. The proposed method offers a means for doing this with a systematic mathematical procedure; furthermore, it lends itself to parallel or distributed computer processing.

Before applying the proposed method to a problem, the decomposition must be defined. This implies a definition of the different subproblems and the choice of their design variables and constraints. The structure of the controls must be identified as well. For the sake of generality, the developments of this chapter make the assumption that each

subproblem controls each lower level subproblem; as a consequence, each subproblem responds to each higher level subproblem. Clearly, this situation is undesirable from an economic standpoint. An expensive item in the scheme remains the calculation of the sensitivity derivatives, as these require calculation of second-order behavioral derivatives (Chap. 2). Therefore, as a general rule, the number of controls should be kept as low as possible. Practical experience should help in determining what control or response must be accounted for. In particular, controls or responses yielding typically low sensitivity derivatives ($\partial\varepsilon^*_{ij}/\partial CI_{ij}$ and $\partial\varepsilon^*_{ij}/\partial RI_{ij}$ in Eq. 3.10) should be ignored.

A key point of this discussion is the approach chosen for finding individual subproblem designs (solution of Problems 3.1, 3.7, and 3.13). Two additional variables are introduced in each subproblem. These monitor the most violated equality and inequality constraints. This particular formulation was used because i) it permits equality constraints to be treated numerically, and ii) it is compatible with the use of a usable-feasible direction algorithm for solving the individual subproblems. It must be noted that other approaches could be used as well. Reference 21 discusses an example based on a penalty

function formulation, where a cumulative measure involving all the constraints of the problem (except side constraints and move limits) is minimized.

Chapter IV

APPLICATION OF THE ALGORITHM TO THE DESIGN OF A SAILPLANE WING

This chapter demonstrates the applicability of the proposed algorithm to the problem of designing a high-performance sailplane wing. To achieve this goal, we describe the proposed decomposition. We identify the subproblems, their design variables, and the different control and response vectors. The objective of the overall problem is taken to be the optimization of a classical performance index called the cross-country speed. Clearly, to efficiently design an airplane, one must optimize its entire configuration all at once. However, in order to reduce the problem size, we focus our efforts on the wing design, in effect solving the problem of redesigning the wing of an existing sailplane. We assume that the description of the other sailplane components is entirely known. The variables of the overall problem describe the wing shape and its structure. The decomposition has four levels (see Fig. 4).

The top level of the hierarchy is occupied by a subproblem that selects global performance parameters. This drives an aerodynamic subproblem on the second level where the wing shape is designed to the specified performance characteristics. The synthesis of the wing structure is

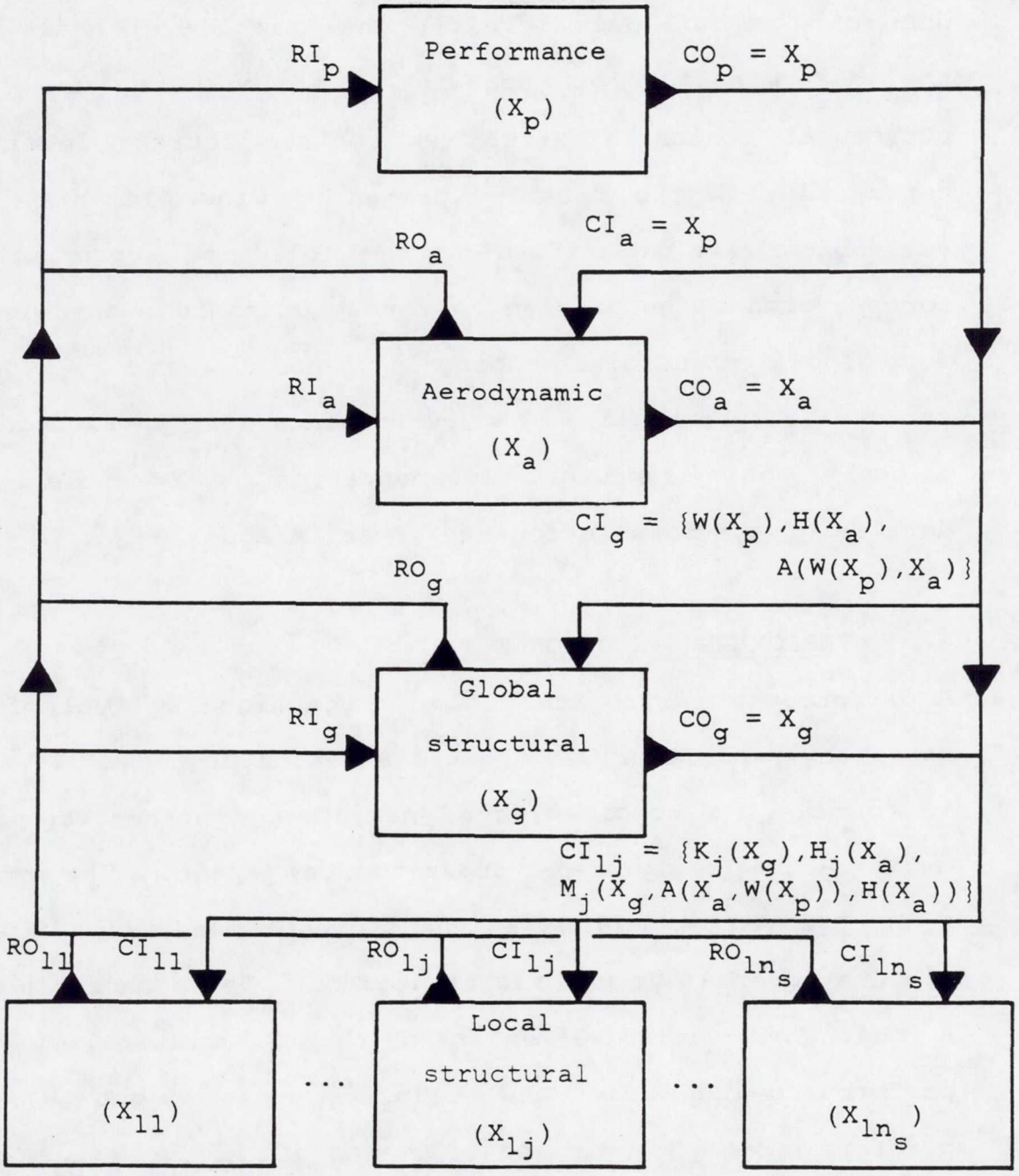

Figure 4: Four-level hierarchy for performance sailplane wing design problem.

done on the two lower levels. The third level deals with the determination of spanwise distributions of global structural characteristics, and the fourth level is concerned with the detailed design of wing elements. The subproblems are identified by the following subscripts: p for performance subproblem, a for aerodynamic subproblem, g for global structural subproblem, and lj for j^{th} local structural subproblem. The developments were carried out to a point where computer implementation is possible. The details of the formulation are given in Apps. A-D.

4.1 PERFORMANCE SUBPROBLEM

A performance subproblem occupies the highest level of the hierarchy, and it drives the whole design process. Its task is to select a combination of performance parameters which maximize the sailplane's cross-country speed. The cross-country speed is defined as the average speed the sailplane achieves over a typical flight segment. It is shown in App. A that the variables entering the calculation of that performance index are: the sailplane gross weight (W), its planform area (S), the coefficients (C_{D0}, C_{D1}, C_{D2}) of a performance curve called the drag polar, and the maximum lift coefficient (C_{Lmax}). These variables will be taken as the performance variables.

$$X_p^T = \{W, S, C_{D0}, C_{D1}, C_{D2}, C_{Lmax}\} \tag{4.1}$$

The design will be subjected to the constraint that the sailplane be capable of a minimum rate of climb in a typical thermal updraft. The variables may be divided into two groups. On the one hand, the weight selected on the basis of performance considerations controls the structural design by determining the amount of structural material available. On the other hand, the remaining variables (referred to as aerodynamic performance variables) control the aerodynamic design by specifying the aerodynamic characteristics required from the wing. This is, of course, a statement that optimization of an airplane entails carefully integrated aerodynamic and structural designs. The control outputs of the performance subproblem are therefore the performance variables themselves.

$$CO_p = X_p \tag{4.2}$$

4.2 AERODYNAMIC SUBPROBLEM

The wing is narrow, unswept, and twisted, and it has a double taper (see Fig. 14). Its airfoil is chosen from a standard catalog which details its parameters. The objective of the aerodynamic subproblem is the selection of

the wing geometry which corresponds to the values of planform area, drag polar coefficients and maximum lift coefficient specified in the performance subproblem (these will be referred to as target aerodynamic performance variables). As detailed in App. B, the aerodynamic variables include the wing semispan (b) and the spanwise position of the taper change (b_b). Also included among the variables are the section chord at the root, break, and tip (c_r, c_b, c_t), the section maximum thickness at the root, break, and tip (t_r, t_b, t_t), and, finally, the wing twist angle at the break and the tip ($\varepsilon_b, \varepsilon_t$). Hence,

$$X_a^T = \{b, b_b, c_r, c_b, c_t, t_r, t_b, t_t, \varepsilon_b, \varepsilon_t\} \tag{4.3}$$

Once these variables are known, it is possible to calculate the resulting wing aerodynamic performance variables. By requiring that these must equal the target values specified in the performance subproblem, we obtain six equality constraints among the components of X_a. Furthermore, one inequality constraint is added which forces the initiation of stall at an inboard wing section. As explained in App. B, the calculation of sailplane aerodynamic performance characteristics takes into account the effect of the Reynolds number, and therefore, the sailplane weight must be known. The vector of control inputs into the aerodynamic

subproblem includes then the target values for the aerodynamic performance characteristics and also the sailplane weight.

$$CI_a = X_p \tag{4.4}$$

The aerodynamic design controls the structural design through two major elements: the wing shape and the aerodynamic loads. The former determines the root bending moment as well as the size of the load bearing part of the section; the latter clearly influences the total distribution of loads. All the aerodynamic variables are required for calculating the wing shape and the aerodynamic loads, therefore

$$CO_a = X_a \tag{4.5}$$

Finally, the vector of response outputs from the aerodynamic subproblem is given by Eq. 3.11.

$$RO_a^T = \left\{ \varepsilon_a^* , \frac{\partial \varepsilon_a^*}{\partial X_p} , \frac{\partial \varepsilon_a^*}{\partial RI_a} , \frac{\partial \varepsilon_a^*}{\partial X_a^o} , \eta_a^* , \frac{\partial \eta_a^*}{\partial X_p} , \frac{\partial \eta_a^*}{\partial RI_a} , \frac{\partial \eta_a^*}{\partial X_a^o} \right\} \tag{4.6}$$

4.3 GLOBAL STRUCTURAL SUBPROBLEM

The sailplane gross weight was specified in the performance subproblem. Since the weight of the other sailplane

components is fixed, the weight allocated to the wing (the target weight) is known. At this level, the wing is modeled as a straight beam. This subproblem objective is the selection of global wing structural characteristics, that is: the spanwise distributions of weight per unit length, bending and torsional stiffnesses. These are written as superpositions of interpolating polynomials, the coefficients of which are taken as the subproblem design variables and are referred to as wing stiffnesses (see App. C),

$$X_g^T = \{w_o,\ldots,w_{n_s},EI_o,\ldots,EI_{n_s},GJ_o,\ldots,GJ_{n_s}\} \qquad (4.7)$$

The compatibility between w_j, EI_j and GJ_j is enforced at the lowest level when the detailed synthesis forces the element designs to match the global level stiffnesses. The design is subjected to one equality constraint that specifies that the total wing weight equals the target weight selected in the performance subproblem. In addition, two global structural inequality constraints are added. The wing bending displacements must be limited, and its torsional divergence speed must exceed a given minimum. The calculation of these constraints requires the wing shape, a number of aerodynamic load parameters and, of course, the target weight. The wing shape (vector H) is a function of

the aerodynamic variables, while the target weight (W) is a function of the performance variables. The aerodynamic load parameters (vector A) are themselves functions of the wing shape and the sailplane weight as shown in App. B. Hence, the vector of control inputs into the subproblem is

$$CI_g^T = \{W(X_p), H^T(X_a), A^T(X_a, W(X_p))\} \tag{4.8}$$

The choice of the wing stiffnesses controls the design of the details of structure, hence

$$CO_g = X_g \tag{4.9}$$

The response outputs from the global structural subproblem are given by Eq. 3.11.

$$RO_g^T = \left\{ \varepsilon_g^*, \frac{\partial \varepsilon_g^*}{\partial W}, \frac{\partial \varepsilon_g^*}{\partial H}, \frac{\partial \varepsilon_g^*}{\partial A}, \frac{\partial \varepsilon_g^*}{\partial RI_g}, \frac{\partial \varepsilon_g^*}{\partial X_g^o}, \right.$$
$$\left. \eta_g^*, \frac{\partial \eta_g^*}{\partial W}, \frac{\partial \eta_g^*}{\partial H}, \frac{\partial \eta_g^*}{\partial A}, \frac{\partial \eta_g^*}{\partial RI_g}, \frac{\partial \eta_g^*}{\partial X_g^o} \right\} \tag{4.10}$$

4.4 LOCAL STRUCTURAL SUBPROBLEMS

The fourth level of the hierarchy is devoted to designing the details of the wing to match the stiffness distributions chosen by the global level subproblem. To achieve this, the wing is divided into n_s constant property elements (see Fig.

22), each of which is designed in a separate subproblem. The design variables describing one element include the cross-sectional dimensions of the spar caps (a, t_c), the thicknesses of the sandwich panels constituting the leading and trailing edge shells (t_f, t_{fs}) and the spar webs (t_w, t_{fw}), and the rib spacing (d). Hence,

$$X_{lj}^T = \{a_j, t_{cj}, t_{sj}, t_{fsj}, t_{wj}, t_{fwj}, d_j\} \tag{4.11}$$

The variables are subjected to three equality constraints insuring that the element stiffnesses equal the target values (vector K_j) specified at the global structural level. Furthermore, it is required that the elements withstand applied end loads (vector M_j) without failure or local buckling. App. D shows that the calculation of the stiffnesses involves the element gross dimensions (vector H_j); these are functions of the aerodynamic variables. Also, the applied end loads (M_j) computation must be based on the vector describing the wing shape (H), a function of the aerodynamic variables, the vector of aerodynamic load parameters (A), a function of aerodynamic variables and weight, and the global structural variables (X_g) to account for the effect of inertia loads. Hence,

$$CI_{lj}^T = \{K_j^T(X_g), H_j^T(X_a), M_j^T[X_g, A(X_a, W(X_p)), H(X_a)]\} \tag{4.12}$$

Equation 3.5 gives the response outputs from subproblem 1j, a lowest level subproblem.

$$RO_{1j}^T = \left\{ \varepsilon_{1j}^*, \frac{\partial \varepsilon_{1j}^*}{\partial K_j}, \frac{\partial \varepsilon_{1j}^*}{\partial H_j}, \frac{\partial \varepsilon_{1j}^*}{\partial M_j}, \eta_{1j}^*, \frac{\partial \eta_{1j}^*}{\partial K_j}, \frac{\partial \eta_{1j}^*}{\partial H_j}, \frac{\partial \eta_{1j}^*}{\partial M_j} \right\} \tag{4.13}$$

4.5 RESPONSE INPUTS TO THE DIFFERENT SUBPROBLEMS

The vector of response inputs into a subproblem above the lowest level is given by Eq. 3.12. For the global structural subproblem, we have

$$RI_g^T = \{\{\varepsilon_{11g}^*\}^T, \ldots, \{\varepsilon_{1n_s g}^*\}^T, \{\eta_{11g}^*\}^T, \ldots, \{\eta_{1n_s g}^*\}^T\}$$

where, for example

$$\{\varepsilon_{1jg}^*\}^T = \left\{ \Psi_{1g} \varepsilon_{1j}^*, \frac{\partial \varepsilon_{1j}^*}{\partial M_j} \frac{\partial M_j}{\partial X_g}, \frac{\partial \varepsilon_{1j}^*}{\partial K_j} \frac{\partial K_j}{\partial X_g} \right\} \tag{4.14}$$

The vector of response inputs into the aerodynamic subproblem is

$$RI_a^T = \{\{\varepsilon_{ga}^*\}^T, \{\varepsilon_{11a}^*\}^T, \ldots, \{\varepsilon_{1n_s a}^*\}^T,$$
$$\{\eta_{ga}^*\}^T, \{\eta_{11a}^*\}^T, \ldots, \{\eta_{1n_s a}^*\}^T\}$$

$$\{\varepsilon^*_{ga}\}^T = \left\{\Psi_{ga}\left(\varepsilon^*_g + \frac{\partial\varepsilon^*_g}{\partial RI_g}\Delta RI_g + \frac{\partial\varepsilon^*_g}{\partial X^o_g}\Delta X^o_g\right),\right.$$

$$\left.\frac{\partial\varepsilon^*_g}{\partial A}\frac{\partial A}{\partial X_a}\ ,\ \frac{\partial\varepsilon^*_g}{\partial S}\frac{\partial S}{\partial X_a}\right\}$$

and

$$\{\varepsilon^*_{lja}\}^T = \left\{\Psi_{la}\varepsilon^*_{lj}\ ,\ \frac{\partial\varepsilon^*_{lj}}{\partial M_j}\frac{\partial M_j}{\partial A}\frac{\partial A}{\partial X_a}\ ,\ \frac{\partial\varepsilon^*_{lj}}{\partial M_j}\frac{\partial M_j}{\partial H}\frac{\partial H}{\partial X_a}\ ,\ \frac{\partial\varepsilon^*_{lj}}{\partial H_j}\frac{\partial H_j}{\partial X_a}\right\}$$

(4.15)

Finally, the response inputs into the performance subproblem are

$$RI^T_p = \{\{\varepsilon^*_{ap}\}^T, \{\varepsilon^*_{gp}\}^T, \{\varepsilon^*_{11p}\}^T, \ldots, \{\varepsilon^*_{ln_sp}\}^T,$$

$$\{\eta^*_{ap}\}^T, \{\eta^*_{gp}\}^T, \{\eta^*_{11p}\}^T, \ldots, \{\eta^*_{ln_sp}\}^T\}$$

$$\{\varepsilon^*_{ap}\}^T = \left\{\varepsilon^*_a + \frac{\partial\varepsilon^*_a}{\partial RI_a}\Delta RI_a + \frac{\partial\varepsilon^*_a}{\partial X^o_a}\Delta X^o_a\ ,\ \frac{\partial\varepsilon^*_a}{\partial W}\frac{\partial W}{\partial X_p}\right\}$$

Also

$$\{\varepsilon^*_{gp}\}^T = \left\{\Psi_{gp}\left(\varepsilon^*_g + \frac{\partial\varepsilon^*_g}{\partial RI_g}\Delta RI_g + \frac{\partial\varepsilon^*_g}{\partial X^o_g}\Delta X^o_g\right),\right.$$

$$\left.\frac{\partial\varepsilon^*_g}{\partial A}\frac{\partial A}{\partial X_p}\ ,\ \frac{\partial\varepsilon^*_g}{\partial W}\frac{\partial W}{\partial X_p}\right\}$$

and, finally

$$\{\varepsilon^*_{ljp}\}^T = \left\{\Psi_{lp}\varepsilon^*_{lj}\ ,\ \frac{\partial\varepsilon^*_{lj}}{\partial M_j}\frac{\partial M_j}{\partial A}\frac{\partial A}{\partial W}\frac{\partial W}{\partial X_p}\right\} \tag{4.16}$$

According to Eqs. 3.4.d and 3.10.d., we must further require

$$\Psi_{lg}+\Psi_{la}+\Psi_{lp} = 1$$

$$\Psi_{ga}+\Psi_{gp} = 1 \tag{4.17}$$

Note that we have specified $\Psi_{ap} = 1$ (Eq. 4.16) as there is only one subproblem controlling the aerodynamic subproblem. Furthermore, we assume the participation of each subproblem into the local structural subproblem designs to be equal, for example

$$\Psi_{l1g} = \Psi_{l2g} = \ldots = \Psi_{ln_sg} = \Psi_{lg}$$

The coefficients Ψ_{la} and Ψ_{lp} are defined similarly.

3.1 FINAL REMARK

This decomposition conforms to the general form defined in Chap. III; in particular, it does not contain reverse or network controls. This is because the following effects are neglected (see Apps. B and C): i) effect of wing flexibility on aerodynamic characteristics, ii) effect of changes in wing section elastic axis position on torsional divergence speed, and, iii) effect of changes in wing section center of gravity position on inertia-force-induced torque. To account for i), one must include reverse controls between the global structural and aerodynamic subproblems. Effects ii) and iii) require reverse controls between local structural and global structural subproblems.

Chapter V

TWO-LEVEL MINIMUM WEIGHT WING DESIGN

A complete numerical application of the algorithm presented in Chap. III is appropriate, but it was decided that computer implementation of the four-level high-performance sailplane design problem formulated in Chap. IV and Apps. A-D would be a task well beyond the scope of this research. A more limited and manageable but still significant application of the algorithm is the minimum weight design of the sailplane wing. This corresponds to the two lower levels of the hierarchy described by Fig. 4, except that the objective function of the overall problem, and therefore of the top level of the decomposed problem, is now the total wing weight. The global structural subproblem now has the form of Problem 3.13. The objective function ($F(X_{11}) = F(X_g)$) is the weight, and there are three inequality constraints ($g_{11}(X_{11}) = g_g(X_g)$); two set upper and lower limits on the wing tip displacement, one provides a lower bound for the wing torsional divergence speed (see App. C). The weight and stiffness distributions are Lagrangian interpolations defined on five equal length intervals ($n_s = 5$), thereby requiring six coefficients per distribution, for a total of eighteen global level variables (X_g). The five

local structural subproblems are formulated as in Problem 3.1. Each one is described by seven design variables (X_{1j}). The vector of constraints ($g_{1j}(X_{1j})$) contains twelve constraints on stresses, five on buckling (only the buckling of the sandwich panels is considered, that of the spar caps is ignored, see App. D). Also three constraints are included which limit the ratios of spar cap width to element chord and of sandwich panel total thickness to face sheet thickness (see App. E). Finally, three equality constraints ($e_{1j}(X_{1j})$) require that the element weight per unit length, bending and torsional stiffnesses equal the target values specified at the global structural level (see App. D).

The multilevel decomposition for this two-level problem corresponds to the two lower levels of the hierarchy of Fig. 4 except that the definition of the wing planform is now assumed fixed so that the vectors of wing shape (H) and element gross shape (H_j) are constant throughout the optimization. Furthermore, the effect of the sailplane weight ($W(X_p)$) on the aerodynamic parameters is ignored so that vector A is constant as well. The control inputs into local structural subproblem 1j (CI_{1j}) are then the vectors of target stiffnesses (K_j) and end loads (M_j). The response outputs from that subproblem are given by Eq. 4.13, without the sensitivity derivative with respect to H_j. The response

inputs into the global structural subproblem are given by Eq. 4.14 where the participation factor Ψ_{lg} is set to unity as the global structural subproblem is the only one that controls the local structural level subproblems. The numerical values of the parameters needed for the calculations of Apps. A-D are given in App. E.

5.1 TEST DESCRIPTION

Two test cases will be described. The first starts from the feasible domain, all the constraints being satisfied with ample margins. The second starts from the infeasible domain. It is such that, at the global level, the tip displacement exceeds its upper limit by 130%, while the divergence dynamic pressure is 10% below its lower limit. With the exception of the tip element, all the wing elements have a large proportion of stress and buckling constraints violated, resulting in measures of inequality constraint violation (ε_{lj}) ranging from -3.0 to -6.0. In both cases, an initial design was given for each wing element and the stiffnesses of these elements were calculated. Trial and error was then used to determine the global level stiffnesses whose averages would yield back the local level stiffnesses just calculated, in accordance with Eq. C.23.

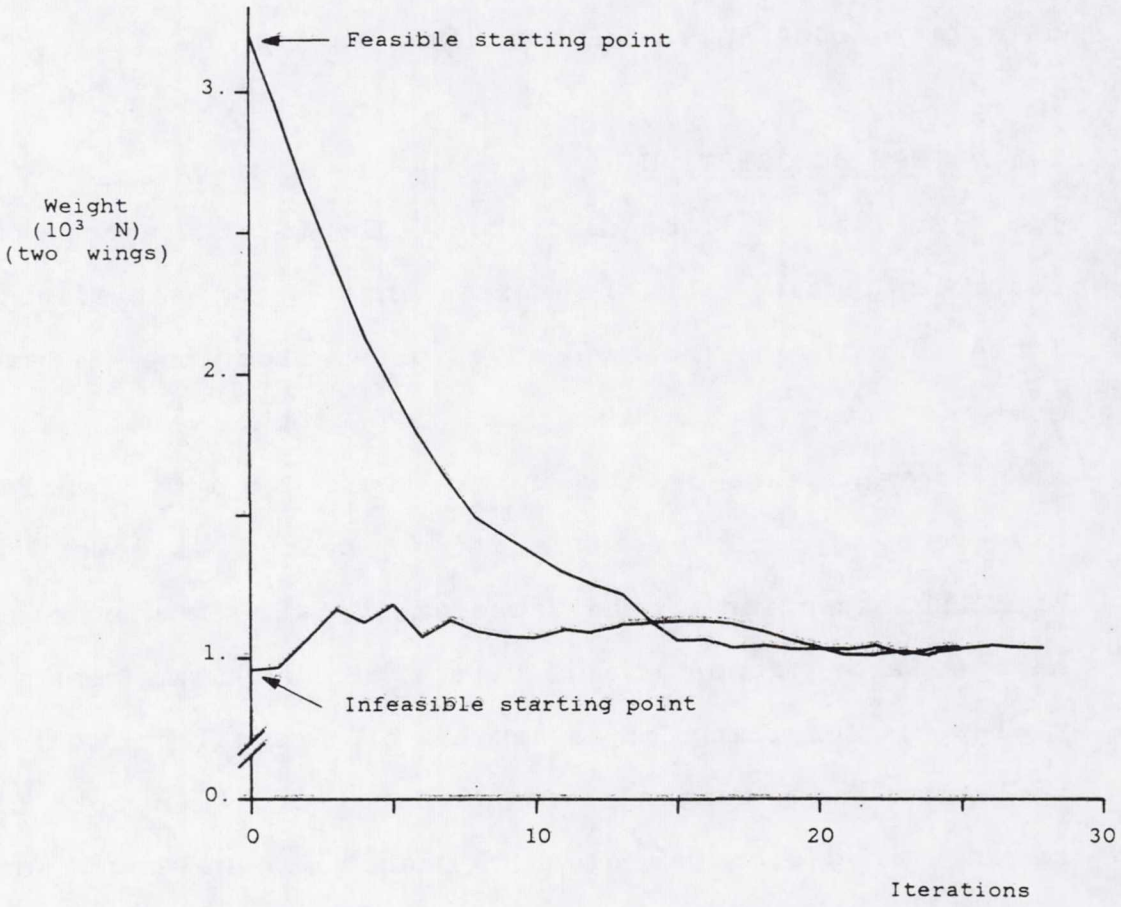

Figure 5: Two-level wing design, weight convergence history.

Figure 5 gives the convergence history for the test cases. Both optimizations took 28 iterations[3] to produce a feasible design with a stabilized weight of 1030 N. (for two wings), with the differences in the final values being less than 1%. The design started in the feasible domain achieves a weight reduction of 68%. That begun in the infeasible region gains barely 6% of weight as it redistributes the structural material in an attempt to satisfy the violated constraints. Both final solutions have the divergence constraint critical, while the upper displacement constraint is satisfied with a margin of about 25%. The designs of wing elements 1 (inboard), 2 and 4 are critical or near critical ($-.01 \leq \varepsilon \leq .07$), while those of elements 3 and 5 (outboard) are not ($\varepsilon > .10$). The active constraints for the critical elements are: i) the stress constraints in the carbon fiber spar caps, and primarily in the lower one, ii) the shear buckling constraint for the upper and lower sandwich panels of the trailing edge shell and the rear spar web, iii) the constraint setting an upper limit on the spar cap width to section chord ratio (a/c). Furthermore, for each element, the rib spacing d is against its upper limit,

---

[3] Unless otherwise specified, one iteration corresponds to one complete optimization of the overall problem. It entails one optimization of the global structural subproblem, one optimization and one sensitivity analysis for each local structural subproblem.

while the spar web face sheet thickness is against its lower limit. The parameter b in the local level subproblem objective function (Problem 3.3) was set to 100. At the global level, the objective function parameters (c and d, see Problem 3.14) were chosen so that, at the beginning of each global level optimization, the penalty term in the objective function ($-c\varepsilon_{11}+d\eta_{11}$) was ten times the weight ($F(X_{11})$). As a consequence, all equality constraints were satisfied, after most system iteration, to within 1%, or less ($\eta \leq .01$).

5.2 COMPARISON OF GLOBAL AND LOCAL DESIGNS

Figure 6 shows the global and target local weights for the initial and final designs of both tests. The same information is given for the bending stiffnesses on Fig. 7. On these figures, the straight-line segments join stiffnesses corresponding to the same (initial/final) design; they do not represent the global level stiffness distributions, as these are obtained with Lagrangian interpolations and have no slope discontinuities. The figures show good agreement between the final target values (open symbols) toward the wing root, and the agreement worsens somewhat toward the wing tip. The variability is even more marked with the final global level variables

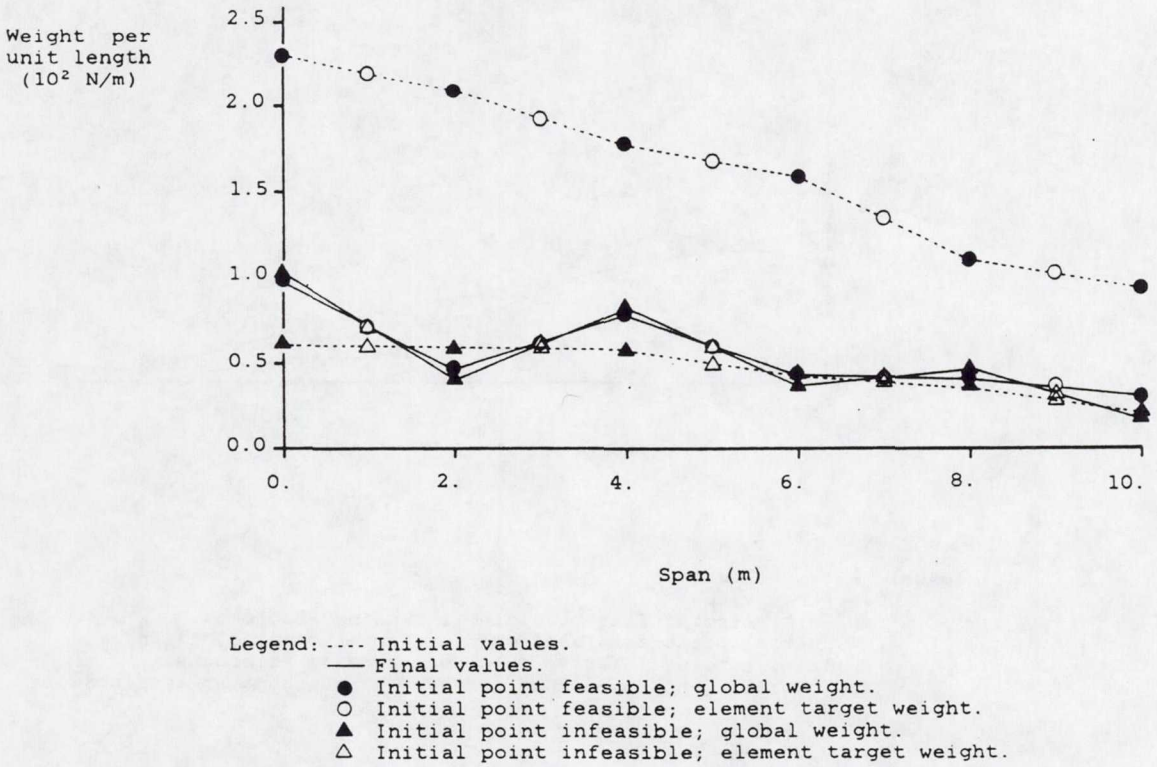

Figure 6: Two-level wing design, comparison of initial and final global and target weights per unit length.

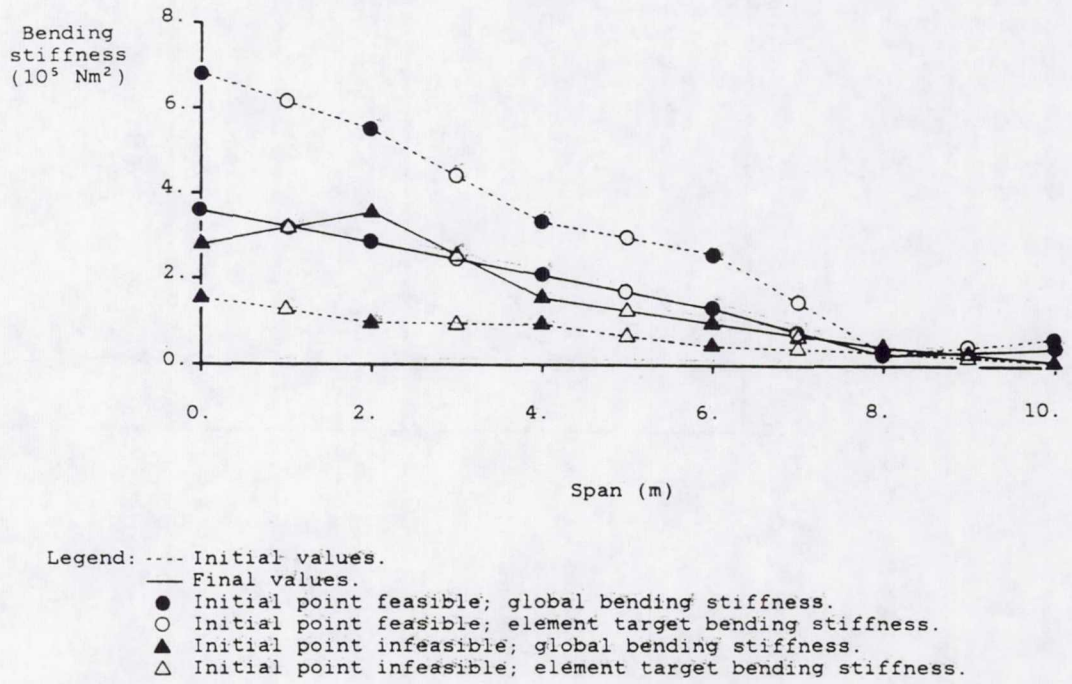

Figure 7: Two-level wing design, comparison of initial and final global and target bending stiffnesses.

(solid symbols). This is probably evidence that the optimum is fairly "flat". In other words, the global level design may be perturbed without drastically changing the overall design quality measured in terms of minimum objective function and constraint satisfaction. Three factors may be contributing to that situation. First, due to the relationship between the number of coefficients in the global level wing model (6 per distribution of weight per unit length, bending and torsional stiffnesses) and the number of wing elements (5), there is an infinite number of global level designs which yield the same local level target values. Second, it may be proven algebraically that all the combinations of global level weights which result in the same local level target weights actually result in the same total wing weight (this can be shown easily for Lagrangian interpolations based on an odd number of equal length intervals). Third, all the global level constraints (in the untransformed subproblem) are integral constraints (see App. C). The integration process should be expected to smooth out the effect of variations in global level stiffness distributions.

The distributions of stiffnesses are wavy; this must be related to the order of the interpolating polynomials used to model them. These polynomials are of the fifth order in

the present model. It would be interesting to model the wing weight and stiffness distributions with lower-order polynomials; this should reduce the wavyness while necessitating fewer variables in the global structural subproblem and making the global and local structural models independent. This would, however, require a new definition of the relationship between the global level weights and stiffnesses and the corresponding local level target values (Eq. C.23).

Table 1 compares numerically the initial and final designs for the inboard and outboard elements. As expected, the trend observed among the target stiffnesses is repeated at the lower level; the two designs obtained for the inboard wing element are very close, while those for the outboard element differ substantially. This general trend can be intuitively understood as the overall wing response must be more sensitive to the design of the wing root which carries the total wing load than to that of the wing tip which is almost unloaded.

5.3 QUALITY OF SENSITIVITY-DERIVATIVE-BASED EXTRAPOLATIONS

Figure 8 depicts a typical evolution of optimum measures of inequality and equality constraint violation (ε_{1j} and η_{1j}). The example corresponds to the design of the second wing

TABLE 1

Two-level wing design, comparison of initial and final designs for the inboard and outboard elements.

Wing Element		Inboard				Outboard			
Initial Point		Feasible		Infeasible		Feasible		Infeasible	
Design		Initial	Final	Initial	Final	Initial	Final	Initial	Final
a^*	$x10^{-2}$	3.00	9.01	3.00	9.22	3.00	3.44	3.00	1.28
t_c	$x10^{-3}$	20.00	2.48	3.00	2.37	20.00	4.38	3.00	11.10
t_s	$x10^{-3}$	10.00	5.98	3.00	5.96	10.00	3.92	3.00	3.91
t_{fs}	$x10^{-4}$	20.00	5.13	5.00	5.15	20.00	7.13	5.00	5.22
t_w	$x10^{-3}$	7.00	9.57	3.50	9.50	7.00	2.76	3.50	7.61
t_{fw}	$x10^{-4}$	10.00	5.00**	5.00	5.00**	10.00	5.00**	5.00	5.00**
d	$x10^{-1}$	2.50	5.00**	5.00	5.00**	2.50	5.00**	5.00	5.00**

* All dimensions are in meters.

** Variables against side constraints.

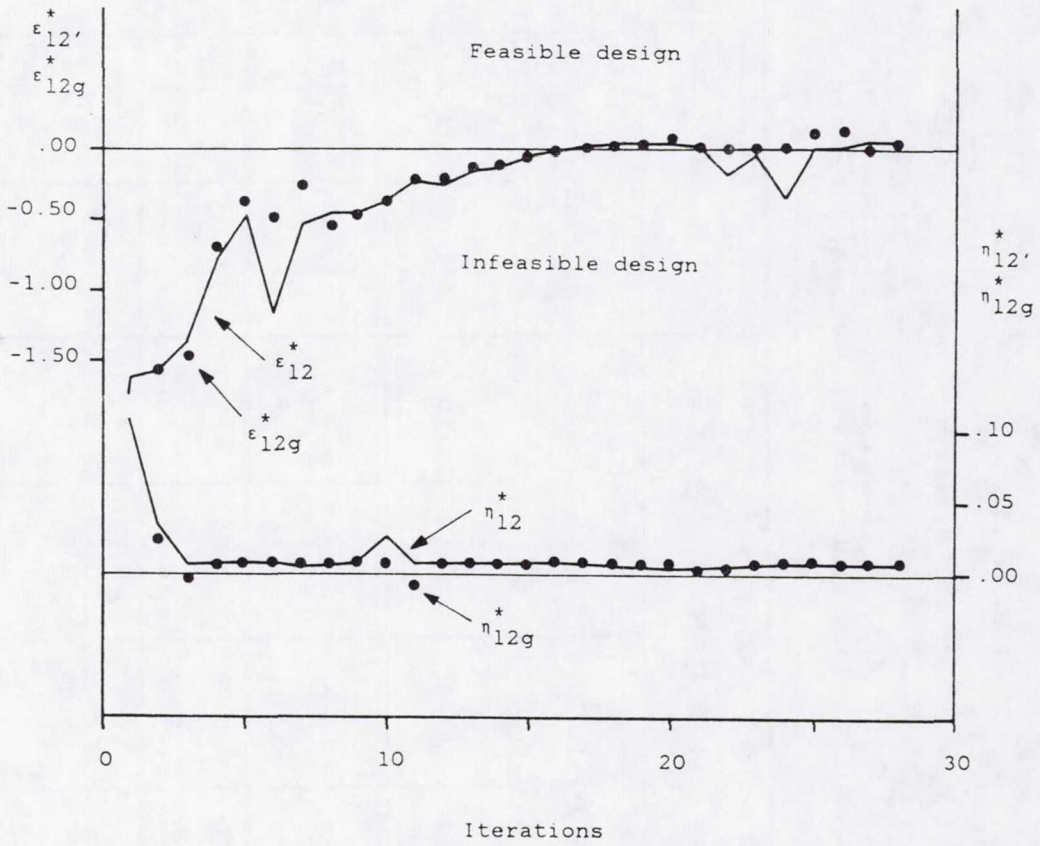

Figure 8: Two-level wing design, typical history of measures of constraint violation. Wing element 2, infeasible initial design.

element when optimization is started from the infeasible domain. A short digression is necessary to explain the physical meaning of variables ε and η. For an infeasible design, ε measures the violation of the most violated constraint; for a feasible design it gives an indication of the margin associated with the constraint which is the closest to being critical. For example, if we refer to a design problem involving a single inequality constraint on displacement u ($g(X) = u(X)/u_{max}-1 \leq 0$), a value of -1.5 for ε indicates that displacement u exceeds its maximum value u_{max} by 150%, while a value of 0.5 means that the displacement is only 50% of its upper limit. Variable η measures the violation of the most violated equality constraint of a subproblem. Considering a subproblem subjected to the requirement that a function f of its design variables remain equal to a target value f_t ($e(X) = f(X)/f_t-1 = 0$), a value of .25 for η means that f(X) is 25% away from f_t.

Returning to Fig. 8, the solid lines give the evolution of ε^*_{12} and η^*_{12}. They describe the evolution of these optimum quantities throughout the design process, each value being obtained at the end of a complete optimization of subproblem 12. The dots correspond to the estimates of these as generated on the basis of optimum sensitivity

analysis in the global structural subproblem. They are, respectively, $\varepsilon^*_{\mu\nu 11} = \varepsilon^*_{12g}$ and $\eta^*_{\mu\nu 11} = \eta^*_{12g}$ in the notation of Chap. III (see Problem 3.13). The interpretation of the graph may be aided by an example. At the end of iteration 3, ε^*_{12} is -1.35; the global structural subproblem improves its design at the beginning of iteration 4 and predicts that this will result in a change to -.68 while ε^*_{12} actually is reduced to -.78 when local structural subproblem 12 is optimized.

From Fig. 8, one can observe that the algorithm effectively reduces the violation of inequality constraints while keeping the violation of equality constraints within 1%, most of the time. The success is a result of the generally good prediction of these measures by the global structural subproblem. Occasionally, however, the predictions are poor, as for iterations 6, 22 and 24 for ε^*_{12}, and 10 for η^*_{12}. The bad predictions can be correlated with changes in the set of constraints determining the successive solutions to subproblem 12; as discussed in Sec. 2.4, these changes do introduce discontinuities in the sensitivity derivatives. This slows down the convergence process, but the algorithm appears robust enough to overcome the difficulty; this observation is consistent with the results of Ref. 21. It must be noted

that the occurrence of active constraint switching does not always produce discontinuities as significant as those observed here. As a matter of fact, about 60% of the optimizations included in the example presented end with changes in the active constraint set, but only 15% seem really affected by the change.

5.4 ADDITIONAL COMMENTS

As was pointed out in Chap. III, limits must be set on the global level variables to insure that the sensitivity-derivative-based linear extrapolations of the local level measures of constraint violation are not used beyond their range of validity. Upper and lower bounds could be estimated for these limits, using Eqs. 2.25 and 2.16. However, it was elected not to do so in this study. The two test cases presented here were started with move limits allowing changes of ± 10% in the global level variables at each iteration of the overall problem (δ = .10 in Eq. 3.13.f). As the process neared the optimum solution, these limits were reduced as discussed in Sec. 3.6. For example, in the test case started from the infeasible starting point, the move limits were kept at 10% during the first 5 iterations, 5% for iterations 6-21, 2.5% for iterations 22-25, and finally, 1% for the last three iterations. It

must be pointed out that no attempt was made to refine the bound selection strategy nor to identify the widest usable bounds for the first steps of the process. Doing so could probably improve the convergence characteristics of the algorithm.

The impact of active constraint switching on the rate of convergence is related to the specifics of the solution of the individual subproblems. This approach tracks the most violated equality and inequality constraints. Therefore, a relatively large number of changes in the active constraint set may be expected. By contrast, the approach of Ref. 21 combines most constraints (except upper and lower bounds and move limits) in a penalty function which is continuous in the constraints. That approach should not result in so many changes. The question of which approach provides the best rate of convergence may be answered only by using both approaches to solve the same design problem.

Early tests with this algorithm revealed a situation that deserves comment. In some circumstances, the subproblem solution may not be unique. An example of this is depicted on Fig. 9 where the subproblem involves one equality constraint that is parallel to one of the sides of the domain defined by the inequality constraints. Assuming that the equality constraint is satisfied at the outset of the

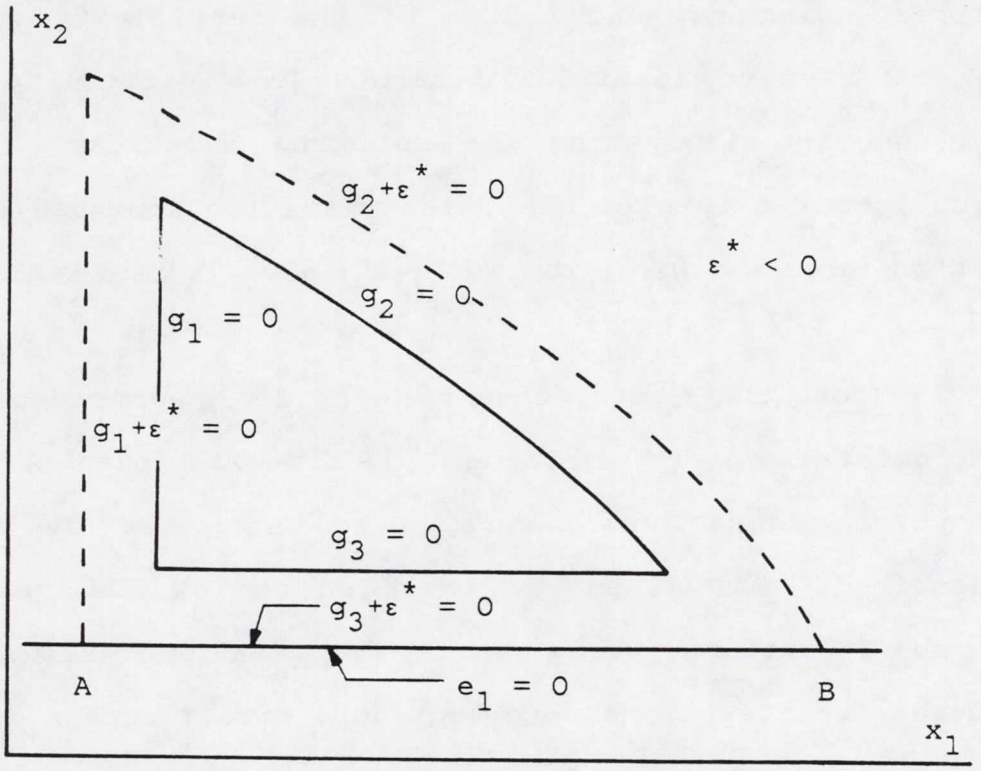

Figure 9: Situation where a subproblem has an infinite number of solutions.

optimization, we see that each point of segment AB is a solution. This situation does not cause difficulties during optimization of the subproblem. However, it leads to singular sensitivity matrices. This can be shown on the example. As none of the subproblem objective function ($e^{-\varepsilon}+b\eta$) or active constraints depend on variables x_2, the corresponding row and column of the sensitivity equations (Eq. 2.14) are identically zero. This difficulty may be overcome by eliminating the null row and column from the equation. In this problem, the situation appeared when the design process was started with all variables at lower bounds.

To conclude this chapter, a few words about the implementation are in order. A special purpose FORTRAN computer program was developed to carry out the examples described. It was run in batch on an IBM 3081 processor. Three iterations were run at a time and results from successive iterations were kept on a direct access data file so as to provide the capability for restarting the optimization from any iteration. Individual subproblems were optimized with the usable-feasible direction algorithm implemented in subroutine CONMIN (Ref. 28). For the two examples discussed, convergence was achieved in 28 iterations; a typical iteration took 30-35 CPU seconds. Of

that time, about 60% was devoted to optimizing the global structural subproblem, while the remaining 40% was split evenly between optimization and sensitivity analysis of the 5 local level subproblems. During one iteration of the overall problem, optimization of the global level subproblem took an average of 18 iterations to converge. Each global level iteration required about 21 function evaluations (weight, wing tip displacement and wing divergence dynamic pressure). At the local level, a wing element design took an average of 38 iterations. Each local level iteration required about 11 function evaluations (stiffnesses, stresses and buckling constraints), while each local level sensitivity analysis required 531 function evaluations. The numbers of function evaluations reported above include those required for derivative calculations. For reasons of convenience, all derivatives for optimization were obtained by forward difference formulae; those for sensitivity analysis were found by central difference formulae.

Chapter VI

DISCUSSION AND RECOMMENDATIONS

This work centers on a multilevel decomposition approach to the optimization of large problems. The starting point is Sobieski's original idea (Ref. 20) of using optimum sensitivity analysis to account for the coupling between the different subproblems of a decomposed problem. The objective of this research was the investigation of the applicability of Sobieski's algorithm to the design of complex engineering systems. The three major contributions of this dissertation are: i) a presentation of an extended version of the algorithm, ii) an illustration of the applicability of the algorithm to a realistic multidisciplinary design problem, and, iii) an application of the proposed algorithm. This chapter summarizes these developments and offers some recommendations.

6.1 ON THE PROPOSED ALGORITHM

The algorithm we developed is very general; in contrast with previously introduced multilevel approaches, it does not make restrictive assumptions as to the mathematical nature of the problem considered nor is it developed for a specific class of physical problems. Rather, it is devised for the

optimization of large systems which may be decomposed into subsystems.

We hypothesize an existing decomposition of the overall problem into smaller subproblems. It is assumed that the decomposition is multilevel and hierarchical; that is, the subproblems are organized on levels corresponding to progressively more refined models of the system designed and, furthermore, the subproblems on a given level exert control on the design of the subproblems on lower levels. The controls must be defined with the hierarchy. It is finally assumed that the subproblems entail finding a design that satisfies a set of equality and inequality constraints.

An iterative procedure is then used where each subproblem is designed separately by minimization of a measure of constraint violation, for fixed values of the controls imposed by higher level subproblems. Sensitivity derivatives of the resulting subproblem solution are generated which constitute the response of that subproblem to the higher level subproblem controls. Each subproblem is designed with additional constraints which require improvement of the lower level subproblem responses. This algorithm specifically allows for the extreme situation where a subproblem controls each lower level subproblem, and, as a consequence, each subproblem responds to each

higher level subproblem. The highest level of the hierarchy is occupied by a single subproblem which drives the whole design process. Its task is the optimization of the overall problem objective with respect to variables which describe the system in very general terms. This subproblem also manipulates its controls to improve the lower level subproblem designs.

The specifics of the solution of the individual subproblems differ from those of Ref. 21, where equality constraints are handled analytically by elimination of dependent variables, while the independent variables are found by minimization of a penalty function. The present approach introduces two additional variables which measure i) the violation of the most violated inequality constraint (or the margin of the constraints which are the closest to being critical), and ii) the violation of the most violated equality constraint. These variables are then combined in a cumulative measure of violation which is minimized to find the "best" subproblem design. The advantage of this approach is that it is more general in that it handles equality constraints numerically. Furthermore, it is compatible with the use of a usable-feasible direction algorithm.

C-2

This discussion shows that when the decomposition contains more than two levels, it becomes necessary to consider the sensitivity of a given subproblem above the lowest level not only to the control inputs into that subproblem, as shown in Ref. 20, but also to the response inputs into that subproblem, as well as to the initial design for that subproblem. Of course, it may be argued that ignoring such effects will only slow down the convergence of the overall process while resulting in fewer sensitivity analyses and in an easier implementation. This question must be resolved by testing a simple three-level problem for which a solution is known or easy to generate.

All that is required before using this algorithm is a choice of the decomposition of the overall problem into subproblems, and of the controls between the subproblems. These choices must be made on the basis of practical experience accumulated with the type of systems considered. The decomposition must correspond to the general description given above. Intuitively, the number of controls should be kept to a minimum; the decision of whether to include a specific control or not could be helped by analysis of the sensitivity of the optimum of the subproblem being controlled to the control considered.

6.2 ON THE APPLICABILITY OF THE ALGORITHM

The applicability of the algorithm was illustrated by formulation of a realistic multidisciplinary design problem: the simultaneous aerodynamic and structural design of sailplane wing for maximum cross-country speed. A multilevel decomposition conforming to the desired general form was developed. The highest level is occupied by a subproblem which selects the sailplane performance parameters that maximize the cross-country speed. Then follows an aerodynamic subproblem which determines the wing shape that produces the aerodynamic performance parameters selected at the level above and meets a stall-related constraint. On the third level, a global structural subproblem chooses the distributions of wing weight and stiffnesses which satisfy constraints on wing tip displacement and divergence dynamic pressure for a total weight equal to that selected in the performance subproblem. Finally, at the lowest level, a number of structural subproblems are concerned with finding wing element designs which yield the stiffnesses specified by the global structural subproblem while satisfying stress and buckling constraints.

The controls of this decomposition were chosen by considering the rigorous functional dependence of a given

subproblem optimum on the variables of the higher level subproblems. As a consequence, the weight, a performance variable, controls all subproblems below the highest level; likewise, the wing shape vector, a combination of aerodynamic variables, controls the two structural levels. This underscores the need for an algorithm that allows each subproblem to control each lower level subproblem.

The formulation of this design problem was carried to a point where computer implementation is possible. Its completion can prove to be a very instructive exercise, especially as the initial theoretical developments related to the proposed algorithm show that handling problems with more than two levels may require calculations that were not necessary for two-level problems.

6.3 ON THE EXAMPLE PROBLEM

The proposed algorithm has been applied to the two-level minimum weight design of the sailplane wing. The tests show that it is effective at producing low weight feasible designs whether optimization is started from the feasible domain or the infeasible one.

The numerical experiments conducted confirm that as optimization progresses, changes occur in the sets of constraints defining the optima of the different

subproblems. These changes occasionally cause discontinuities in the sensitivity derivatives, and these may even result in oscillations about the optimum solution. Although the algorithm successfully overcomes these discontinuities, they still result in delayed convergence. The susceptibility of a particular algorithm to active constraint switching depends on the specific approach used to optimize the individual subproblems. This point should be investigated carefully prior to undertaking any large-scale implementation of the algorithm. A good basis for comparison could be obtained by solving a small two-level problem using all candidate subproblem formulations.

REFERENCES

1. Lasdon, L. S., Optimization Theory for Large Systems, Macmillan Series in Operations Research, MacMillan Publishing Co., Inc, N. Y., 1970.

2. Ho, J. K., "Optimal Design of Multi-Stage Structures: a Nested Decomposition Approach," Technical Report 74-2, Systems Optimization Laboratory, Department of Operations Research, Stanford University, Stanford, California, March 1974.

3. Woo, T.-H., "Decomposition in Structural Synthesis," Ph.D. Dissertation, University of California, Los Angeles, California, 1977.

4. Tsach, U., "Optimum Design of Trusses Subject to Vulnerability Constraints," M. S. Thesis, Illinois Institute of Technology, Chicago, Illinois, 1978.

5. Chang, C., "Minimum Weight Design of Trusses Subject to Damage Tolerance Constraints," M. S. Thesis, Illinois Institute of Technology, Chicago, Illinois, 1981.

6. Bellman, R., Dynamic Programming, Princeton University Press, Princeton, N. J., 1957.

7. Kirsch, U., Optimum Structural Design, McGraw-Hill Book Co., N. Y., 1981.

8. Twisdale, L. A., and Katchaturian, N., "Multistage Optimization of Structures," Journal of the Structural Division, ASCE, ST5, May 1975, pp. 1005-1020.

9. Mesarovic, M. D., Macko, D., and Takahara, Y., Theory of Hierarchical, Multilevel, Systems, Academic Press, N. Y., 1970.

10. Kirsch, U., "Multilevel Approach to Optimum Structural Design," Journal of the Structural Division, ASCE, ST4, April 1975, pp. 957-974.

11. Kirsch, U., and Moses, F., "Decomposition in Optimum Structural Design," Journal of the Structural Division, ASCE, ST1, January 1979, pp. 85-100.

12. Ginsburg, S., and Kirsch, U., "Multilevel Optimization of Arrays of Protective Structures," Presented at the International Symposium on Optimal Structural Design, 11th ONR Naval Structural Mechanics Symposium, held at the University of Arizona, Tucson, Arizona, October 19-22 1981.

13. Giles, G. L., "Procedure for Automating Aircraft Wing Structural Design," Journal of the Structural Division, ASCE, Vol 97, January 1971, pp. 97-113.

14. Sobieszczanski-Sobieski, J., "An Integrated Computer Procedure for Sizing Composite Airframe Structures," NASA TP 1300, February 1979.

15. Kirsch, U., Reiss, M., and Shamir, U., "Optimum Design by Partitioning into Substructures," Journal of the Structural Division, ASCE, ST1, January 1972, pp. 249-267.

16. Sobiezczanski-Sobieski, J., and Loendorf, D., "A Mixed Optimization Method for Automated Design of Fuselage Structures," Journal of Aircraft, Vol. 9, December 1972, pp. 805-811.

17. Hughes, O. F., Mistree, F., and Zanic, V., "A Practical Method for the Rational Design of Ship Structures," Journal of Ship Research, Vol. 24, No. 2, June 1980, pp. 101-113.

18. Schmit, L. A., Jr., and Ramanatham, R. K., "Multilevel Approach to Minimum Weight Design Including Buckling Constraints," AIAA Journal, Vol. 16, No. 2, February 1978, pp. 97-104.

19. Schmit, L. A., Jr., and Mehrinfar, M., "Multilevel Optimum Design of Structures with Fiber-Composite Stiffened-Panel Components," AIAA Paper 80-0723, presented at the 21st AIAA/ASME/ASCE/AHS Structures, Structural Dynamics and Materials Conference, May 12-14 1980, Seattle, Washington.

20. Sobiezczanski-Sobieski, J., "A Linear Decomposition Method for Large Optimization Problems - Blueprint for Development," NASA TM 83248, February 1982.

21. Sobiezczanski-Sobieski, J., James, B., and Dovi, A., "Structural Optimization by Multilevel Decomposition," AIAA Paper No. 83-0832-CP, presented at the 24th AIAA/ASME/ASCE/AHS Structures, Structural Dynamics and Materials Conference, Lake Tahoe, Nevada, May 2-4 1983.

22. Sobiezczanski-Sobieski, J., Barthelemy, J.-F., and Riley, K. M., "Sensitivity of Optimum Solutions to Problem Parameters," AIAA Journal, Vol. 20, No. 9, September 1982, pp. 1291-1299.

23. Schmit, L. A., Jr., and Chang, K. J., "Optimum Design Sensitivity Based on Approximation Concepts and Dual Methods," Proceedings of the AIAA/ASME/ASCE/AHS 23rd Structures, Structural Dynamics and Materials Conference, New-Orleans, La., may 10-12 1982, AIAA Paper No. 82-0713-CP.

24. Haftka, R. T., "Damage Tolerant Design Using Collapse Technique," Proceedings of the AIAA/ASME/ASCE/AHS 23rd Structures, Structural Dynamics and Materials Conference, New-Orleans, La., may 10-12 1982, AIAA Paper No. 82-0718.

25. Barthelemy, J.-F., and Sobiezczanski-Sobieski, J., "On Optimum Sensitivity Derivatives of Objective Functions in Nonlinear Programming," to appear in the AIAA Journal in May or June 1983.

26. Barthelemy, J.-F., and Sobiezczanski-Sobieski, J., "Extrapolation of Optimum Design Based on Sensitivity Derivatives," AIAA Journal, Vol. 21, No. 5, May 1983, pp. 797-799.

27. Pope, G. G., "Sequences of Linear Programs," Structural Design Applications of Mathematical Programming Techniques, AGARDograph No. 149, 1971, pp. 48-54.

28. Vanderplaats, G. N., "CONMIN - a FORTRAN Program for Constrained Function Minimization: User's Manual," NASA TM X-62,282, August 1973.

29. Conway, C., The Joy of Soaring - Manual of Instruction, The Soaring Society of America, Inc., Los Angeles, California, 1970.

30. Temmes, K., "Finding the Best Speed for Cross-Country Soaring," Soaring, January-February 1950, pp. 6-8.

31. Carmichael, B. H., "What Price Performance," Soaring, May-June 1954, pp. 6-10.

32. Helwig, G., "Wing Shape Optimization for Maximum Cross-Country Speed, with Mathematical Programming," Science and Technology of Low Speed and Motorless Flight, NASA CP 2085, Part. 1, 1979, pp. 203-217.

33. MacReady, P. B., Jr., "Optimum Airspeed Selector," Soaring, March-April 1954, pp. 8-9.

34. McMasters, J. H., "An Introduction to Geometric Programming and its Application to Sailplane Design," Motorless Flight Research, 1972, NASA CR-2315, November 1973, pp. 119-146.

35. Chen, M. K., and McMasters, J. H., "From Paleoaeronautics to Altostratus - A Technical History of Soaring," AIAA paper 81-1611, presented at the AIAA Aircraft Systems and Technology Conference, August 11-13 1981, Dayton, Ohio.

36. Loftin, K. L., Jr., and Smith, H. A., "Aerodynamic Characteristics of 15 NACA Airfoil Sections at Seven Reynolds Numbers from 0.7×10^6 to 9.0×10^6," NACA TN-1945, Oct. 1949.

37. Bisplinghoff, R. L., Ashley, H., and Halfman, R. L., Aeroelasticity, Addison-Wesley Pub. Co., Inc., 1955, Chapters 5 and 9.

38. Peery, D. J., Aircraft Structures, McGraw-Hill Book Company, 1950, Chapter 9.

39. Torenbeek, E., Synthesis of Subsonic Airplane Design, Delft University Press, 1976, Chapter 9, Appendices A, E, F.

40. Federal Aviation Agency, Basic Glider Criteria Handbook, Flight Standards Service, Washington, D. C., 1961.

41. Beyer, W. H., Ed., CRC Standard Mathematical Tables, 25th Edition, CRC Press, Inc., West Palm Beach Florida, 1978.

42. Muser, D., "Advanced Composites in Sailplane Structures: Application and Mechanical Properties," Science and Technology of Low Speed and Motorless Flight, NASA CP-2085, Part 2, 1979, pp. 467-483.

43. Thielemann, W. F., "Experience with Composites as Obtained from Gliders," Impact of Composite Materials on Aerospace Vehicles and Propulsion Systems, AGARD CP112, May 1973, pp. 11-1-7.

44. Bruhn, E. F., Analysis and Design of Flight Vehicle Structures, Tri-State Offset Company, 1973.

45. Jones, R. M., Mechanics of Composite Materials, Scripta Book Company, Washington, D. C., 1975.

46. U. S. Munitions Board Aircraft Committee, Sandwich Construction for Aircraft, Part II, Materials Properties and Design Criteria, ANC23, 1951.

47. Lekhnitskii, S. G., Anisotropic Plates, Gordon and Breach Science Publishers, New York, 1968.

Appendix A

PERFORMANCE SUBPROBLEM

The design of an airplane is always driven by the desire to obtain the best possible value of a given performance index. In this application, we will maximize the sailplane best cross-country speed, that is, maximize the best average speed the sailplane can achieve over a segment of flight which starts with a high-speed glide and follows with a circling climb in a thermal to recover the height lost during the glide. In addition, we will require that the sailplane achieves a minimum rate of climb in a typically weak thermal. The design variables optimized in this subproblem are the sailplane weight, wing area, maximum lift coefficient, and the parameters relating its drag coefficient to its lift coefficient.

This appendix describes the calculations required to obtain the sailplane best cross-country speed and rate of climb as required for the optimization of the performance subproblem.

A.1 NOMENCLATURE

C_D : sailplane drag coefficient.

C_{D0}, C_{D1}, C_{D2}: coefficients of the drag polar (Eq. A.1).

C_L : sailplane lift coefficient.

D : drag force.

d : horizontal distance flown in typical flight segment (Subsec. A.3.2)

h : height lost and recovered in typical flight segment.

g : acceleration of gravity.

K : Eq. A.8.

L : lift force.

r : radius of thermal or circling flight.

$r_{1/2}$: radius where thermal strength is reduced to one half of the maximum strength v_{thmax}.

S : wing planform area.

t_1 : time expended in gliding flight.

t_2 : time expended in climbing flight.

V : horizontal flight speed.

v_c : sailplane rate of climb in thermal flight.

V_{cc} : cross-country speed.

v_{ith} : rate of sink of air between thermals.

v_s : sailplane rate of sink with respect to ambient air in straight flight.

v_{sc} : sailplane rate of sink with respect to ambient air in circling flight.

v'_{sc} : projection of v_{sc} in sailplane plane of symmetry.

V_t : absolute flight speed.

v_{th} : rate of climb of air in thermal.

v_{thmax} : maximum value of v_{th}.

W : sailplane gross weight.

ϕ : sailplane bank angle.

ρ : mass density of air.

A.2 SAILPLANE PERFORMANCE CURVES

A.2.1 Drag Polar

The performance of a sailplane in gliding flight may be described by a curve that relates total drag coefficient to total lift coefficient. That curve is named the drag polar, it is essentially parabolic in shape; we will assume the following form

$$C_D = C_{D0}+C_{D1}C_L+C_{D2}C_L^2 \qquad (A.1)$$

where the coefficients C_{D0}, C_{D1} and C_{D2} depend mainly on the sailplane aerodynamic design and on its weight.

A.2.2 Speed Polar

As a sailplane flies unaccelerated on a straight trajectory in undisturbed air the lift and the drag combined equilibrate exactly the weight (see Fig. 10). The similarity between the triangles of speeds and forces yields

$$v_s/V = D/L = C_D/C_L \qquad (A.2)$$

or, with Eq. A.1

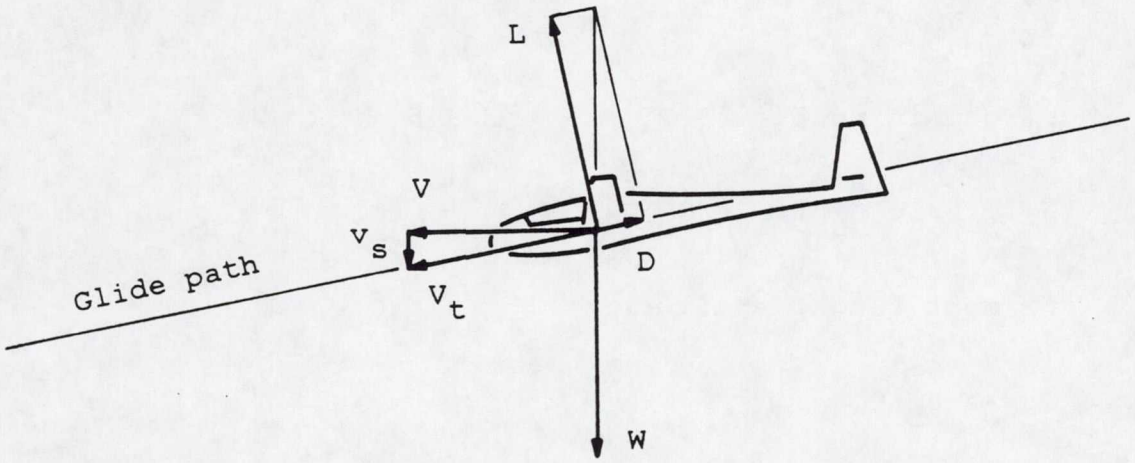

Figure 10: Sailplane in unaccelerated flight, definition of forces and speeds.

$$v_s = V(C_{D0}/C_L + C_{D1} + C_{D2}C_L) \tag{A.3}$$

The equilibrium of the forces acting on the sailplane yields

$$W = (L^2+D^2)^{1/2}$$

$$= .5\rho S V_t^2 (C_L^2+C_D^2)^{1/2} \tag{A.4}$$

while, from the speed triangle, we know

$$V_t^2 = V^2+v_s^2 \tag{A.5}$$

or, combining Eqs. A.2, A.4 and A.5

$$W = .5\rho S V^2 C_L [1+(C_D/C_L)^2]^{3/2} \tag{A.6}$$

For most flight attitudes

$$C_L >> C_D$$

and

$$W \simeq L \simeq .5\rho S V^2 C_L \tag{A.7}$$

The lift coefficient is thus related to the horizontal flight speed by

$$C_L = K/V^2$$

$$K = 2W/\rho S \tag{A.8}$$

So that the sailplane rate of sink (Eq. A.3) is now related to its horizontal flight speed as follows

$$v_s = (C_{D0}/K)V^3 + C_{D1}V + C_{D2}K/V \qquad (A.9)$$

This equation is the speed polar. It is quite important to the sailplane pilot since it allows him to know the altitude loss per unit time corresponding to his horizontal flight speed.

A.2.3 Circling Polar

A sailplane circling at constant speed in undisturbed air is depicted in Fig. 11. It flies on a helical trajectory of constant radius r about a vertical axis. In the plane of symmetry of the sailplane, the similarity between the triangles of speeds and forces yields

$$v'_{sc}/V = D/L = C_D/C_L \qquad (A.10)$$

In the vertical plane containing the center of gravity of the sailplane, we see that the vertical rate of sink v_{sc} is now related to the rate of sink in the plane of symmetry v'_{sc} and the bank angle ϕ by

$$v_{sc} = v'_{sc}/\cos\phi \qquad (A.11)$$

so that

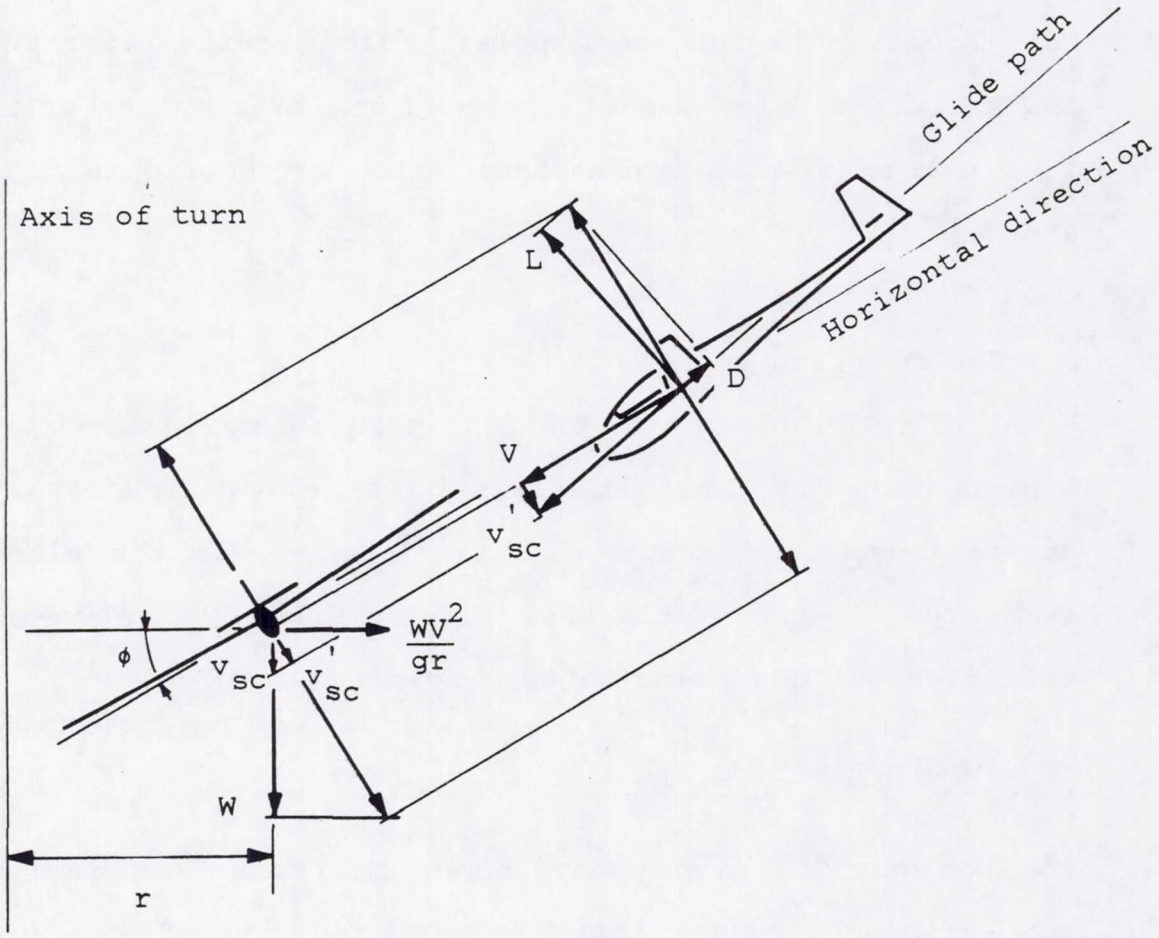

Figure 11: Sailplane in constant speed circling flight, definition of forces and speeds.

$$v_{sc} = \frac{V}{\cos\phi}\frac{C_D}{C_L} \tag{A.12}$$

Following a development similar to the one conducted in the previous subsection, we relate the sailplane lift to its weight by

$$L \simeq .5\rho SV^2 C_L \simeq W/\cos\phi \tag{A.13}$$

and the horizontal flight speed is now given by

$$V = [K/(C_L\cos\phi)]^{1/2} \tag{A.14}$$

where K is defined in Eq. A.8. The vertical rate of sink is obtained by combining Eqs. A.12 and A.14

$$v_{sc} = \frac{C_D K^{1/2}}{(C_L\cos\phi)^{3/2}} \tag{A.15}$$

The bank angle ϕ is found from the inertia forces

$$\cos\phi = \frac{W}{[W^2+(WV^2/gr)^2]^{1/2}}$$

$$= [1+(V^2/gr)^2]^{-1/2} \tag{A.16}$$

We may eliminate V from Eqs. A.14 and A.16 and that yields

$$\cos\phi = [1-(K/C_L gr)^2]^{1/2} \tag{A.17}$$

Finally, from Eqs. A.1, A.15 and A.17 we obtain

$$v_{sc} = \frac{(C_{DO}+C_{D1}C_L+C_{D2}C_L^2)K^{1/2}}{[C_L^2-(K/gr)^2]^{3/4}} \qquad (A.18)$$

Equation A.18 is known as the circling polar. For a given sailplane, it relates the sailplane rate of sink in circling flight to the radius of turn and the specific lift coefficient selected by the pilot.

A.3 A SAILPLANE PERFORMANCE INDEX: THE CROSS-COUNTRY SPEED

A.3.1 Soaring

A sailplane is usually towed to altitude by another airplane, a winch or even a car. If the pilot encounters only motionless air, he will trade his altitude for the speed needed to sustain flight. To keep his altitude and really soar, the pilot must find regions of rising air. Three soaring techniques are frequently used: thermal soaring, ridge soaring and wave soaring (See Ref. 29).

In thermal soaring, the source of lift (lift is meant here as upward force) is columns of rising air. During sunny days, radiation from the sun heats the surface of the earth which, in turn, heats the air in contact with it. The heating of the air is conditioned by the nature of the underlying surface. By buoyancy, the warmer air rises with respect to the cooler air. The regions of rising air are

called thermals. Once a pilot finds a thermal, he usually tries to circle in it to gain altitude.

When the wind blows on a mountain ridge, it is deflected upwards. By flying in a direction generally parallel to the ridge, on its upwind side, the pilot can remain at about constant altitude for as long as the ridge is uninterrupted, provided it is reasonably straight. This is called ridge soaring. The maximum altitude achievable in ridge lift is only a few hundred meters over the mountain.

When a mass of air flows across a mountain top, a system of standing waves may develop downwind from the ridge. Regions of rising and descending air alternate. Those regions may extend very high in altitude, up to ten times the height of the ridge. This source of lift is always used to establish altitude records. This type of flying is referred to as wave soaring.

From this very brief discussion of soaring, it is clear that a sailplane may be flown at quite different flight regimes. Therefore, it is difficult to define a performance index for the design of a sailplane without making some assumptions as to the type of soaring it will be used for. In this work, we will design the sailplane for thermal soaring.

A.3.2 The Cross-Country Speed

To cover a given distance, a pilot alternates slow circling flight in thermals with fairly fast glides between thermals. A portion of such a flight is sketched on Fig. 12. It includes a glide in a region of air descending at constant speed v_{ith}. The sailplane flies at horizontal speed V, its rate of sink with respect to the surrounding air is v_s, it covers the distance d in a time t_1, losing height h. The sailplane then reaches a thermal assumed to have the shape of a vertical cylinder. The pilot begins circling flight, and the height h is recovered in the thermal in a time t_2.

The rate of climb in the thermal is obtained by combining the sailplane rate of sink in circling flight v_{sc} with the rate of climb of the thermal air v_{th} which is assumed to depend on the distance r between the sailplane and the thermal axis,

$$v_c = v_{th}(r) - v_{sc} \qquad (A.19)$$

The cross-country speed is defined as the distance covered divided by the time required to reach the thermal and recover the altitude lost.

$$V_{cc} = d/(t_1+t_2) \qquad (A.20)$$

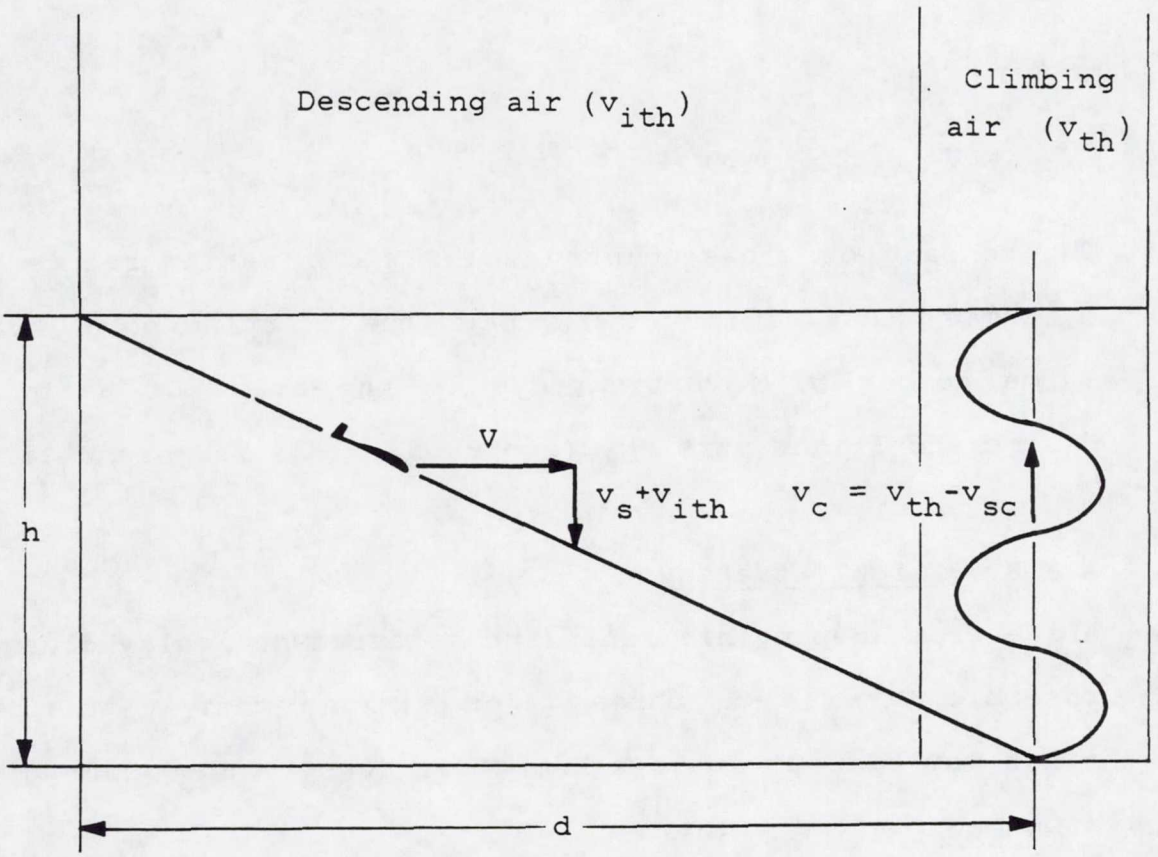

Figure 12: Model of flight used in the definition of cross-country speed.

Now

$$t_1 = d/V = h/(v_s+v_{ith})$$

$$t_2 = h/v_c \qquad (A.21)$$

so that

$$V_{cc} = Vv_c/(v_{ith}+v_c+v_s) \qquad (A.22)$$

The concept of cross-country speed was first introduced by K. Temmes (Ref. 30). It has been the starting point for a large number of investigations in the areas of sailplane design and flight strategy (see Refs. 31-33 for example).

A.3.3 Flight Strategy

Aside from keeping his sailplane as aerodynamically clean as possible, there are three major actions that a sailplane pilot may take to improve his cross-country speed for given atmospheric conditions.

i) Achieve the best rate of climb in the thermal. Intuitively, the best value of V_{cc} will be obtained with the best rate of climb in thermals v_c. The pilot must carefully select his position in the thermal to obtain the best possible lift.

ii) Select the best interthermal speed. From the development on the speed polar (Eq. A.9), we know

that the rate of sink in straight flight v_s is directly related to the horizontal flight speed V. For a given interthermal downdraft v_{ith} and a given anticipated achieved rate of climb, the pilot is left with the choice of the horizontal speed. Intuitively, if the next thermal is expected to be strong, the pilot should dive toward it at high speed. This may cause him to lose a lot of altitude in interthermal flight, but that loss will be recovered quickly in the strong thermal, and the cross-country speed will be high. Alternatively, if the pilot anticipates a weak thermal, he should choose a slow speed in interthermal flight.

iii) Adjust the sailplane weight. To increase the weight of a sailplane alters its speed polar in such a way that a given rate of sink occurs at a higher horizontal flight speed. This is favorable in interthermal flight. However, the price to pay for that is a lower achievable rate of climb in a given thermal. It turns out that heavy weight is advantageous in typical strong thermal conditions but disadvantageous in typical weak conditions. Therefore, sailplanes are equipped with water tanks (water ballasts) in the wings. The pilot may

select the amount of water to carry on the basis of the thermal conditions for the flight.

In the next two subsections, we will discuss how to evaluate the best achievable rate of climb for a sailplane in a given thermal and the best cross-country speed for fixed rate of climb and interthermal downdraft.

A.4 BEST RATE OF CLIMB IN THERMAL FLIGHT

A.4.1 Thermal Model

A difficulty in any study of sailplane performance is the choice of the thermal model. We will follow Carmichael (Ref. 31) and assume the thermals to be cylinders with vertical axes. The distribution of vertical airspeed is given as a function of the distance r to the thermal axis by

$$\frac{v_{th}(r)}{v_{thmax}} = \cos^2\left(\frac{\pi r}{4r_{1/2}}\right) \quad \text{if} \quad \frac{r}{r_{1/2}} < 2$$

$$= 0 \qquad \text{if} \quad \frac{r}{r_{1/2}} \geq 2 \qquad \text{(A.23)}$$

where v_{thmax} is the maximum vertical airspeed (on the thermal axis) and $r_{1/2}$ is that radius where the vertical airspeed is reduced to one half of v_{thmax}. This distribution is plotted in Fig. 13, where typical values are given for the parameters.

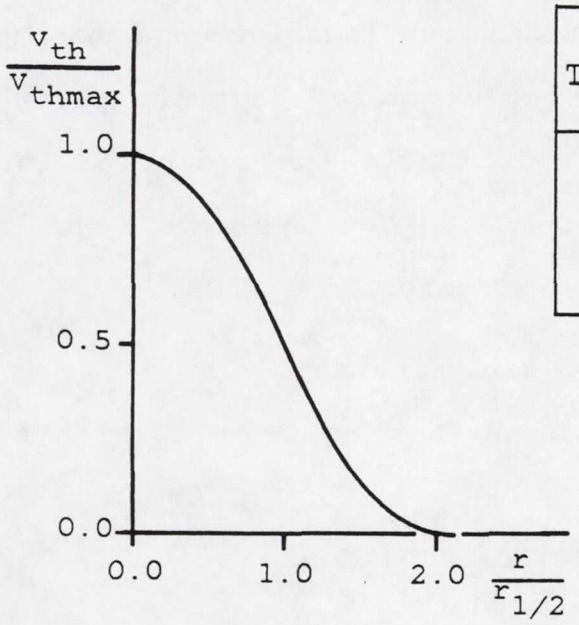

Thermal	v_{thmax} (m/s)	$r_{1/2}$ (m)
Strong	6.0	60.
Wide	4.5	120.
Weak	3.0	60.

Figure 13: Thermal models (arranged from Ref. 31).

A.4.2 Best Rate of Climb

From Eqs. A.18 and A.19 we obtain the sailplane rate of climb.

$$v_c = v_{th}(r) - \frac{(C_{D0}+C_{D1}C_L+C_{D2}C_L^2)K^{1/2}}{[C_L^2-(K/gr)^2]^{3/4}} \qquad (A.24)$$

For a given sailplane (fixed weight) in given atmospheric conditions, there are only two variables that the pilot can control to improve his rate of climb: the radius of turn r and the lift coefficient C_L. To evaluate the best achievable rate of climb, we specify

$$\frac{\partial v_c}{\partial r} = \frac{\partial v_c}{\partial C_L} = 0 \qquad (A.25)$$

This yields the following set of equations

$$\frac{\partial v_{th}}{\partial r} + \frac{3(C_{D0}+C_{D1}C_L+C_{D2}C_L^2)K^{5/2}}{2g^2r^3[C_L^2-(K/gr)^2]^{7/4}} = 0 \qquad (A.26.a)$$

$$r = \frac{K}{g\left[C_L^2 - \dfrac{3(C_{D0}C_L+C_{D1}C_L^2+C_{D2}C_L^3)}{2(C_{D1}+2C_{D2}C_L)}\right]^{1/2}} \qquad (A.26.b)$$

These equations are nonlinear and must be solved numerically.

Experiments with typical sailplane parameters have shown that the solution may yield an unrealistically high lift coefficient. When that happens, the lift coefficient must be set to its maximum allowable value C_{Lmax} and Eq. A.26.a solved for r.

A.5 BEST CROSS-COUNTRY SPEED

The cross-country speed is given by Eqs. A.9 and A.22 combined

$$V_{cc} = \frac{Vv_c}{(v_{ith}+v_c)+[(C_{D0}/K)V^3+C_{D1}V+C_{D2}K/V]} \qquad (A.27)$$

For a given sailplane (fixed weight) and known rate of climb and interthermal downdraft the pilot controls his cross-country speed by adjusting the horizontal flight speed. To evaluate the best available cross-country speed, we set

$$\frac{\partial V_{cc}}{\partial V} = 0 \qquad (A.28)$$

This yields

$$\frac{C_{D0}}{K^2} V^4 - \frac{v_c + v_{ith}}{2K} V - C_{D2} = 0 \qquad (A.29)$$

To obtain the best cross-country speed a given sailplane may reach in given atmospheric conditions, we proceed as follows:

i) Determine the radius r and lift coefficient C_L to use in the thermal from Eq. A.26.

ii) Find the resulting rate of climb from Eq. A.24.

iii) Determine the horizontal speed to select in interthermal flight from Eq. A.29.

iv) Find the resulting best achievable cross-country speed from Eq. A.27.

Appendix B

AERODYNAMIC SUBPROBLEM

The objective of the aerodynamic subproblem is to design the wing so as to obtain the aerodynamic characteristics requested by the performance subproblem. These characteristics are the wing area, the coefficients of the drag polar, and the maximum sailplane lift coefficient. The design is subjected to the constraint that stall must begin at an inboard station of the wing so as to preserve lateral control in high angle of attack conditions. The variables of this subproblem are coefficients of the spanwise distributions of wing chord, thickness and geometric twist.

The calculations of the contribution of the wing to the aerodynamic characteristics will be performed using accurate prediction methods since the wing design is the object of this subproblem. In particular, finite span and Reynolds number effects will be accounted for while estimating wing lift and drag (as suggested in 34). However, the wing will be assumed rigid, neglecting aeroelastic lift redistribution and similar phenomena. The effect of the remaining sailplane components on the aerodynamic characteristics of interest will be found using more approximate methods. This will enable us to keep the computational cost to a minimum

while still obtaining realistic estimates for these parameters.

This appendix describes the calculations for obtaining the sailplane polar curve, its maximum lift coefficient and for estimating the position of the wing station where stall begins. In addition, it details the developments giving the control vectors A, H, and H_j (see Chap. IV).

B.1 NOMENCLATURE

$\{A\}$: vector of aerodynamic load parameters.

$\{A^1\}$, $\{A^2\}$, $\{A^3\}$: subvectors of A.

A_h : horizontal tailplane aspect ratio.

A_v : fuselage maximum cross-sectional area.

[AS] : aerodynamic matrix.

b : wing semispan.

b_b : spanwise position of break in wing planform.

b_f : fuselage maximum width.

b_i : width of wing element i.

{B}, {B1}, {B2} : Eqs. B.18 and B.20.

c; c_r, c_b, c_t; c_i : section chord; chord for root, break and tip sections; chord for wing element i.

$\bar{c}$: mean aerodynamic chord.

c_{dp}, c_{dpmin}, c_{dpl} : airfoil profile drag, minimum profile drag, profile drag for unit lift coefficients.

c'_{dpo}, c'_{dpl}, c'_{dp2} : Eq. B.41.

c_l, c_{li}, c_{lmax}, $c_{l\alpha}$: airfoil lift coefficient, design lift coefficient, maximum lift coefficient, lift curve slope.

c'_l, c'_{lo}, $c'_{l\alpha}$: airfoil three-dimensional lift, lift for zero fuselage angle of attack, lift curve slope coefficients.

c_{mac} : airfoil coefficient of moment about aerodynamic center.

C_{mac}, C_{macw} : coefficients of aerodynamic moment for wing fuselage combination, for wing alone.

C_C : coefficient of aerodynamic forces acting on sailplane parallel to mean aerodynamic chord.

C_D, C_{Dw}: total coefficients of drag for sailplane, for wing.

C_DS : drag area.

C_F : skin friction coefficient.

C_L, C_{Lo}, $C_{L\alpha}$: sailplane trimmed lift, trimmed lift at zero fuselage angle of attack, untrimmed lift curve slope.

C_{Lh}, $C_{Lh\alpha}$: horizontal tailplane lift, lift curve slope coefficients.

C_{Lw}, C_{Lwo}, $C_{Lw\alpha}$: wing lift, zero fuselage angle of attack lift, lift curve slope coefficients.

C_{Lwf} : lift coefficient for wing fuselage combination.

ORIGINAL PAGE IS
OF POOR QUALITY

C_N, C_{Nw} : coefficients of aerodynamic forces acting normal to mean aerodynamic chord on sailplane, on wing.

d_C, d_N : chordwise and normal moment arms of aerodynamic forces with respect to axis Y (Fig. 18).

f_{aN}, f_{aC} : aerodynamic forces per unit length acting normal and parallel to mean aerodynamic chord (Fig. 18).

h_h, h_f : Fig. 16.

H, H_j : vectors describing shape of wing, shape of wing element j.

i_w : wing angle of incidence (Fig. 14).

K_I, K_{II}: Eq. B.26.

l_f, l_{fn}, l_h : Fig. 16.

m_{aY} : aerodynamic moment per unit length about spanwise axis.

n_a : number of wing stations in integration of lifting line equation.

n_C : longitudinal sailplane load factor.

n_s : number of wing elements at local structural level.

n_f : number of intervals in discretization of spanwise distributions of aerodynamic load parameters.

n_N, n_{Nw}: normal sailplane, wing load factors.

Re : Reynolds number.

S : wing planform area.

S_f, S_{fw}, S_{fwet} : fuselage planform area, wetted area, portion of wing area inside fuselage outline (Fig. 16).

S_h, S_v : planform areas for horizontal and vertical tail.

t; t_t, t_b, t_r; t_i : wing thickness; thickness for root, break and tip sections; thickness for wing element i.

V_f : fuselage volume.

V_t : indicated airspeed.

W : sailplane gross weight.

x_{ac}, x_{cg}, x_n : longitudinal position of aerodynamic center of sailplane without tail, of sailplane center of gravity and neutral point; datum is at leading edge of mean aerodynamic chord.

x_{ac}, x_{cg}, x_{mt} : dimensional chordwise position of airfoil aerodynamic center, area center of gravity, maximum thickness; datum is at leading edge.

$\{X_a\}$: vector of variables of aerodynamic subproblem.

$\{X_p\}$: vector of performance variables.

y : dimensional spanwise coordinate.

$\bar{y}$: spanwise position of mean aerodynamic chord.

z_{ac}, z_{cg}, z_{mt} : dimensional position of airfoil aerodynamic center, area center of gravity, maximum thickness normal to airfoil chord; datum is at airfoil chord, positive up.

α, α_c, α_{ol}, α_{olr}, α_f : angles of attack (Fig. 14).

$\alpha_{ol}\varepsilon_{at}$: Eqs. B.24.

ε; ε_b, ε_t: section geometric twist; geometric twist for break and tip wing sections.

$\bar{\varepsilon}$: geometric twist at section of mean aerodynamic chord.

ζ, η, γ: z_{ac}, z_{cg}, z_{mt} normalized with respect to the section chord.

η : non-dimensional spanwise coordinate (y/b).

λ_h : horizontal tailplane taper ratio.

ρ : mass density of air.

ϕ : non-dimensional spanwise coordinate (Eq. B.15).

χ, δ, β: x_{ac}, x_{cg}, x_{mt} normalized with respect to section chord.

ν : kinematic viscosity of air.

Commonly used superscripts

1, 2, 3 : aerodynamic load parameters related to the various structural design requirements.

' : three-dimensional airfoil aerodynamic quantity (i.e., a quantity corrected for finite span effects).

T : transposed vector or matrix.

-1 : inverse matrix.

Commonly used subscripts

i as in A_i: element i of vector A, or

: discretized value of function A(y), i.e., $A_i = A(y_i)$.

ij : element ij of matrix.

b : wing section at planform break.

f : fuselage.

h : horizontal tail.

m : miscellaneous.

r : wing section at root.

t : wing section at tip.

v : vertical tail.

wf : wing fuselage combination.

Special symbols

{ } as in {A} : vector A, or

: discrete values of function A(y) collected

: in vector $\{A\}^T = \{A(y_1), A(y_2), \ldots\}$.

[ ] : square matrix.

B.2 WING DESCRIPTION

B.2.1 Wing Shape

The wing aerodynamic model is described in Fig. 14. It is a straight cantilever wing with linearly varying chord c, thickness t and geometric twist ε. The wing is positioned so that the chord of the root section is at an angle i_w (wing angle of incidence) with respect to the fuselage axis.

The chord of the wing section at station y makes an angle $\varepsilon(y)$ with respect to the chord of the root section. The sections are arranged so that the line joining their point of maximum thickness is straight and perpendicular to the sailplane plane of symmetry.

In terms of the spanwise coordinate y, we have

$$c(y) = c_r\left(1-\frac{y}{b_b}\right) + c_b\left(\frac{y}{b_b}\right) \qquad y<b_b$$

$$= c_b\left(1-\frac{y-b_b}{b-b_b}\right) + c_t\left(\frac{y-b_b}{b-b_b}\right) \qquad y\geq b_b \qquad \text{(B.1)}$$

$$t(y) = t_r\left(1-\frac{y}{b_b}\right) + t_b\left(\frac{y}{b_b}\right) \qquad y<b_b$$

$$= t_b\left(1-\frac{y-b_b}{b-b_b}\right) + t_t\left(\frac{y-b_b}{b-b_b}\right) \qquad y\geq b_b \qquad \text{(B.2)}$$

$$\varepsilon(y) = \varepsilon_b\left(\frac{y}{b_b}\right) \qquad y<b_b$$

$$= \varepsilon_b\left(1-\frac{y-b_b}{b-b_b}\right) + \varepsilon_t\left(\frac{y-b_b}{b-b_b}\right) \qquad y\geq b_b \qquad \text{(B.3)}$$

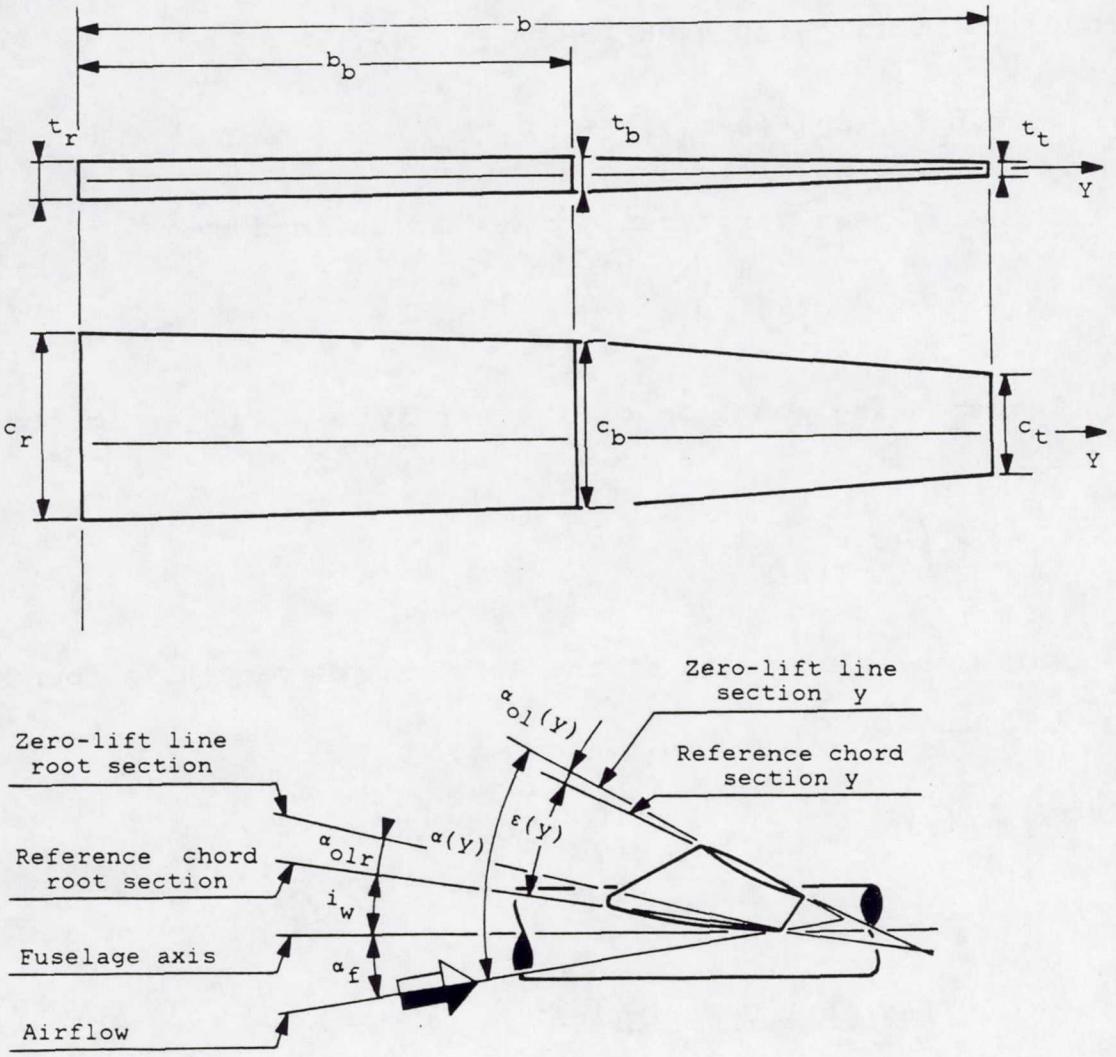

Figure 14: Wing definition.

The quantities b, b_b, c_r, c_b, c_t, t_r, t_b, t_t, ε_b and ε_t are the design variables of the aerodynamic optimization subproblem; they are collected in vector X_a.

The total wing area is

$$S = b_b(c_r+c_b)+(b-b_b)(c_b+c_t) \tag{B.4}$$

The wing mean aerodynamic chord is defined by

$$\bar{c} = \frac{2}{S}\int_o^b c^2(y)dy \tag{B.5}$$

The spanwise position of the aerodynamic center is obtained from

$$\bar{y} = \frac{2}{S}\int_o^b c(y)ydy \tag{B.6}$$

while the wing twist at the aerodynamic center is found from Eq. B.3 as

$$\bar{\varepsilon} = \varepsilon(\bar{y}) \tag{B.7}$$

B.2.2 Airfoil Description

In the past thirty years, sailplane wings have been built with specially tailored, laminar-flow airfoils (see Ref. 35). However, for this application, we will use airfoils from the NACA 6-series, a class typical of immediate post World War II sailplane design. This choice was conditioned by the availability of experimental data. The specific

airfoil family chosen is the NACA 64-4XX which is extensively described in Ref. 36. For the purpose of this application, linear regressions were developed from the data collected in Ref. 36. These laws relate the airfoil performance characteristics to their thickness ratio (t/c) and the Reynolds number based on the chord ($Re=Vc/\nu$). The data from Ref. 36 is valid for the following ranges of thickness ratio and Reynolds number

$$.09<t/c<.18 \text{ and } 630000<Re<6300000 \qquad (B.8)$$

Typical Reynolds number for sailplanes may be as low as 400000; therefore, the laws are somewhat deficient. However, no sufficient set of data was found for Reynolds numbers less than 630000.

The following performance laws are used (see Fig. 15).

i) Lift coefficient (c_l) versus angle of attack (α_c).

$$c_l = c_{l\alpha}(\alpha_c-\alpha_{ol}) \qquad c_l<c_{lmax}$$

$$= 0 \qquad c_l \geq c_{lmax}$$

$$\alpha_{ol} = (-98.13+12.429\log Re)+(1964.96-249.921\log Re)(t/c)$$
$$+(-13785.2+1722.21\log Re)(t/c)^2$$
$$+(32757.-4056.\log Re)(t/c)^3$$

$$c_{l\alpha} = (-.12661+.03509\log Re)+(1.1562-.16571\log Re)(t/c)$$

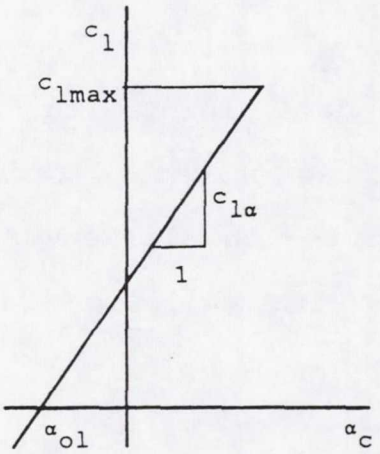

a) Lift coefficient.

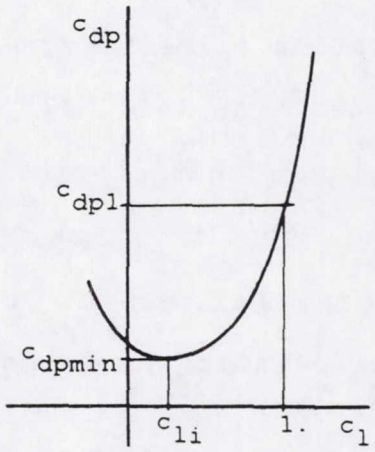

b) Profile drag coefficient.

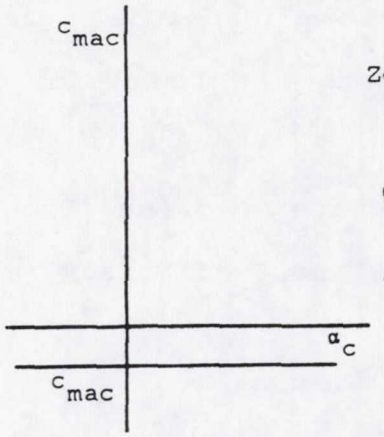

c) Moment Coefficient
(about aerodynamic center).

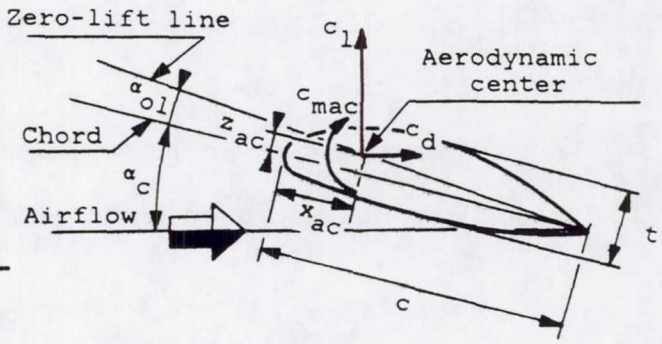

d) Definition of geometry
and aerodynamic coefficients.

Figure 15: Wing section, definition of geometry and aerodynamic performance coefficients. Each curve corresponds to one Re and t/c combination.

$$c_{lmax} = (1.756-.2058\log Re)+(-66.826+12.840\log Re)(t/c)$$
$$+(306.11-56.746\log Re)(t/c)^2 \qquad (B.9)$$

ii) Moment coefficient about aerodynamic center (c_{mac}).

$$c_{mac} = -.075+.0556(t/c) \qquad (B.10)$$

iii) Profile drag coefficient (c_{dp}) versus lift coefficient.

$$c_{dp} = c_{dpmin}+(c_{dpl}-c_{dpmin})\left(\frac{c_l-c_{li}}{1-c_{li}}\right)^2$$

$$c_{dpmin} = (.1315-.041135\log Re+.0032813\log^2 Re)$$
$$+(.1956-.027286\log Re)(t/c)$$

$$c_{dpl} = (8.026-2.248796\log Re+.1573704\log^2 Re)$$
$$+(-126.0558+33.68397\log Re-2.22887\log^2 Re)(t/c)$$
$$+(583.6108-139.0277\log Re+7.8373\log^2 Re)(t/c)^2$$
$$+(-656.255+96.296\log Re)(t/c)^3$$

$$c_{li} = .4 \qquad (B.11)$$

iv) Aerodynamic center position (x_{ac} and z_{ac}).

$$x_{ac} = \chi c$$

$$\chi = -6.2579+2.7958\log Re-.4202\log^2 Re+.021123\log^3 Re$$
$$+(9.308-.494\log Re+.0223\log^2 Re)(t/c)$$
$$+(-54.81+.28\log Re)(t/c)^2+130.7(t/c)^3$$

$$z_{ac} = \zeta c$$

$$\zeta = -1.8143-.1911\log Re+.1627\log^2 Re-.014757\log^3 Re$$
$$+(69.045-18.325\log Re+1.3378\log^2 Re)(t/c)$$
$$+(-94.67+5.24\log Re)(t/c)^2+164.6(t/c)^3 \qquad (B.12)$$

v) Maximum thickness point position (x_{mt}, z_{mt}).

$$x_{mt} = \beta c \quad \beta = .37$$

$$z_{mt} = \gamma c \quad \gamma = .02 \qquad (B.13)$$

vi) Area center of gravity position (x_{cg}, z_{cg}).

$$x_{cg} = \delta c \quad \delta = .42$$

$$z_{cg} = \eta c \quad \eta = .02 \qquad (B.14)$$

B.3 LIFT AND AERODYNAMIC MOMENT CALCULATION

B.3.1 Wing Lift

The three-dimensional spanwise distribution of lift coefficient may be obtained by integration of Prandtl's lifting line equation. This classical integral equation is developed in Refs. 37 and 38 where it is said to be applicable to straight, high aspect ratio wings in imcompressible flow. Several solution schemes exist for Prandtl's equation. We will use Glauert's method, which is based on Fourier series.

A new coordinate is defined along the wing by

$$\phi = \cos^{-1}(y/b) \tag{B.15}$$

where the angle ϕ varies between 0 at the wing tip and $\pi/2$ at the wing root. Stations are chosen along the semispan at equal interval $\Delta\phi$. If there are n_a intervals

$$\Delta\phi = \pi/(2n_a) \tag{B.16}$$

The three-dimensional lift coefficient (c_l') at an arbitrary section along the wing is given by

$$c_l' = \frac{2b}{c(\phi)} \sum_{j=1}^{n_a} B_j \sin[(2j-1)\phi] \tag{B.17}$$

For a symmetric lift distribution, the coefficients B_j are obtained from

$$\{B\} = [AS]\{\alpha\}$$

$$[AS]^{-1}_{ij} = \left[\frac{2b}{c_{l\alpha}(i\Delta\phi)c(i\Delta\phi)} + \frac{(2j-1)}{4\sin(i\Delta\phi)}\right]\sin[i(2j-1)\Delta\phi]$$

$$\alpha_i = \alpha(i\Delta\phi) \qquad (B.18)$$

$\alpha(i\Delta\phi)$, the angle of attack for section i, is measured with respect to the zero lift line of that section. The lift curve slope of the airfoil $c_{l\alpha}(i\Delta\phi)$ is a known function of the section chord $c(i\Delta\phi)$ and thickness $t(i\Delta\phi)$ defined in Subsec. B.2.1 and, also, of the Reynolds number ($Re=Vc(i\Delta\phi)/\nu$).

From Fig. 14 we see that

$$\alpha_i = \alpha_f + \alpha_i'$$

$$\alpha_i' = i_w + \varepsilon_i - \alpha_{oli} \qquad (B.19)$$

If we define

$$\{B1\} = [AS]\{u\}$$

$$\{B2\} = [AS]\{\alpha'\}$$

$$\{u\}^T = \{1,1,\ldots,1\} \qquad (B.20)$$

we obtain the three-dimensional wing lift distribution as a function of the sailplane angle of attack

$$c_l'(y) = c_{l\alpha}'(y)\alpha_f + c_{lo}'$$

$$c_{l\alpha}'(y) = \frac{2b}{c(y)} \sum_{j=1}^{n_a} B1_j \sin[(2j-1)\phi(y)]$$

$$c_{lo}'(y) = \frac{2b}{c(y)} \sum_{j=1}^{n_a} B2_j \sin[(2j-1)\phi(y)] \qquad (B.21)$$

where, of course, $\phi(y)$ is given by Eq. B.15.

The total wing lift coefficient is now obtained from

$$C_{Lw} = \frac{2}{S}\int_o^b c(y)c_l'(y)dy$$

or, using Eq. B.21

$$C_{Lw} = C_{Lw\alpha}\alpha_f + C_{Lwo}$$

$$C_{Lw\alpha} = (\pi b^2 B1_1)/S$$

$$C_{Lwo} = (\pi b^2 B2_1)/S \qquad (B.22)$$

For subsequent calculations, it is convenient to write the wing lift coefficient as

$$C_{Lw} = C_{Lw\alpha}(\alpha_f + i_w - \alpha_{olr} - \alpha_{ol}\varepsilon_{at}) \qquad (B.23)$$

Comparing Eqs. B.22 and B.23, we obtain

$$\alpha_{ol}\varepsilon_{at} = i_w - \alpha_{olr} - \frac{C_{Lwo}}{C_{Lw\alpha}} \qquad (B.24)$$

The quantity α_{ol} is called the change in zero-lift angle of attack of the wing per unit of positive aerodynamic twist at the wing tip, ε_{at} being the aerodynamic twist at the wing tip. It must be emphasized that in order to complete these calculations, the Reynolds number Re and the fuselage angle of attack α_f must be known. This point will clarified in Subsec. B.4.3

B.3.2 Sailplane Trimmed Lift

In Ref. 39, the total trimmed lift is given as,

$$C_L = C_{Lwf}\left(1+\frac{x_{cg}-x_{ac}}{l_h}\right)+\frac{\bar{c}}{l_h}c_{mac} \qquad (B.25)$$

The lift coefficient for the wing fuselage combination C_{Lwf}, the distance between the sailplane center of gravity and its aerodynamic center $x_{cg}-x_{ac}$ and the aerodynamic moment coefficient about the sailplane aerodynamic center for the complete aircraft minus horizontal tail c_{mac} will be calculated in this section. The mean aerodynamic chord $\bar{c}$ was defined in Subsec. B.2.1, and the tail length l_h is a fixed parameter of the design problem.

The lift coefficient for the wing-fuselage combination is given for a mid-wing configuration by

$$C_{Lwf} = K_I C_{Lw\alpha}[\alpha_f - \alpha_{ol}\varepsilon_{at} + \frac{K_{II}}{K_I}(i_w - \alpha_{olr})]$$

$$K_I = (1+2.15b_f/b)(1-S_{fw}/S) + \frac{2\pi b_f^2}{C_{Lw\alpha}S}$$

$$K_{II} = (1+.7b_f/b)(1-S_{fw}/S) \qquad (B.26)$$

The quantities b_f and S_{fw} are fixed parameters in this design problem and they are defined in Fig. 16. The longitudinal distance between the aircraft center of gravity and its aerodynamic center (tail effects not included) may be written

$$x_{cg}-x_{ac}=(x_{cg}-x_n)+(x_n-x_{ac}) \qquad (B.27)$$

where x_n defines the stick-fixed neutral point, i.e., that position of the center of gravity for which the sailplane is neutrally stable for constant elevator angle. The quantity $(x_n-x_{cg})/\bar{c}$ is called the static margin; it is a measure of longitudinal static stability and should be positive for stability. It may be taken as a fixed parameter for the problem. The quantity (x_n-x_{ac}) may be obtained as follows for an aircraft with a T-tail

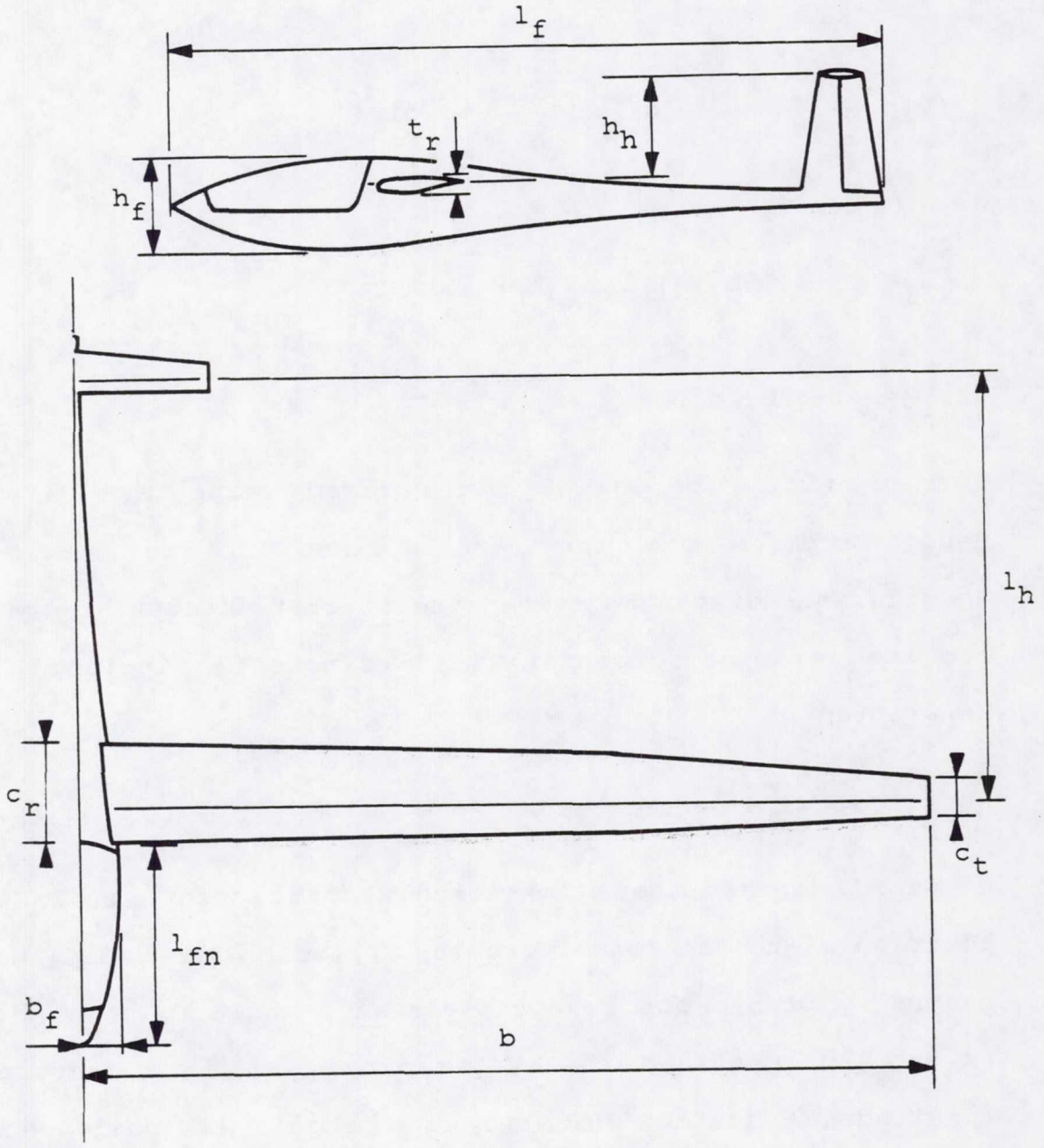

Figure 16: Geometric description of the sailplane.

$$\frac{x_n - x_{ac}}{\bar{c}} = \frac{C_{Lh\alpha}}{C_{L\alpha}}\left(1 - \frac{d\varepsilon}{d\alpha}\right)\frac{S_h l_h}{S\bar{c}}$$

$$C_{L\alpha} = K_I C_{Lw\alpha} + C_{Lh\alpha}\frac{S_h}{S}\left(1 - \frac{d\varepsilon}{d\alpha}\right) \tag{B.28}$$

The tailplane lift curve slope $C_{Lh\alpha}$ may be estimated by

$$C_{Lh\alpha} = \frac{2\pi}{1 + \frac{2(1+2\lambda_h)}{A_h(1+\lambda_h)}} \tag{B.29}$$

where A_h, λ_h and S_h are the tailplane aspect ratio, taper ratio and total planform area; they are fixed parameters. The downwash gradient $d\varepsilon/d\alpha$ is found from

$$\frac{d\varepsilon}{d\alpha} = .438\,\frac{SC_{Lw\alpha}}{\pi b^2\left(\frac{c_t l_h}{c_r b}\right)^{.25}\left(1 + \left|\frac{h_h}{b}\right|\right)} \tag{B.30}$$

where b is the wing semispan, l_h and h_h are dimensions related to the tail (Fig. 16). To trim the sailplane, the horizontal tailplane must exert a lift given by the coefficient

$$C_{Lh} = \frac{S\bar{c}}{S_h l_h}\left[C_{mac} + C_{Lwf}\left(\frac{x_{cg} - x_{ac}}{\bar{c}}\right)\right] \tag{B.31}$$

B.3.3 Pitching Moment Coefficient

For the sailplane without horizontal tail, the pitching moment coefficient is given by

$$C_{mac} = C_{macw} + \Delta_f C_{mac} \tag{B.32}$$

The wing moment coefficient is given for straight wings by

$$C_{macw} = \frac{2}{S\bar{c}} \int_o^b c_{mac}(y) c^2(y) dy \tag{B.33}$$

where c_{mac} is the airfoil pitching moment coefficient. It is a known function of the thickness ratio (t/c) as explained in Sec. B.2.2.

The effect of the fuselage on the pitching moment coefficient is (see Ref. 39)

$$\Delta_f C_{mac} = -.9\left(1-5.\frac{b_f}{l_f}\right)\frac{\pi b_f h_f l_f C_{Lo}}{S c K_I C_{Lw\alpha}} \tag{B.34}$$

All the elements in Eq. B.34 were calculated before or are defined in Fig. 16 except for C_{Lo}, the total sailplane lift coefficient at zero fuselage angle of attack (α_f). Combining Eqs. B.25-26, B.32 and B.34, we obtain

$$C_{Lo} = \frac{K_I C_{Lw\alpha}\left[-\alpha_{ol}\varepsilon_{at} + \frac{K_{II}}{K_I}(i_w - \alpha_{olr})\right]\left(1+\frac{x_{cg}-x_{ac}}{l_h}\right) + \frac{\bar{c}}{l_h} C_{macw}}{1+1.8\left(1-5.\frac{b_f}{l_f}\right)\frac{\pi b_f h_f l_f}{2 S l_h K_I C_{Lw\alpha}}} \tag{B.35}$$

B.3.4 Maximum Lift Coefficient

The information obtained in the previous sections may be used to estimate approximately the sailplane maximum lift coefficient.

The three-dimensional distribution of wing lift coefficient is given by Eq. B.21. Assuming that stall occurs in a given wing section when that section lift coefficient equals its maximum local lift coefficient obtained from experimental data (Eq. B.9), we may define the fuselage angle of attack for which stall occurs in section y as

$$\alpha_{fs}(y) = [c_{lmax}(y)-c'_{lo}(y)]/c'_{l\alpha}(y) \qquad (B.36)$$

The wing section where stall initiates (at spanwise station y_s) is such that $\alpha_{fs}(y)$ is minimum. It may be determined by numerical minimization of $\alpha_{fs}(y)$ with respect to y. The resulting angle of attack may be used with Eq. B.25 to determine the maximum sailplane lift coefficient C_{Lmax}. This approach is described in Ref. 39. The $c'_{l\alpha}(y)$, $c'_{lo}(y)$ and $c_{lmax}(y)$ distributions are Reynolds number dependent, as was pointed out earlier. Therefore, the procedure should be repeated iteratively. Such a refinement does not seem appropriate in view of the approximate character of the method; the above mentioned distributions

will be calculated with Reynolds numbers based on a typical (slow) flight speed.

B.4 SAILPLANE DRAG PREDICTION

B.4.1 Wing Drag

In this subsection, we develop expressions for the vortex induced drag distribution, the total drag distribution and the total wing drag.

The local vortex induced drag coefficient is given in Ref. 38 as

$$c'_{di}(y) = c'_l(y)[\alpha(y)-c'_l(y)/c_{l\alpha}(y)] \qquad (B.37)$$

where the (') emphasizes the fact that the vortex induced drag coefficient c'_{di} and the lift coefficient c'_l include finite span effects. Now, from Fig. 14

$$\alpha(y) = \alpha_f+i_w+\varepsilon(y)-\alpha_{ol}(y) \qquad (B.38)$$

The total drag distribution on the wing is

$$c'_d(y) = c'_{di}(y)+c'_{dp}(y) \qquad (B.39)$$

where the local airfoil profile drag coefficient c'_{dp} is known once the local lift coefficient c'_l, the local Reynolds number and the local thickness ratio are known, as shown in Subsec. B.2.2.

The total drag on the wing is found as

$$(C_D S)_w = 2\int_o^b c_d'(y)c(y)dy \qquad (B.40)$$

It may be calculated once the flight speed, the fuselage angle of attack and the wing geometry are known.

For the calculation of the loads on the wing, it will prove necessary to know the wing drag as a function of the fuselage angle of attack. Using Eqs. B.11, B.21, and B.37-40, we obtain

$$C_{Dw} = C_{Dw2}\alpha_f^2 + C_{Dw1}\alpha_f + C_{Dw0}$$

$$C_{Dwj} = \frac{2}{S}\int_o^b c_{dj}'(y)c(y)dy; \qquad j=0,1,2$$

$$c_{do}'(y) = c_{lo}'(y)\left[i_w+\varepsilon(y)-\alpha_{ol}(y)-\frac{c_{lo}'(y)}{c_{l\alpha}(y)}\right]+c_{dpmin}(y)$$

$$+[c_{dpl}(y)-c_{dpmin}(y)]\left[\frac{c_{lo}'(y)-c_{li}}{1.-c_{li}}\right]^2$$

$$c_{dl}'(y) = c_{l\alpha}'(y)\left[i_w+\varepsilon(y)-\alpha_{ol}(y)-\frac{c_{lo}'(y)}{c_{l\alpha}'(y)}\right]+c_{lo}'(y)\left[1-\frac{c_{l\alpha}'(y)}{c_{l\alpha}(y)}\right]$$

$$+2[c_{dpl}(y)-c_{dpmin}(y)]\frac{c_{l\alpha}'(y)[c_{lo}'(y)-c_{li}]}{(1.-c_{li})^2}$$

$$c'_{d2}(y) = c'_{l\alpha}(y) - \frac{c'^{2}_{l\alpha}(y)}{c_{l\alpha}(y)} + [c_{dpl}(y) - c_{dpmin}(y)] \left[\frac{c'_{l\alpha}(y)}{1. - c_{li}}\right]^2 \tag{B.41}$$

B.4.2 Total Sailplane Drag

The various contributions to the sailplane drag from sources other than the wing will be given in this subsection, following Ref. 39.

B.4.2.1 Fuselage Drag

The drag of the fuselage includes viscous and induced components.

$$(C_D S)_f = .15\alpha_f^2 V_f^{2/3} + C_F S_{fwet}(1+\phi_f) + S_f|\sin^3\alpha_f|$$

$$\phi_f = \frac{2.2}{\lambda_{eff}^{1.5}} + \frac{3.8}{\lambda_{eff}^{3}}$$

$$\lambda_{eff} = \frac{l_f}{(4A_c/\pi)^{1/2}} \tag{B.42}$$

The quantities V_f, S_{fwet}, S_f, A_c and l_f are, respectively: the fuselage volume, wetted area, planform area, maximum cross-sectional area and length; they are fixed parameters

of the design problem. The angle α_f is the fuselage angle of attack. C_f is the skin friction coefficient; it is a function of the Reynolds number and the location of the boundary layer transition on the body considered. For lack of sufficient information, we will assume that transition occurs at the nose of all sailplane components, a conservative assumption. Then

$$C_F = \frac{.4550}{(\log Re)^{2.58}} \tag{B.43}$$

For the fuselage, the Reynolds number is based on the total fuselage length (l_f).

B.4.2.2 Wing-Fuselage Interaction Drag

The drag due to wing-fuselage interaction may be obtained for straight wings from:

$$(C_D S)_{wf} = \frac{.138(b_f/b)C_{Lo}^2 S^2}{(1+c_t/c_r)\pi b^2}(2-\pi b_f/b) + 6.75 C_F c_r t_r \tag{B.44}$$

In this equation, c_r, t_r, b, and S are, respectively: the wing root chord, root thickness, semispan and total area. The lift coefficient for zero fuselage angle of attack (C_{Lo}) was obtained in Subsec. B.3.3. Also, b_f is the fuselage radius. The skin friction coefficient C_f is obtained from

Eq. B.43, with the Reynolds number based on the nose-wing distance.

B.4.2.3 Horizontal Tailplane Drag

Combining the drag due to the tailplane lift and the tailplane viscous drag, we find

$$(C_D S)_h = 1.35 \frac{C_{Lh}^2 S_h}{\pi A_h} + 2C_F[1+2.75(t/c)_h]S_h \qquad (B.45)$$

S_h, A_h, $(t/c)_h$ are, respectively: the tailplane planform area, aspect ratio, and thickness ratio; they are fixed parameters in this problem. The tailplane lift coefficient C_{Lh} was obtained in Subsec. B.3.2. The skin friction coefficient and the thickness ratio are based on the average tailplane chord.

B.4.2.4 Vertical Tailplane Drag

The main contribution to the vertical tailplane drag is viscous in nature, it is given by:

$$(C_D S)_v = 2C_F[1+2.75(t/c)_v]S_v \qquad (B.46)$$

S_v and $(t/c)_v$ are the vertical tailplane planform area and thickness ratio. The skin friction coefficient as well as the thickness ratio are based on the average vertical tailplane chord.

B.4.2.5 Miscellaneous Drag Contributions

A sailplane is aerodynamically clean in design. The only drag contribution that will be considered in addition to those already mentioned is that due to the gaps of the flaps and control surfaces. For movable surfaces along the entire trailing edge of the wing and the vertical tailplane, we have:

$$(C_D S)_m = 2(S+S_V)10^{-4} \tag{B.47}$$

B.4.3 Drag Polar Calculation

The total sailplane drag coefficient is now given by

$$C_D = \frac{1}{S}[(C_D S)_w + (C_D S)_f + (C_D S)_{wf} + (C_D S)_h + (C_D S)_v + (C_D S)_m] \tag{B.48}$$

The various contributions were obtained in the two previous subsections.

To evaluate the drag polar (Subsec. A.2.1) for known weight and geometry, we proceed as follows.

i) Choose a lift coefficient value and determine an approximate flight speed by equating the lift to the known weight (Eq. A.8). At this point, the local Reynolds number is known for all sailplane components.

ii) Proceed with the calculations of Subsec. B.3.1 and obtain all the information on the wing lift. The fuselage angle of attack α_f is still unknown at this step.

iii) Calculate all the terms in the sailplane trimmed lift equation (B.25), as shown in Subsecs. B.3.2-3.

iv) Find the fuselage angle of attack from the information obtained in iii) and the lift coefficient selected in i).

v) Continue with the calculations of the various drag components as described in Subsecs. B.4.1-2.

The drag polar is obtained point by point by repeating this procedure for different lift coefficients. In this application, the curve is modeled by a parabola; therefore, the process must be repeated only three times to obtain the coefficients in Eq. A.1.

B.5 CONTROLS CALCULATION

B.5.1 Wing Shape (Vector H)

In order to design the structure of the wing, the global structural subproblem must have access to the wing shape. The shape information to send from the aerodynamic subproblem to the global structural subproblem is collected in vector H

$$\{H\}^T = \{b, b_b, c_r, c_b, c_t\} \tag{B.49}$$

To obtain a linear approximation to the constraint satisfactions in the global structural subproblem, we need the matrix $\partial H/\partial X_a$ (see Chap. IV). This matrix is easily obtained from Eq. B.49.

B.5.2 Wing Element Shape (Vector H_j)

When performing the detailed structural design, the wing is modelled by n_s cylindrical elements of equal length and constant geometric and structural properties. The element properties are chosen to be those of their middle section in the actual wing. Three shape parameters must be known for the analysis of any one element. They are given for element j by the vector

$$\{H_j\}^T = \{b_j, c_j, t_j\} \tag{B.50}$$

where b_j, c_j and t_j are, respectively the element length, chord and thickness. The element length is

$$b_j = b/n_s \tag{B.51}$$

If we define

$$m_j = (2j-1)/(2n_s) \tag{B.52}$$

The reference station for wing element j is determined by

$$y_j = m_j b \tag{B.53}$$

The element chord (c_j) and thickness (t_j) are now found from Eqs. B.1-2, where y is set to y_j.

While optimizing the aerodynamic subproblem, we need linear approximations to the constraint satisfaction in the local structural subproblems in terms of the aerodynamic variables (see Chap. IV). These linear expansions contain the matrix $\partial H_j/\partial X_a$, which may be obtained from Eq. B.50. Its non zero entries are as follows.

$$\partial b_j/\partial b = 1/n_s$$

$$\partial c_j/\partial b = [m_j(c_b-c_r)]/b_b \qquad y_j<b_b$$

$$= [(1-m_j)(c_t-c_b)b_b]/(b-b_b)^2 \qquad y_j\geq b_b$$

$$\partial c_j/\partial b_b = [m_j(c_r-c_b)b]/b_b^2 \qquad y_j<b_b$$

$$= [(1-m_j)(c_b-c_t)b]/(b-b_b)^2 \qquad y_j\geq b_b$$

$$\partial c_j/\partial c_r = \partial t_j/\partial t_r = 1-m_jb/b_b \qquad y_j<b_b$$

$$= 0 \qquad y_j\geq b_b$$

$$\partial c_j/\partial c_b = \partial t_j/\partial t_b = m_jb/b_b \qquad y_j<b_b$$

$$= 1-(m_jb-b_b)/(b-b_b) \qquad y_j\geq b_b$$

$$
\begin{aligned}
\partial c_j/\partial c_t &= \partial t_j/\partial t_t = 0 && y_j < b_b \\
&= (m_j b - b_b)/(b - b_b) && y_j \geq b_b \\
\partial t_j/\partial b &= [m_j(t_b - t_r)]/b_b && y_j < b_b \\
&= [(1-m_j)(t_t - t_b)b_b]/(b-b_b)^2 && y_j \geq b_b \\
\partial t_j/\partial b_b &= [m_j(t_r - t_b)b]/b_b^2 && y_j < b_b \\
&= [(1-m_j)(t_b - t_t)b]/(b-b_b)^2 && y_j \geq b_b
\end{aligned} \tag{B.54}
$$

B.5.3 Aerodynamic Loads Calculation

The Federal Aviation Agency requires that the structural integrity of the sailplane be verified for a number of different load cases (see Ref. 40). The cases considered in this study correspond to symmetric wing loadings, and their selection will be discussed in App. C. Each symmetric load case is uniquely defined by an indicated airspeed V_t and a wing load factor n_{Nw}. The total load on the wing is then given in coefficient form by

$$C_{Nw} = 2\frac{n_{Nw}W}{\rho S V_t^2} \tag{B.55}$$

The total wing load is assumed to act in a direction perpendicular to the reference chord of the section corresponding to the mean aerodynamic chord, as shown on

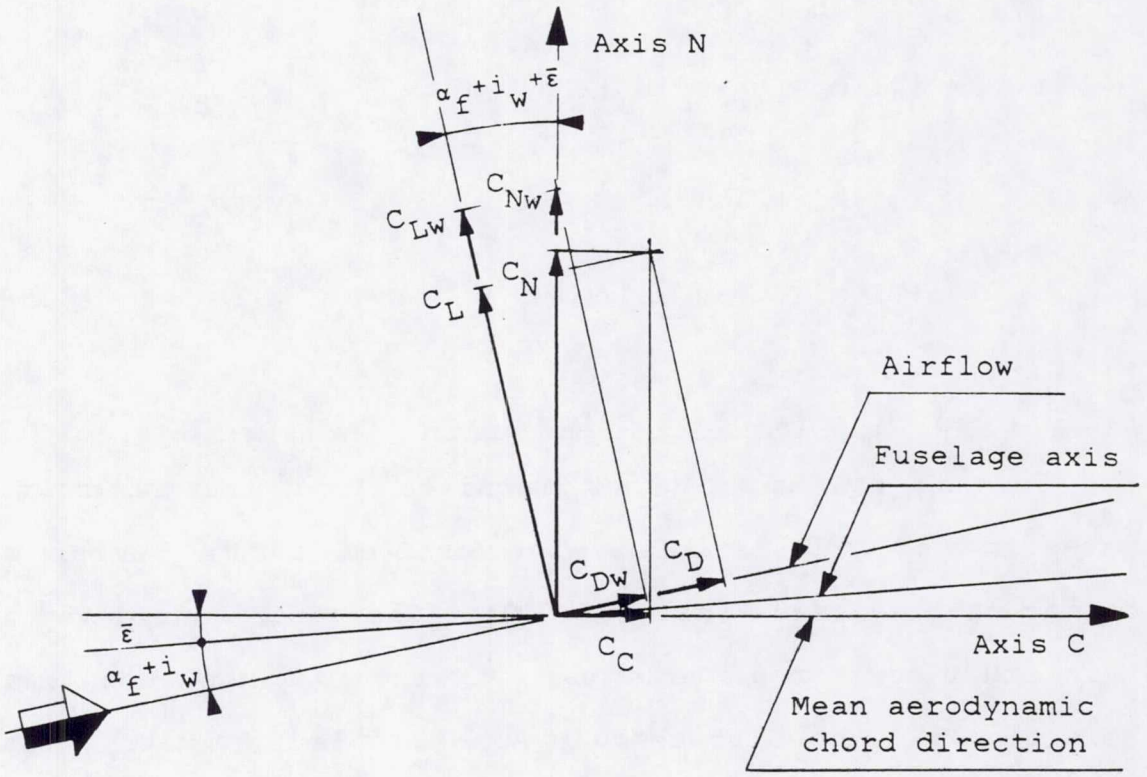

Figure 17: Definition of force coefficients for the wing alone and the total sailplane.

Fig. 17.

To determine the spanwise distributions of aerodynamic forces and moment we must find the fuselage angle of attack α_f which corresponds to c_{Nw}. Following the developments outlined in Subsecs. B.3.1 and B.4.1, we obtain the wing lift and drag coefficients (C_{Lw} and C_{Dw}) as functions of α_f (Eqs. B.22 and B.41), the Reynolds number being based on V_t. Then it is clear from Fig. 17 that

$$C_{Nw} = C_{Lw}(\alpha_f)\cos(\alpha_f+i_w+\bar{\varepsilon})+C_{Dw}(\alpha_f)\sin(\alpha_f+i_w+\bar{\varepsilon}) \qquad (B.56)$$

In what follows we will assume that the load cases are selected so that $\alpha_f+i_w+\bar{\varepsilon}$ is small, so

$$C_{Nw} = C_{Lw}(\alpha_f) \qquad (B.57)$$

The only unknown in Eq. B.57 is the angle of attack α_f, which may be easily solved for. Then, the spanwise distributions of lift c_l' and drag c_d' are found from Eqs. B.21 and B.41, respectively. The distribution of coefficient of pitching moment about the section aerodynamic center c_{mac} is taken from Eq. B.10, ignoring finite span effects. This situation is summarized on Fig. 18 for an arbitrary wing section. For subsequent calculations, we express the aerodynamic forces and moments in a system of axes centered in the plane of symmetry of the sailplane with:

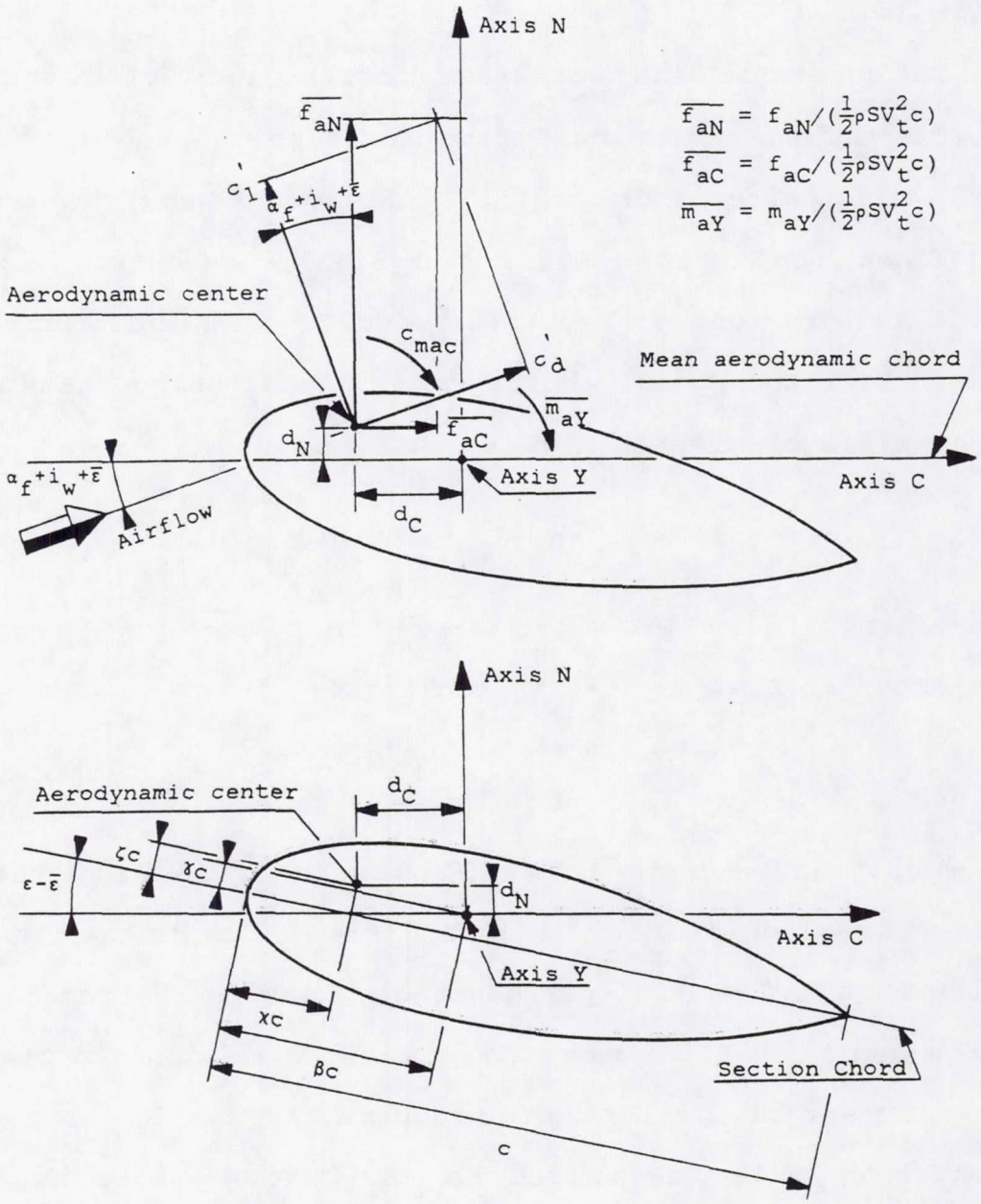

Figure 18: Wing section: aerodynamic forces applied and corresponding geometric parameters.

i) axis Y previously defined, spanwise and perpendicular to the plane of symmetry,

ii) axis C in the plane of symmetry and parallel to the mean aerodynamic chord,

iii) axis N in the plane of symmetry also and perpendicular to axes Y and C.

Note that axis Y joins the points of maximum thickness for each section. Those points are located at distances βc from the leading edge of the section and γc above the chord line; β and γ are constants characteristic of the selected airfoil and are given by Eq. B.13.

At section y, the forces per unit length reduce to (see Fig. 18)

$$f_{aN}(y) = .5\rho V_t^2 c(y) c_l'(y)$$

$$f_{aC}(y) = .5\rho V_t^2 c(y) c_d'(y) \qquad \text{(B.58)}$$

These forces act at the aerodynamic center of the section, which is located at distances $\chi(y)c(y)$ from the leading edge and $\zeta(y)c(y)$ above the chord line. χ and ζ are also given in Sec. B.1; like the other airfoil parameters, they are functions of the thickness ratio and the Reynolds number. Measured positively along the axes C and N, the moment arms of the forces with respect to axis Y are (see Fig. 18)

$$d_C(y) = -[\beta - \chi(y)]c(y)$$

$$d_N(y) = -[\gamma - \zeta(y)]c(y) \qquad \text{(B.59)}$$

The total moment per unit length of the aerodynamic forces at section y (positive clockwise) is finally

$$m_{aY}(y) = .5\rho V_t^2 c^2(y) c_{mac}(y) - f_{aN}(y) d_c(y) + f_{aC}(y) d_N(y) \qquad \text{(B.60)}$$

We conclude this subsection by finding the total sailplane load factors. At this point we know the angle of attack yielding the wing load factor n_{Nw} and, also, the flight speed V_t and, therefore, the Reynolds number. We perform the calculations described in Subsecs. B.3.1-3 and B.4.1-2 to find the lift and drag coefficients C_L and C_D. Then, from Fig. 18 the aerodynamic force coefficients in the YCN set of axes are (again for small $(\alpha_f + i_w + \bar{\varepsilon})$)

$$C_N = C_L$$

$$C_C = C_D \qquad \text{(B.61)}$$

The total sailplane load factors are

$$n_N = \frac{\rho S V_t^2 C_N}{2W}$$

$$n_C = \frac{\rho S V_t^2 C_C}{2W} \qquad \text{(B.62)}$$

B.5.4 Load Parameters (Vector A)

The wing will be designed so as to meet three structural requirements (see App. C). The aerodynamic parameters needed to perform the structural design will be calculated in the aerodynamic subproblems and communicated to the global structural subproblem through vector A, which will be partitioned into three vectors, one per structural requirement.

$$\{A\}^T = \{\{A^1\}^T, \{A^2\}^T, \{A^3\}^T\} \tag{B.63}$$

Requirement 1 limits the displacement of the wing tip. This necessitates the knowledge of the sailplane normal load factor n_N and of the spanwise distribution of aerodynamic force normal to the mean aerodynamic chord f_{aN}. The latter will be transmitted to the global structural subproblem as a vector $\{f_{aN}\}$ containing the values of $f_{aN}(y)$ calculated at (n_f+1) points along the wing; those points being equally spaced and including the wing root and tip. Therefore

$$\{A^1\}^T = \{n_N^1, \{f_{aN}^1\}^T\} \tag{B.64}$$

Requirement 2 is that no failure or buckling occur in the wing elements in a high-speed positive pull-up maneuver. To perform the necessary calculations, the sailplane load

factors n_N and n_C as well as the corresponding spanwise distributions of aerodynamic transverse force f_{aN} and moment m_{aY} must be known. Hence

$$\{A^2\}^T = \{n_N^2, n_C^2, \{f_{aN}^2\}^T, \{m_{aY}^2\}^T\} \tag{B.65}$$

where $\{f_{aN}^2\}$ and $\{m_{aY}^2\}$ are obtained by the process described above. While structural design to requirement 2 is the object of the local structural subproblems (App. D), vector $\{A^2\}$ must first be transmitted to the global structural subproblem so as to account for the effect of inertia on the spanwise distributions of forces and moment.

Finally, requirement 3 is that the wing torsional divergence speed must exceed a given limit. As will be shown in App. C, the spanwise distributions of lift curve slope $c'_{l\alpha}$ and chordwise position of the aerodynamic center χ are required for the calculation of the divergence speed. Therefore

$$\{A^3\}^T = \{\{c'^3_{l\alpha}\}^T, \{\chi^3\}^T\} \tag{B.66}$$

where, again, $\{c'^3_{l\alpha}\}$ and $\{\chi^3\}$ contain appropriate values of $c'_{l\alpha}(y)$ and $\chi(y)$ for equally spaced wing stations.

The matrices $\partial A/\partial X_a$ and $\partial A/\partial X_p$ are needed when constructing linear extrapolations to the measures of constraint satisfaction in the global structural subproblem

(App. C). These matrices will be found by finite differences.

Appendix C

GLOBAL STRUCTURAL SUBPROBLEM

The global structural subproblem objective is to design the wing structure so as to achieve the total sailplane weight specified in the performance subproblem. Once a weight is chosen for the sailplane fuselage, tailplane, equipment and pilot, the available weight for structural and non-structural wing elements is known. The design variables of this subproblem are the coefficients in the spanwise distributions of weight and flexural and torsional stiffnesses. The optimization is subjected to the constraints that the wing tip deflection is limited in high speed straight flight and that the torsional divergence speed is beyond a set limit.

The wing shape and aerodynamic load parameters are obtained from the aerodynamic subproblem. The wing flexural and torsional responses are investigated using Rayleigh-Ritz analyses. The redistribution of aerodynamic forces due to the wing elastic deformations is neglected.

Optimization and sensitivity analysis require that derivatives of the wing weight, tip displacement and divergence dynamic pressure be calculated with respect to the subproblem variables and parameters. Unless otherwise

specified, these derivatives are found by finite differences.

C.1 NOMENCLATURE

$\{A\}$: vector of aerodynamic load parameters.

$\{A^1\}$, $\{A^2\}$, $\{A^3\}$: subvectors of $\{A\}$.

b : wing semispan.

c : wing chord.

c'_{le}, $c'_{l\alpha}$: section three-dimensional elastic lift, lift curve slope coefficients.

e_C, e_N : Fig. 19.

EI, EI_i, EI_{ej} : distribution of wing bending stiffness, ith coefficient in that distribution (Eq. C.1), target bending stiffness for element j.

EI^1, EI^1_o : bending stiffness distribution for the linear wing model, root bending stiffness for that model.

f_{aN}, f_{aNi}, f'_{aN} : distribution of aerodynamic forces normal to the mean aerodynamic chord, aerodynamic force at spanwise station i, distribution estimated by Lagrangian interpolation (Eq. C.4).

f_N : distribution of total forces normal to the mean aerodynamic chord.

f^1, f^1_o : distribution of transverse forces on the linear model, root value of that distribution.

F_j : vector containing the end forces acting on wing element j.

$\{H\}$: vector containing parameters describing the wing shape.

GJ, GJ_i, GJ_{ej} : distribution of wing torsional stiffness, ith coefficient in that distribution (Eq. C.1), target torsional stiffness for element j.

K_j : vector containing the target stiffnesses for element j.

m : distribution of moment of forces about spanwise axis including effect of elastic deformations.

m_{aY}, m_{aYi}, m'_{aY} : distribution of aerodynamic moment about spanwise axis, aerodynamic moment at spanwise station i, distribution estimated by Lagrangian interpolation (Eq. C.4).

m_{eaY} : distribution of elastic aerodynamic moment about spanwise axis.

m^*_{eaY}, m^*_{eaYi} : Eqs. C.16-17.

m_Y : distribution of total moment of forces about spanwise axis, includes aerodynamic and inertia forces.

M_i : bending moment in section i.

n_C : sailplane longitudinal load factor.

n_f : number of intervals in the discretization of the distributions of aerodynamic characteristics.

n_N, n_{Nw}: sailplane normal load factor, wing normal load factor.

n_s : number of intervals in the discretization of the distributions of wing weight and stiffnesses at the global level, number of wing elements in the discretization of the wing at the local level.

P_i, P_i' : Lagrange polynomials, Eqs. C.1, C.4.

q, q_D : dynamic pressure, divergence dynamic pressure.

S_f : ultimate safety factor.

T_i : torque at wing station i.

u, u^*, u_t, u_{tmax} : wing bending mode, non-dimensional bending mode, bending deflection at the wing tip, maximum value for u_t.

V_t, V_d, V_D, V_{Dmin} : indicated flight speed, maximum indicated dive speed, divergence speed, minimum divergence speed.

V_i : shear force at wing station i.

w, w_i, w_{ej} : spanwise distribution of wing weight per unit length, ith coefficient in that distribution (Eq. C.1), target weight per unit length for element j.

W : sailplane gross weight.

W_{nw} : weight of sailplane without wings.

y, y_i : spanwise coordinate, spanwise coordinate for station i.

$\{X_g\}$: vector containing global structural subproblem design variables.

α : slope of the force distribution on the linear wing model (Eq. C.9).

α_r : wing section rigid angle of attack.

β : slope of the stiffness distribution on the linear wing model (Eq. C.9)

β, δ : chordwise position of the section elastic axis, and center of gravity with respect to section leading edge, normalized with respect to section chord (Fig. 19).

ε, ε : wing geometric twist (see Subsec. B.2.1), wing twist at the mean aerodynamic chord.

γ, η : normal position of the section elastic axis and center of gravity with respect to section chord, normalized with respect to section chord (Fig. 19).

η, η^* : wing bending modes.

χ; χ_i : chordwise position of section aerodynamic center with respect to the section leading edge, normalized with respect to the section chord; value of χ at station i.

ρ : mass density of air.

θ, θ^* : wing torsion modes.

Commonly used superscripts

1, 2, 3 : aerodynamic load parameters related to the various structural design requirements.

' : three-dimensional airfoil aerodynamic quantity (i.e., a quantity corrected for finite span effects).

Commonly used subscripts

i as in A_i : element i of vector A, or

: discretized value of function A(y), i.e., $A_i = A(y_i)$.

ij : element ij of matrix.

Special symbols

{ } as in {A} : vector A, or

: discrete values of function A(y) collected in vector $\{A\}^T = \{A(y_1), A(y_2), \ldots\}$

[ ] : square matrix.

C.2 GLOBAL STRUCTURAL LEVEL WING MODEL

C.2.1 Model Description

To study the wing behavior at the global structural level, we model it as a straight beam aligned with the previously defined spanwise axis Y. We consider only two types of wing deformations.

i) Bending deformations in a direction normal to the wing mean aerodynamic chord, or, along axis N defined in Subsec. B.5.3.

ii) Twisting deformations about the spanwise axis Y.

This neglects chordwise bending.

The parameters necessary to the description of the wing global structural behavior are the distributions of bending stiffness EI(y), torsional stiffness GJ(y) and total wing weight (structural and non-structural) per unit length w(y). It must be noted that the wing is made of composite material as detailed in App. D. However the lay-ups are chosen so that no bending-torsion coupling exists. Therefore, the parameters retained will be adequate.

The distributions will be written as follows

$$EI(y) = \sum_{i=0}^{n_s} EI_i P_i(y)$$

$$GJ(y) = \sum_{i=0}^{n_s} GJ_i P_i(y)$$

$$w(y) = \sum_{i=0}^{n_s} w_i P_i(y)$$

$$P_i(y) = \frac{\prod_{\substack{j=0 \\ \neq i}}^{n_s} (y-y_j)}{\prod_{\substack{j=0 \\ \neq i}}^{n_s} (y_i-y_j)}$$

$$y_i = ib/n_s; \qquad i=0,\ldots,n_s \tag{C.1}$$

These expressions are interpolations based on Lagrangian polynomials (see Ref. 41). The EI_i, GJ_i and w_i are stiffnesses and weight values at selected, equally spaced stations y_i along the wing. They are the design variables of the global structural subproblem. They are collected in vector X_g and will be referred to as global stiffnesses.

C.2.2 Elastic Axis and Center of Gravity Position

The structural model described in the previous subsection is such that the elastic axis is assumed to lie on the spanwise axis Y. Clearly, the elastic axis position depends directly on the detailed wing design; it should be treated as a reverse control (see Chap. 3). However, this control will be ignored in a first approach to the design. It turns out that this is probably a very reasonable assumption, considering the detailed structural lay-out chosen (see App. D).

The position of a section center of gravity must be known to properly account for the inertia forces. This is also a reverse control. Initially, the mass center of gravity of a wing section will be assumed at the area center of gravity of that section, that is, at distances δc from the section leading edge and ηc above the reference chord (see Subsec. B.2.2).

C.2.3 Sailplane Weight

The total sailplane weight is

$$W = W_{nw} + 2\int_0^b w(y)dy$$

where W_{nw} includes the weight of the fuselage, tailplane, equipment and pilot; it is a fixed parameter in this design problem. For optimization and sensitivity analysis, the derivatives of the weight with respect to b and the w_i are needed. If we perform the change of variables $y=\eta b$ in Eq. C.1, we find

$$P_i(y) = \frac{\prod_{\substack{j=0 \\ \neq i}}^{n_s} (\eta - j/n_s)}{\prod_{\substack{j=0 \\ \neq i}}^{n_s} (i-j)/n_s} = P_i(\eta)$$

therefore

$$W = W_{nw} + 2b \sum_{i=o}^{n_s} w_i \int_o^1 P_i(\eta) d\eta \qquad (C.2)$$

and, clearly

$$\frac{\partial W}{\partial b} = 2 \sum_{i=o}^{n_s} w_i \int_o^1 P_i(\eta) d\eta$$

$$\frac{\partial W}{\partial w_j} = 2b \int_o^1 P_j(\eta) d\eta \qquad (C.3)$$

C.3 STRUCTURAL DESIGN REQUIREMENTS

In order to obtain certification of an airplane by the appropriate authorities, one must insure that the structure is capable of withstanding a number of predetermined loading conditions. Also, static and dynamic instabilities should not occur within the flight envelope. Reference 40 describes the requirements set by the Federal Aviation Agency (FAA) on sailplane designs. These requirements cover stresses in load cases corresponding to symmetric or non-symmetric flight conditions, towed flight and landing. Some requirements also cover flutter. In addition to satisfying the conditions set by the relevant regulating agency, the designer may have to investigate loading conditions specific to his own design. Clearly, a vast amount of calculation is

required in the structural design phase of a project. While modern optimization methods are perfectly capable of handling multiple design conditions, it is preferable to design the structure for a limited number of appropriately selected load cases and instability modes. The resulting design may then be checked for the remaining conditions and optimization may be performed again with additional load cases and instability modes, if desired.

In this work, the structure will be designed to satisfy the three requirements described below.

i) Requirement 1: limit out-of-plane bending. Sailplane wings are typically long and flexible. Excessive bending flexibility may result in control surface jamming, inappropriate ground clearance during landing or unsatisfactory dynamic behavior. We therefore require that the wing tip deflection be below a maximum limit u_{tmax} at an indicated airspeed V_t = 85 m/s, and a wing load factor n_{Nw} = 1. Since the wing does not present bending-torsion coupling, the constraint will control bending stiffness and weight distributions.

ii) Requirement 2: limit stresses and preclude local instabilities. To size the details of the structure (see App. D), we require that no failure

occurs at a flight condition defined by n_{Nw} = 5.33, V_t = 100. m/s. This corresponds to a pull-up at maximum authorized dive speed. This is a design condition, therefore; an ultimate safety factor S_f = 1.5 must be used when calculating the ultimate loads.

iii) Requirement 3: limit wing divergence dynamic pressure. The FAA specifies that the sailplane must be demonstrated "free of undesirable flight characteristics for speeds below the dive speed" (V_d). The maximum authorized dive speed for this type of sailplane is about V_d = 100 m/s. We require that the wing divergence speed V_D be such that $V_D \geq 120.$ m/s. For straight wings with no bending-torsion coupling, divergence is torsional in nature. This constraint will therefore control the torsional stiffness distribution.

C.4 WING TIP DEFLECTION CALCULATION

C.4.1 Total Spanwise Distributions of Force and Moment

At the end of the optimization of the wing aerodynamic design the spanwise distributions of aerodynamic force $f_{aN}(y)$ and moment $m_{aY}(y)$ as well as the total sailplane load factors n_N and n_C are calculated for the wing load factors

n_{Nw} and flight speeds V_t corresponding to Requirements 1 and 2. Discrete values of force f_{aNi} and moment m_{aYi} for various spanwise stations y_i are transmitted to the global structural subproblem in vectors A^1 and A^2 (see Subsec. B.5.4). The spanwise distributions of force and moment may be approximated by interpolation based on Lagrangian polynomials.

$$f'_{aN}(y) = \sum_{i=0}^{n_f} f_{aNi} P'_i(y)$$

$$m'_{aY}(y) = \sum_{i=0}^{n_f} m_{aYi} P'_i(y)$$

$$P'_i(y) = \frac{\prod_{\substack{j=0 \\ \neq i}}^{n_f} (y-y_j)}{\prod_{\substack{j=0 \\ \neq i}}^{n_f} (y_i-y_j)}$$

$$y_i = ib/n_f; \qquad i=0,\ldots,n_f \tag{C.4}$$

To determine the total spanwise distribution of forces and moments, we add the contributions of inertia to the distributions given in Eq. C.4. The situation is illustrated in Fig. 19 for a wing section at spanwise station y. The inertia forces are assumed to act at the

section area center of gravity. Measured positively along the axes C and N, the moment arm of these inertia forces with respect to axis Y are, for small wing twist (small $\varepsilon(y)-\bar{\varepsilon}$)

$$e_C(y) = (\delta-\beta)c(y)$$

$$e_N(y) = (\eta-\chi)c(y) \qquad (C.5)$$

The distributions of transverse force and moment are, finally

$$f_N(y) = f'_{aN}(y)-n_N w(y)$$

$$m_Y(y) = m'_{aY}(y)+e_C(y)n_N w(y)-e_N(y)n_C w(y) \qquad (C.6)$$

The distribution of chord c(y) is known to the global structural subproblem since it is communicated from the aerodynamic subproblem in vector H (see Fig. 4 and Subsec. B.5.1).

C.4.2 Wing Bending Response

The wing bending model is a cantilever beam of varying bending stiffness EI(y) (Eq. C.1) under varying transverse load $f_N(y)$ (Eq. C.6). In this subsection, we describe the calculation of the wing tip displacement using a single mode Rayleigh-Ritz analysis.

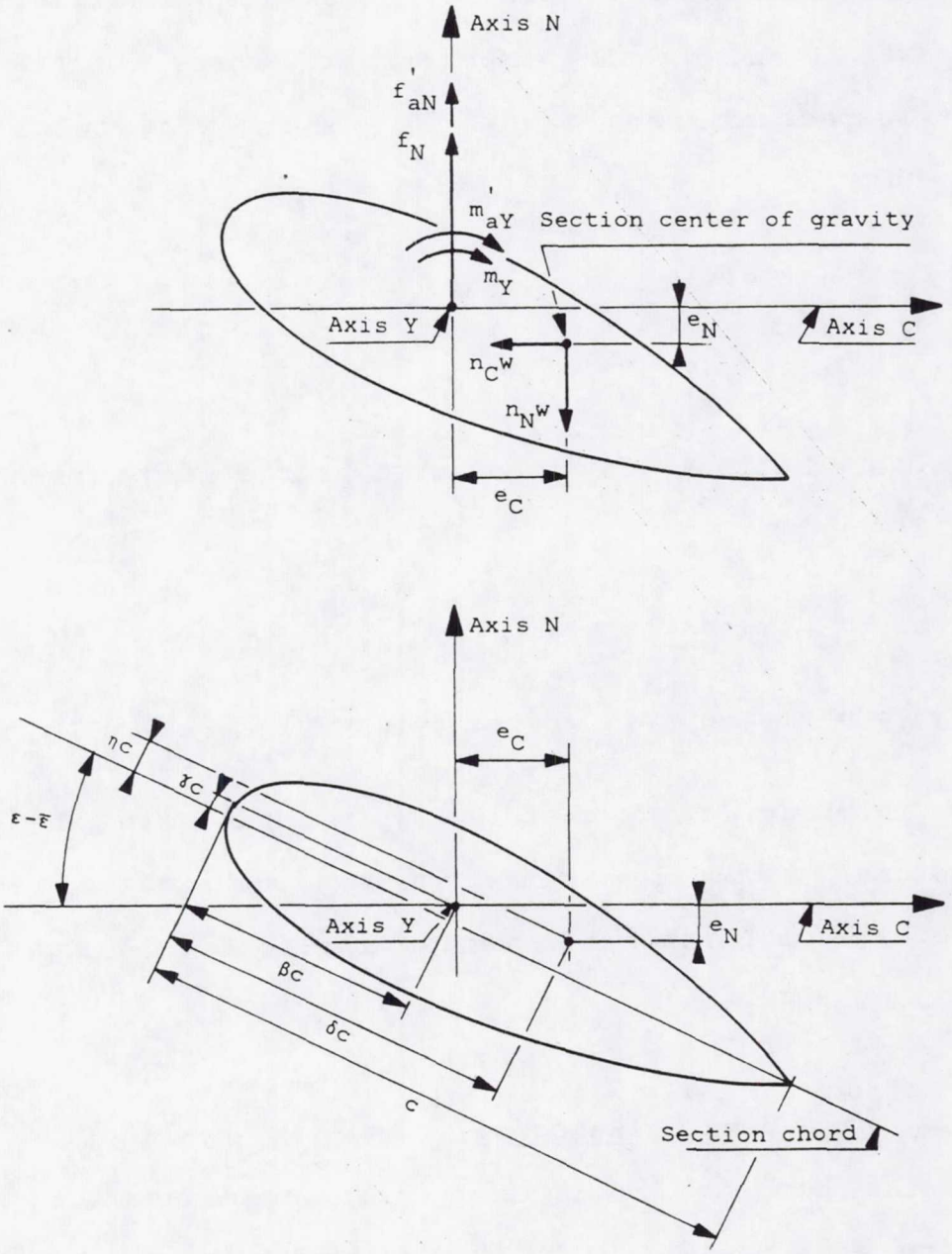

Figure 19: Wing section, forces applied and corresponding geometrical parameters.

C.4.2.1 Wing Tip Deflection

Assume that the displacement mode of the wing is given in terms of the non-dimensional spanwise coordinate $\eta=y/b$ as

$$u(\eta) = Du^*(\eta) \tag{C.7}$$

where D is a constant. The specific expression chosen for $u^*(\eta)$ will be given in the next subsection. By requiring that the work of the external force $f_N(\eta)$ equals the bending strain energy for a virtual displacement about $u^*(\eta)$, we find the tip displacement u_t as

$$u_t = u(1) = u^*(1)b^4 \frac{\int_o^1 f_N(\eta)u^*(\eta)d\eta}{\int_o^1 EI(\eta)[u^{*\prime\prime}(\eta)]^2 d\eta} \tag{C.8}$$

where $(\ )' = \partial(\ )/\partial\eta$ and $(\ )'' = \partial^2(\ )/\partial\eta^2$.

C.4.2.2 Assumed Displacement Mode

The shape of the assumed mode will be taken as the displacement of a beam with linearly varying bending stiffness under linearly varying transverse load (hereafter referred to as model beam). Using the superscript 1 to refer to the model beam, we have

$$EI^1(\eta) = EI_o^1(1+\beta\eta)$$

$$f^1(\eta) = f_o^1(1+\alpha\eta) \tag{C.9}$$

The model beam obeys the following differential equation and boundary conditions

$$[(1+\beta\eta)u''(\eta)]'' = k(1+\alpha\eta)$$

$$k = f_o^1 b^4/EI_o^1$$

$$u(\eta)|_{\eta=0} = u'(\eta)|_{\eta=0} = 0$$

$$(1+\beta\eta)u''(\eta)|_{\eta=1} = [(1+\beta\eta)u''(\eta)]'|_{\eta=1} = 0 \qquad (C.10)$$

The solution to Eq. C.10 is

$$u(\eta) = ku^*(\eta)$$

$$u^*(\eta) = A_4\eta^4+A_3\eta^3+A_2\eta^2+A_1\eta+A_s(1+\beta\eta)\ln(1+\beta\eta)$$

$$A_1 = -[\alpha(-1+3\beta^2+2\beta^3)+3\beta(1+\beta)^2]/6\beta^4$$

$$A_2 = [\alpha(1-3\beta^2)-3\beta(1+2\beta)]/12\beta^3$$

$$A_3 = (3\beta-\alpha)/36\beta^2$$

$$A_4 = \alpha/72\beta$$

$$A_s = -A_1/\beta \qquad (C.11)$$

The mode shape $u^*(\eta)$ in Eq. C.11 will be used together with Eq. C.8 to calculate the displacement of the wing tip.

In order to carry out these calculations, we need to estimate the parameters α and β for the model beam.

Parameter α is found by requiring that the actual load $f_N(\eta)$ and the linear one $f^1(\eta)$ are statically equivalent. That is

$$\int_0^1 f_N(\eta)d\eta = \int_0^1 f^1(\eta)d\eta$$

$$\int_0^1 f_N(\eta)\eta d\eta = \int_0^1 f^1(\eta)\eta d\eta$$

This yields

$$\alpha = (3I_2-1.5I_1)/(I_1-1.5I_2)$$

$$I_1 = \int_0^1 f_N(\eta)d\eta$$

$$I_2 = \int_0^1 f_N(\eta)\eta d\eta \qquad \text{(C.12)}$$

A parallel approach was used to estimate parameter β. However, this occasionaly turned out to result in equivalent linear stiffness distributions that became negative. Therefore, parameter β is obtained by requiring that the actual distribution of stiffness $EI(\eta)$ and the linear $EI^1(\eta)$ have equal end values. This permits one to avoid negative stiffnesses, as the end stiffnesses $EI(0)$ and $EI(1)$ are design variables at the global structural level. They can be kept positive at all time during the optimization process by suitable side constraints. We have

$$EI(\eta)|_{\eta=0} = EI^1(\eta)|_{\eta=0}$$

$$EI(\eta)|_{\eta=1} = EI^{1}(\eta)|_{\eta=1}$$

This gives

$$\beta = EI(1)/EI(0)-1 \qquad (C.13)$$

C.5 WING DIVERGENCE DYNAMIC PRESSURE

A wing section is depicted in Fig. 20. If the wing was rigid, the angle of attack measured with respect to the section reference chord would be α_r. The total twisting moment on the wing would be $m_Y(y)$, as given by Eq. C.6. If the wing flexibility is taken into account, the section undergoes a twist θ which results in an increment in the lift coefficient.

$$c'_{le}(y) = c'_{l\alpha}(y)\theta(y) \qquad (C.14)$$

This elastic lift causes an increment in torque per unit length (elastic torque)

$$m_{eaY}(y) = .5\rho V_t^2 c^2(y)[\beta-x(y)]c'_{l\alpha}(y)\theta(y) \qquad (C.15)$$

or, if we set

$$q = .5\rho V_t^2$$

$$m^*_{eaY}(y) = c^2(y)[\beta-x(y)]c'_{l\alpha}(y)$$

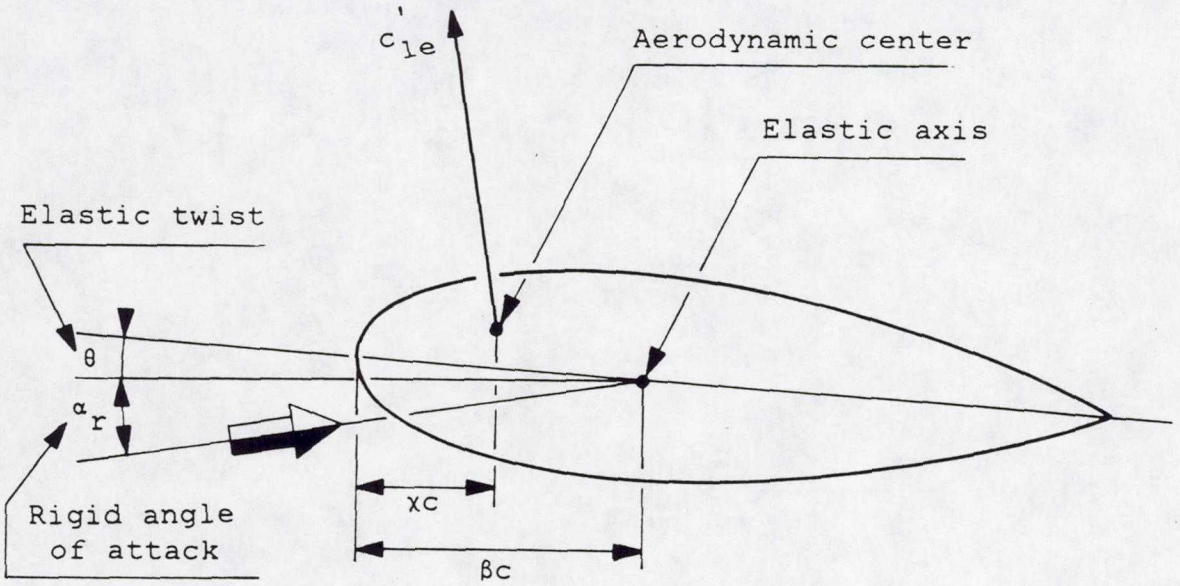

Figure 20: Lift coefficient induced by the wing elastic twist.

we have

$$m_{eaY}(y) = qm^{*}_{eaY}(y)\theta(y) \qquad (C.16)$$

where q is the flight dynamic pressure. m^{*}_{eaY}, the elastic torque per units of length, dynamic pressure and elastic deformation may be estimated on the basis of the information contained in the vectors A (subvector A^3) and H (see Fig 4).

$$m^{*}_{eaY}(y) = \sum_{i=0}^{n_f} m^{*}_{eaYi} P'_i(y)$$

$$m_{eaYi} = c^2(y_i)(\beta - x^3_i)c'^3_{l\alpha i}$$

$$P'_i(y) = \frac{\prod_{\substack{j=0 \\ \neq i}}^{n_f} (y-y_j)}{\prod_{\substack{j=0 \\ \neq i}}^{n_f} (y_i-y_j)}$$

$$y_i = ib/n_f; \qquad i=0,\ldots,n_f \qquad (C.17)$$

Vector H contains what is necessary to calculate $c(y_i)$ (see Eqs. B.1 and B.49), while vector A^3 contains the x^3_i and $c'^3_{l\alpha i}$ (see Eq. B.66).

C.5.1 Wing Divergence Dynamic Pressure Calculation

The torsional model of the wing is a cantilever beam of varying stiffness GJ(y) (Eq. C.1), under varying twisting moment $m(y) = m_Y(y)+m_{eaY}(y)$ (Eqs. C.6 and C.16-17). The divergence dynamic pressure can be calculated using a single mode Rayleigh-Ritz analysis. Using again the normalized coordinate η, we write the wing twist as

$$\theta(\eta) = E\theta^*(\eta) \tag{C.18}$$

For a given dynamic pressure, the wing twist amplitude E may be found by requiring that the work of the external forces $m(\eta)$ equals the torsion strain energy for a virtual displacement about $\theta^*(\eta)$.

$$E = \frac{b^2\int_o^1 m_Y(\eta)\theta^*(\eta)d\eta}{\int_o^1 GJ(\eta)\theta^{*'2}(\eta)d\eta - qb^2\int_o^1 m^*_{eaY}(\eta)\theta^{*2}(\eta)d\eta} \tag{C.19}$$

where, again, $(\ )' = \partial(\ )/\partial\eta$. The divergence dynamic pressure is that which makes E unbounded

$$q_D = \frac{\int_o^1 GJ(\eta)\theta^{*'2}(\eta)d\eta}{b^2\int_o^1 m^*_{eaY}(\eta)\theta^{*2}(\eta)d\eta} \tag{C.20}$$

For this analysis, we will assume the torsion mode to be the divergence mode of a uniform wing with uniform twisting

moment per unit elastic twist (see Ref. 7).

$$\theta^*(\eta) = \sin(\pi\eta/2) \tag{C.21}$$

C.6 CONTROLS CALCULATION

C.6.1 Wing Element Target Stiffnesses (Vector K_j)

When performing the detailed structural design, the wing is modelled by n_s cylindrical wing elements of equal length and constant geometric and structural properties. Therefore, a wing element spans the distance between two consecutive stations used in the definition of the distributions of stiffness at the global level (see Subsec. C.2.1). Three global structural characteristics must be known for the synthesis of any one element; for element j, they are given by the vector

$$\{K_j\}^T = \{EI_{ej}, GJ_{ej}, w_{ej}\} \tag{C.22}$$

These target flexural stiffness, torsional stiffness and weight per unit length will be taken for a given element as the averages between the corresponding global level variables.

$$EI_{ej} = .5(EI_{j-1}+EI_j)$$

$$GJ_{ej} = .5(GJ_{j-1}+GJ_j)$$

$$w_{ej} = .5(w_{j-1}+w_j) \tag{C.23}$$

The matrix $\partial K_j/\partial X_g$ is needed while developing the linear approximation to the constraint violations for local structural subproblem j. That matrix is easily obtained from Eq. C.23.

C.6.2 Element End Forces (Vector F_j)

The detailed structural design of each of the n_s wing elements is made to the values of the forces and moments calculated at the inboard side of the element. This seems justified in view of the type of loading chosen.

The forces acting at the inboard section of element j are collected in vector F_j

$$\{F_j\}^T = \{V_j, M_j, T_j\} \tag{C.24}$$

with V_j, M_j, T_j being respectively shear force, bending moment and twisting moment. To obtain $\{F_j\}$, the flight conditions specified for Requirement 2 (see Sec. C.3) are used to determine the corresponding spanwise distributions of aerodynamic force $f^2_{aN}(y)$ and moment $m^2_{aY}(y)$ (see Subsec. B.5.4); this is done in the aerodynamic subproblem. These quantities are passed in vector A to the global structural subproblem where they are modified to account for inertia effects (see Subsec. C.4.1). Finally, numerical integration is used to obtain the components of $\{F_j\}$.

We have

$$V_j = \sum_{i=o}^{n_f} f_{aNi}^2 \int_{y_j}^{b} P_i'(y)dy - n_N^2 \sum_{i=o}^{n_s} w_i \int_{y_j}^{b} P_i(y)dy$$

$$M_j = \sum_{i=o}^{n_f} f_{aNi}^2 \int_{y_j}^{b} P_i'(y)ydy - n_N^2 \sum_{i=o}^{n_s} w_i \int_{y_j}^{b} P_i(y)ydy$$

$$T_j = \sum_{i=o}^{n_f} m_{aYi}^2 \int_{y_j}^{b} P_i'(y)dy$$

$$+ [n_N^2(\delta-\beta) - n_C^2(\eta-\gamma)] \sum_{i=o}^{n_s} w_i \int_{y_j}^{b} P_i(y)c(y)dy$$

$$y_j = (j-1)b/n_s; \quad j=o,\ldots,n_s \qquad \text{(C.25)}$$

where y_j defines the inboard section of element j.

The matrices $\partial F_j/\partial X_{sg}$, $\partial F_j/\partial A$ and $\partial F_j/\partial H$ are needed for the development of linear approximations to the measures of constraint violation in local subproblem j. The two former matrices can be easily obtained analytically from Eq. C.25, the latter will be calculated by finite differences.

Appendix D

LOCAL STRUCTURAL SUBPROBLEM

The task of the local structural subproblem is to find the detailed design of the wing which corresponds to the spanwise distributions of weight and stiffnesses chosen in the global structural subproblem. The optimization is subjected to the additional constraints that the stresses at selected points in the structure do not exceed appropriate allowables and that the various wing components be free of buckling.

The wing is divided into equal length cylindrical elements, each of which is optimized separately. The overall element dimensions (length, chord, thickness) are fixed by the aerodynamic subproblem. The global structural subproblem imposes target values for the constant weight per unit length and flexural and torsional stiffnesses. It also supplies values for the out-of-plane shear force, bending and twisting moments at the inboard section of the element for stresses and stability calculations. The design variables of the local structural subproblem are the detailed element dimensions. The stresses and the panel buckling loads are found using conventional design methods.

D.1 NOMENCLATURE

a : spar cap width.

A : cell cross-sectional area.

[A] : panel extensional stiffness matrix.

b : wing element length.

c : wing element chord.

d : rib spacing.

D : panel bending stiffness.

E : material extensional stiffness modulus.

EI : wing element target bending stiffness.

e : wing element elastic axis position.

G : material shear stiffness modulus.

GJ : wing element target torsional stiffness.

H_j : vector containing overall dimensions for wing element j.

l : developed length of shell, or, panel dimension.

M : bending moment at element inboard section.

n_l : number of layers in composite laminates.

n_s : number of elements at the local structural level.

N : in-plane end load on element panel.

[Q] : lamina stiffness matrix in panel axes.

s : coordinate along shell midplane.

S : composite allowable shear stress in material axes.

t : thickness of wing element, panels or composite layers.

T : twisting moment at element inboard section.

T' : Eq. D.16.

V : shear force at element inboard section.

w, w_i : target weight per unit length for element, weight per unit length for component i of wing element.

x_{cg}, x_i : chordwise position of element center of gravity, same for element component i.

X : material allowable strength along the fibers.

y : spanwise coordinate.

Y : material allowable strength across the fibers.

z : position of lamina midplane with respect to laminate midplane.

z_{cg}, z_i : element center of gravity position above section chord, same for element component i.

γ : shear strain.

ε : normal strain.

θ : layer orientation with respect to panel axes.

ν : material Poisson's ratio, or ratio between structural and non-structural weight for wing element.

ρ : material weight density.

σ : normal stress.

τ : shear stress.

ϕ : wing section cell twist angle.

Commonly Used Subscripts

c : spar cap.

cr : critical (buckling) value of panel in-plane load.

C, T : compressive or tensile allowable.

fs : leading or trailing edge sandwich panel face sheets.

fw : spar web sandwich panel face sheet.

s : leading and trailing edge shell.

V, T : shear flow induced by shear force or twisting moment.

w : web sandwich panel.

x, y : refer to panel axes.

1-5, 6f, 6r, 7f, 7r : end loads on various element components (Fig. 23).

1, 2, 6: refer to material axes.

α, β : refer to axis system defined for sandwich panel buckling analysis.

Commonly Used Superscripts

c : carbon material.

e : equivalent.

k : layer number in laminate.

r : rib.

s : fiberglass material.

$\{\ \}^T$: transposed vector.

( )' : refer to quantities in material axes.

D.2 LOCAL STRUCTURAL LEVEL WING MODEL

D.2.1 Wing Construction

The wing construction is typical of present day technology (see Refs. 42-43). It is a shell reinforced by a straight spar normal to the plane of symmetry of the sailplane (Fig. 21). The spar caps are built of carbon fibers oriented spanwise and resist most of the bending moment. The shells as well as the spar webs are of symmetric sandwich made of fiberglass face sheets with foam core. The glass fibers are oriented at ± 45° with respect to the spanwise direction, thereby providing high shear stiffness.

Control surfaces (flaps/airbrake and aileron) run the whole length of the trailing edge so that only the portion of the wing between the leading edge and the rear web, the torsion box, is capable of carrying load. Finally, fiberglass ribs are positioned chordwise to increase the buckling loads of the spar caps and the sandwich panels; the rib thicknesses will be held constant during optimization.

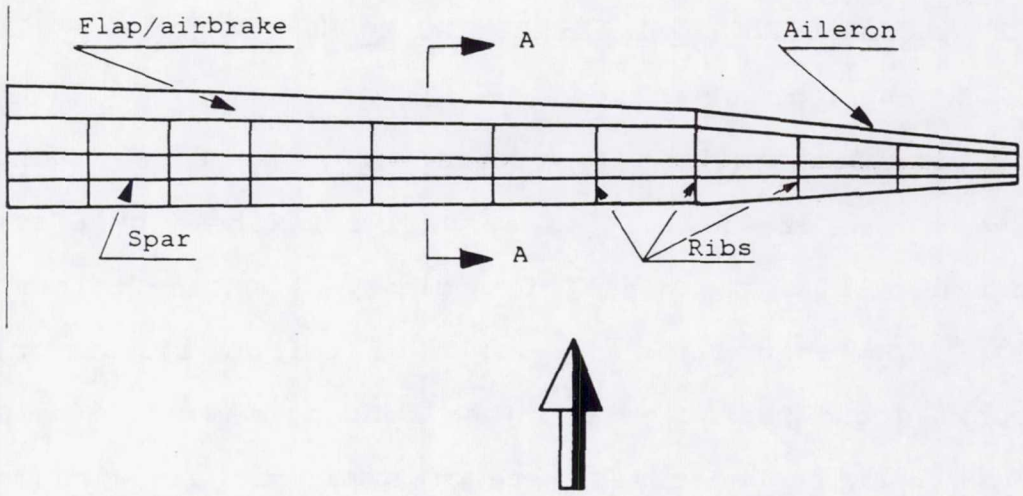

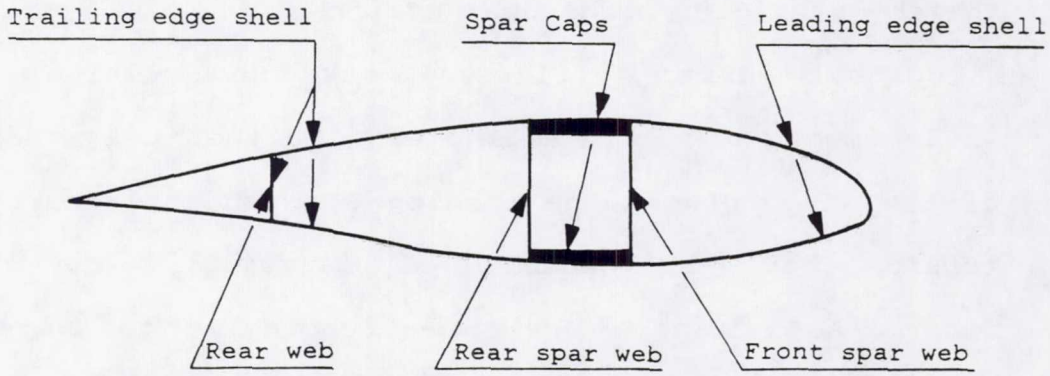

View A-A

Figure 21: Wing structure layout.

D.2.2 Model Description

To conduct the design at the local level, we divide the torsion box into n_s equal length, cylindrical elements (Fig. 22). The chord length c,[4] and the maximum section thickness t of each element are constant; together with the element length b they are communicated to the local structural subproblem from the aerodynamic subproblem in the vector H_i (see Subsec. B.5.2). For each element, the design variables are the spar cap width a and thickness t_c, the leading and trailing edge total thickness t_s and face sheet thickness t_{fs}, the front and rear spar web total thickness t_w and face sheet thickness t_{fw}, and the rib spacing d. Note that, technically, the thicknesses of the composite lay-ups vary in a discrete fashion since integer numbers of plies must be used. Similarly, the rib spacing is a discrete quantity. However, these will be treated as continuous variables to avoid difficulties while optimizing the design.

D.3 INTERNAL FORCE DISTRIBUTION

A wing section under bending moment, shear force and twisting moment is depicted in Fig. 23. The orientation of M, V and T are consistent with the definitions in App. C. This section is concerned with the calculation of the

[4] In this appendix, we drop the subscript j for the quantities relating to element j (i.e., c_j).

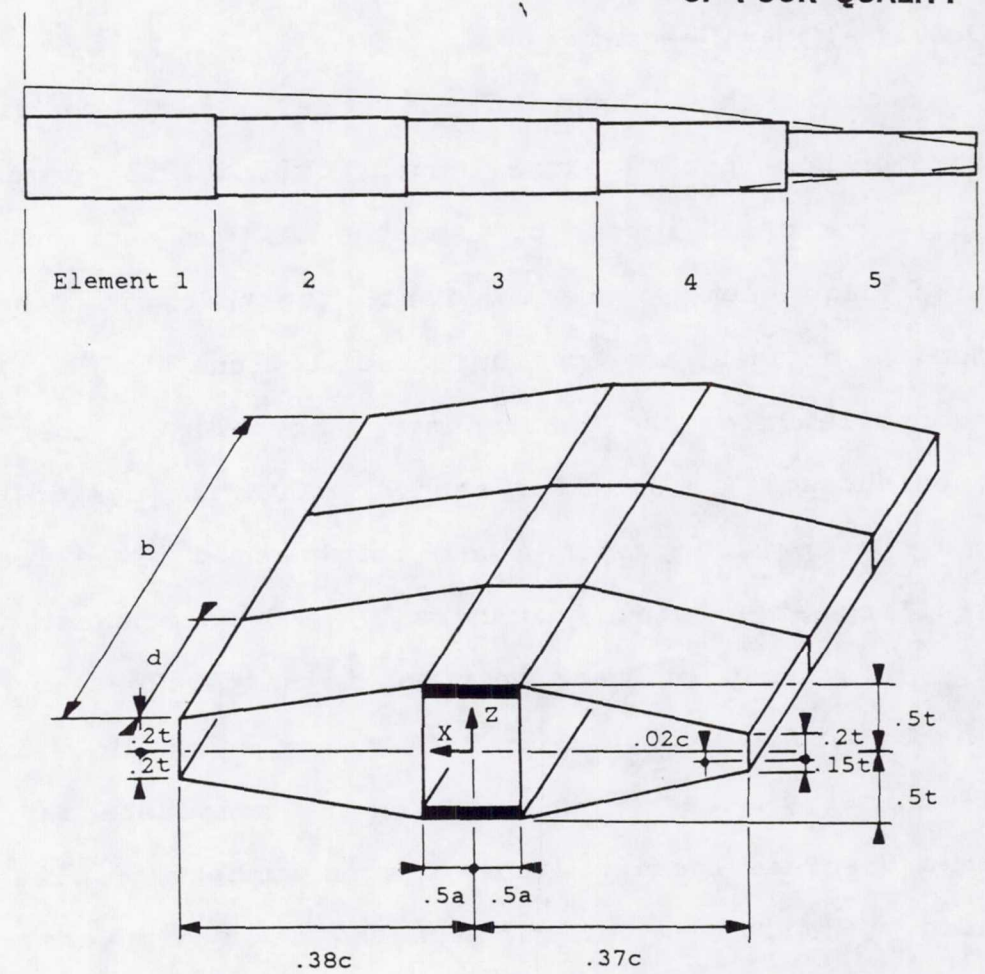

Figure 22: Wing model for local structural design. Details of a wing element. Dimensions are in terms of chord c and thickness t (n_s=5).

internal forces introduced in the wing section by that system of end forces.

D.3.1 Bending Moment Effect

The carbon fiber spar caps are about twenty times stiffer in the spanwise direction than the fiberglass shells (Ref. 42). It is therefore legitimate to assume that the entire bending moment is resisted by these spar caps. Furthermore, they are symmetric and their thickness is small with respect to the distance that separates them. Therefore, we assume them to be subjected to a constant normal load per unit length approximately given by

$$N_1 = \frac{M}{a(t-2t_{fs}-t_c)} \qquad (D.1)$$

D.3.2 Shear Flow Distribution

Shear forces and twisting moments induce shear flows in the panels constituting the wing section. Simple equilibrium arguments (see Ref. 44) show that the shear flows are constant on panels not subjected to normal edge loads and linear on panels subjected to constant normal edge loads.

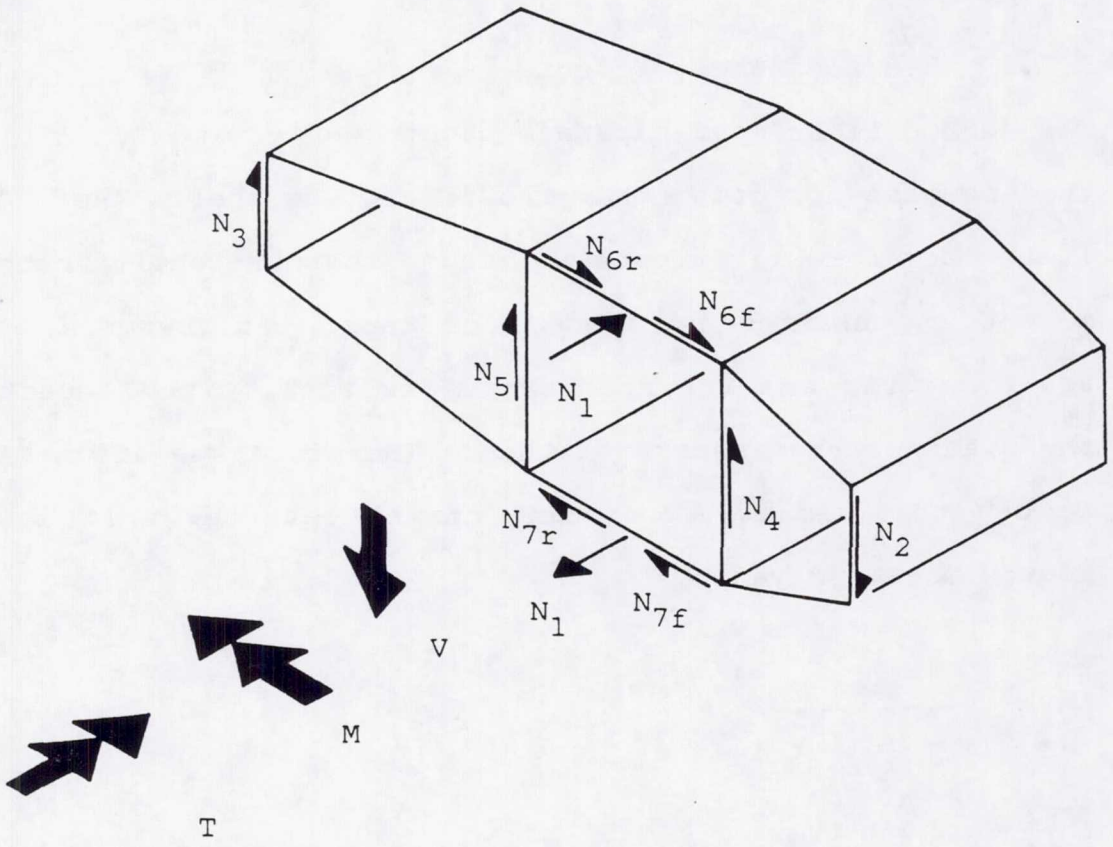

Figure 23: Internal forces induced in a wing section by a combination of shear force, bending moment and twisting moment.

Therefore, as summarized on Fig. 23, constant shear flows exist on the leading edge shell (N_2), the trailing edge shell (N_3), the front spar web (N_4) and the rear spar web (N_5). The shear flows vary linearly between N_{6r} and N_{6f} on the upper spar cap and between N_{7r} and N_{7f} on the lower one.

Four relationships may be written which express shear flow conservation at the junctions of the various panels,

$$N_3+N_5-N_{6r} = 0$$

$$N_3+N_5-N_{7r} = 0$$

$$N_4-N_2+N_{6f} = 0$$

$$N_4-N_2+N_{7f} = 0 \qquad (D.2)$$

Clearly

$$N_{6r} = N_{7r} \quad \text{and} \quad N_{6f} = N_{7f} \qquad (D.3)$$

Equilibrium of the upper spar cap in the spanwise direction yields

$$N_{6r}-N_{6f} = a \frac{dN_1}{dy} \qquad (D.4)$$

Finally, the twist angle per unit length for any of the three cells is given by (see Ref. 44)

$$\phi_i = \frac{1}{2A_i} \oint_i \frac{N(s)ds}{G(s)t(s)} \qquad (D.5)$$

where the integral is carried around the relevant cell. A_i is the cell cross-sectional area and s is a coordinate along the cell perimeter. G(s) is the material shear modulus and t(s) the wall thickness; both may be variable. We assume that only the sandwich face sheets carry shear. The equivalent shear modulus for the spar caps is obtained by specifying the compatibility of shear deformations for the various layers.

$$G^e = \frac{t_c G^c + 2t_{fs} G^s}{t_c + 2t_{fs}} \qquad (D.6)$$

G^c is the shear modulus for the spar cap carbon material. Since the carbon fibers are oriented spanwise,

$$G^c = G^c_{12} \qquad (D.7)$$

where G^c_{12} is the carbon shear modulus in material axes. G^s is the shear modulus for the fiberglass material, the fibers of which run at ± 45° with respect to the spanwise direction. Therefore (see for example Ref. 45)

$$G^s = \frac{E^s_1}{2(1+\nu^s_{12})} \qquad (D.8)$$

where E_1^s and ν_{12}^s are the fiberglass extensional stiffness modulus and Poisson's ratio in material axes. Using the subscripts L, T and S to designate respectively the leading edge, trailing edge and spar cell we have (see Fig. 24)

$$\phi_L = \frac{1}{4G^s A_L}\left[\frac{N_2 l_L}{t_{fs}} + \frac{N_4 t}{t_{fw}}\right]$$

$$\phi_T = \frac{1}{4G^s A_T}\left[\frac{N_3 l_T}{t_{fs}} - \frac{N_5 t}{t_{fw}}\right]$$

$$\phi_S = \frac{1}{2A_S}\left[\frac{(N_{6f}+N_{6r})a}{(t_c+2t_{fs})G^e} + \frac{(N_5-N_4)t}{2t_{fw}G^s}\right] \qquad (D.9)$$

The geometric quantities A_L, A_T, A_S, l_L and l_T are calculated in Subsec. D.4.1.

The relationships developed here will be used in the following subsections to determine the shear flows induced by a shear force and a twisting moment.

D.3.3 Effect of Shear Force at the Elastic Axis

A shear force at the elastic axis of a beam induces only bending deformations. Furthermore, the shear force is related to the bending moment by

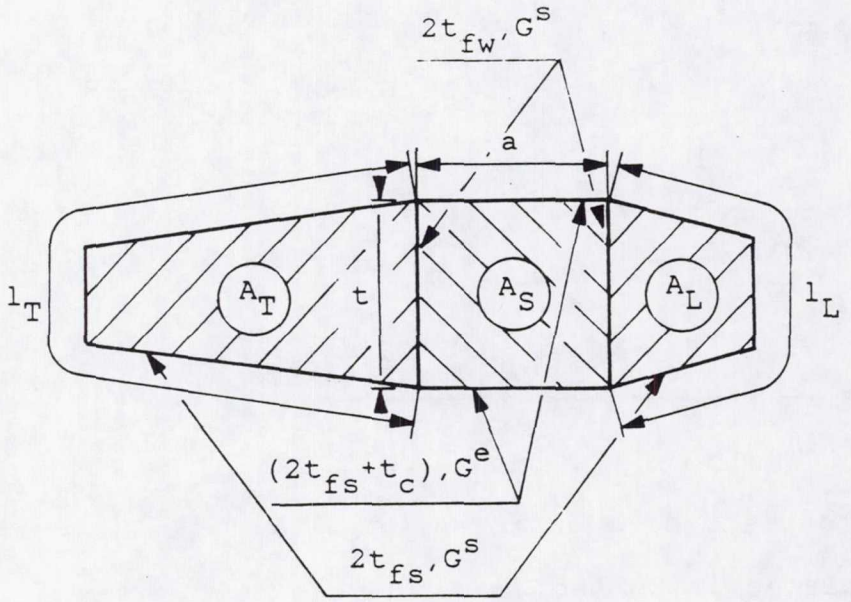

Figure 24: Definition of parameters used in cell twist angle calculation.

$$V = -\frac{dM}{dy}$$

or, from Eq. D.1

$$\frac{dN_1}{dy} = -\frac{V}{a(t-2t_{fs}-t_c)} \qquad (D.10)$$

Equations D.2-4 and D.9-10 may now be used to set up a system of six equations in the six unknown shear flows induced by the shear force. Using the subscript V to emphasize the fact that the shear flows are induced by the shear force, we have

$$N_{3V}+N_{5V}-N_{6rV} = 0$$

$$N_{4V}-N_{2V}+N_{6fV} = 0$$

$$N_{6rV}-N_{6fV} = -\frac{V}{(t-2t_{fs}-t_c)}$$

$$\frac{l_L}{t_{fs}}N_{2V}+\frac{t}{t_{fw}}N_{4V} = 0$$

$$\frac{l_T}{t_{fs}}N_{3V}-\frac{t}{t_{fw}}N_{5V} = 0$$

$$\frac{a}{(t_c+2t_{fs})G^e}(N_{6fV}+N_{6rV})+\frac{t}{2t_{fw}G^s}(N_{5V}-N_{4V}) = 0 \qquad (D.11)$$

The three last equations state the fact that the various cells do not rotate when V is applied through the elastic axis.

D.3.4 Elastic Axis Position

Because we consider the shear force acting normal to the wing plane, we are only interested in the chordwise position of the elastic axis. It is found by stating that the sum of the torques induced about any point of the section by the shear flows of Eq. D.11 is exactly equivalent to the torque caused by the shear force itself (see Ref. 44). Therefore, taking the moments about point P in Fig. 25 a)

$$e = \frac{1}{V}[2N_{3V}A_T - N_{4V}A_S + N_{2V}(2A_L + A_S) + (N_{6fV} + N_{6rV})\frac{at}{2}] \qquad (D.12)$$

D.3.5 Twisting Moment Effect

The shear flows induced by a twisting moment may be obtained from the relationships developed in Subsec. D.3.2 with the added condition that the sum of the torques induced by the shear flows about any point of the section must now be equivalent to the applied twisting moment. By compatibility, the three cells must have the same twist angle,

$$\phi_L = \phi_T = \phi_S \qquad (D.13)$$

Also, there is no normal edge load on the spar caps,

$$N_1 = 0$$

$$N_{6rT} = N_{6fT} \qquad (D.14)$$

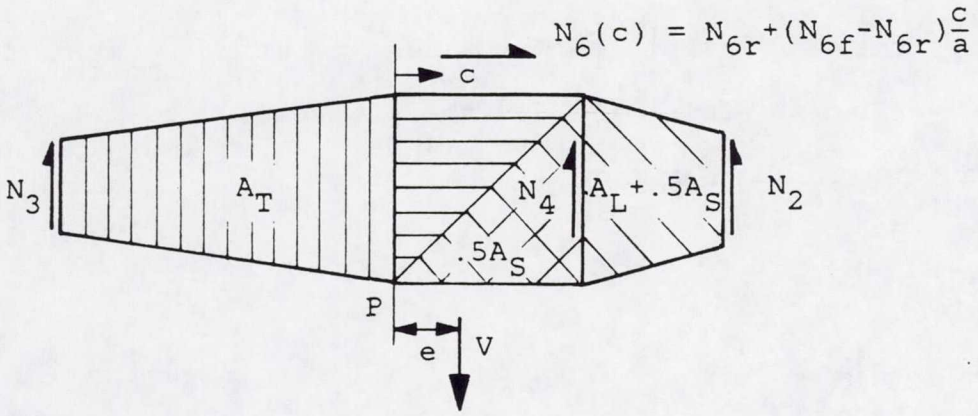

a) Elastic axis position calculation.
(only the shear flows contributing to the twisting moment about P are represented)

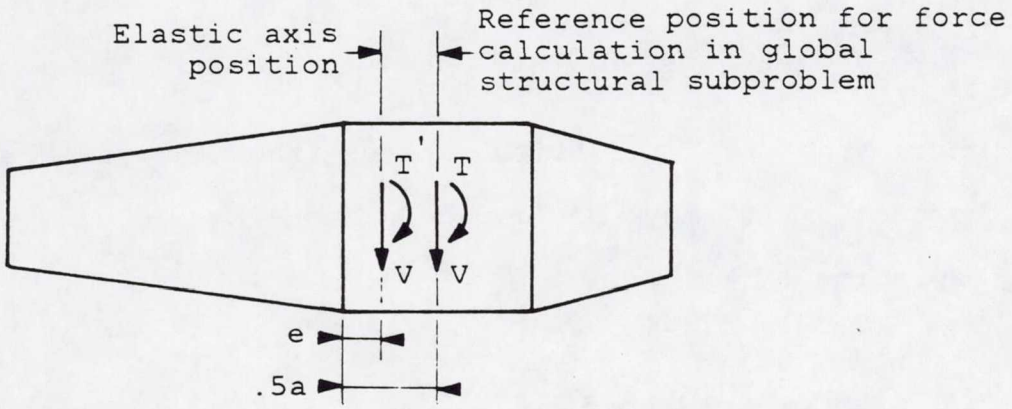

b) Corrected torque calculation.

Figure 25: Elastic axis position and corrected torque calculation.

where the subscript T indicates twisting moment induced shear flows. This yields the following system of five equations in five unknowns.

$$N_{3T}+N_{5T}-N_{6fT} = 0$$

$$N_{4T}-N_{2T}+N_{6fT} = 0$$

$$\frac{l_L}{t_{fs}}N_{2T}+\frac{t}{t_{fw}}N_{4T}-\frac{A_L l_T}{A_T t_{fs}}N_{3T}+\frac{A_L t}{A_T t_{fw}}N_{5T} = 0$$

$$\frac{l_T}{t_{fs}}N_{3T}-\frac{t}{t_{fw}}N_{5T}-\frac{4aA_T G^s}{(t_c+2t_{fs})A_S G^e}N_{6fT}-\frac{tA_T}{t_{fw}A_S}(N_{5T}-N_{4T}) = 0$$

$$2A_T N_{3T}-A_S N_{4T}+(A_S+2A_L)N_{2T}+atN_{6fT} = T \qquad \text{(D.15)}$$

where the last equation states the equivalence of the torques. It may be deduced from Eqs. D.12 and D.14, replacing eV by T.

D.3.6 Combined Loading

The applied values of the shear force, bending and twisting moment to use in the design of a given wing element are supplied by the global structural subproblem. However, the twisting moment is calculated about a point located at the maximum airfoil thickness, halfway between the upper and lower spar surfaces. The twisting moment must be corrected

to account for the offset of that point with respect to the elastic axis. To obtain the internal forces corresponding to any set of applied forces, the following steps must be carried out.

i) Obtain the normal edge load on the spar caps from Eq. D.1.

ii) Calculate the shear flows induced by a shear force assumed to act at the elastic axis using Eq. D.11. The N_{iV} are now known.

iii) Find the elastic axis position from Eq. D12.

iv) Calculate the total moment of the applied forces about the elastic axis (from Fig. 25 b)

$$T' = T+V(\frac{a}{2}-e) \qquad (D.16)$$

v) Calculate the shear flows induced by the complete twisting moment using Eq. D.15, and obtain the N_{iT}.

vi) Combine the N_{iV} from step ii) with the N_{iT} from step v).

D.4 WING SECTION GEOMETRIC PROPERTIES

D.4.1 Shell Developed Lengths and Cell Cross-Sections

Referring to Figs. 22 and 24, we have

$$A_L = .25tc-.34ta$$

$$A_S = ta$$

$$A_T = .27tc-.35ta \tag{D.17}$$

$$l_L = [(.3t+.02c)^2+(.37c-.5a)^2]^{1/2}+.35t$$
$$+[(.35t-.02c)^2+(.37c-.5a)^2]^{1/2}$$

$$l_T = 2[(.3t)^2+(.38c-.5a)^2]^{1/2}+.4t \tag{D.18}$$

D.4.2 Element Weight Data

The calculations for the element weight per unit length and the position of its center of gravity are detailed in Table 2. The position of the various items are given in an X-Z system of axes centered at the chordwise position of maximum airfoil thickness, halfway between the upper and lower surfaces (see Fig. 22). The item numbers are defined in Fig. 26.

The entries in Table 2 are in terms of the variables defined in Fig. 22. ρ^s, ρ^c and ρ^f are the weight densities of, respectively, the fiberglass sandwich face sheets, the carbon fiber spar caps and the sandwich foam core. Item 11 represents the total weight per unit length of the ribs. The wing element is assumed to have b/d ribs, the weight of which is proportional to the torsion box cross-sectional area and the weight per unit area ρ^r. Finally, item 12 is

TABLE 2

Weight and center of gravity position for wing element components.

Item	w_i	z_i	x_i
1	$[(.37c-.5a)^2+(.3t+.02c)^2]^{1/2}\tau^*$	.35t-.01c	-.185c-.25a
2	$.35t\tau$	.025t-.02c	-.37c
3	$[(.37c-.5a)^2+(.35t-.02c)^2]^{1/2}\tau$	-.325t-.01c	-.185c-.25a
4	$t[2t_{fw}\rho^s+(t_w-2t_{fw})\rho^f]$	.0	-.5a
5	$a(t_c\rho^c+2t_{fs}\rho^s)$	.5t	.0
6	$a(t_c\rho^c+2t_{fs}\rho^s)$	-.5t	.0
7	$t[2t_{fw}\rho^s+(t_w-2t_{fw})\rho^f]$	.0	.5a
8	$[(.3t)^2+(.38c-.5a)^2]^{1/2}\tau$	.15t	.19c+.25a
9	$[(.3t)^2+(.38c-.5a)^2]^{1/2}\tau$	-.15t	.19c+.25a
10	$.4t[2t_{fs}\rho^s+(t_s-2t_{fs})\rho^f]$	.0	.38c
11	$(A_L+A_S+A_T)\rho^r/d$	.0	.0
12	$\nu\sum_{i=1}^{11} w_i$	.01c	.46c

$^*\tau = [2t_{fs}\rho^s+(t_s-2t_{fs})\rho^f]$

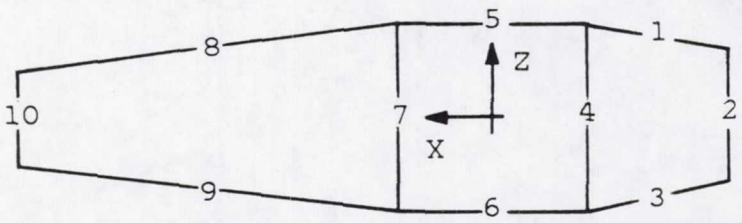

11 Wing ribs

12 Non-structural components

Figure 26: Numbering scheme for element weight and center of gravity calculations.

the total non-structural weight per unit length (control surfaces, control linkages,...). It is assumed to be a fixed percentage of the structural weight (ν) and to be concentrated far behind the spar. The total element weight per unit length is

$$w = \sum_{i=1}^{12} w_i \tag{D.19}$$

Its center of gravity is defined by

$$x_{cg} = \frac{1}{w} \sum_{i=1}^{12} x_i w_i$$

$$z_{cg} = \frac{1}{w} \sum_{i=1}^{12} z_i w_i \tag{D.20}$$

D.4.3 Element Bending Stiffness

Assuming that the entire bending stiffness is provided by the spar caps we have, approximately

$$EI = \frac{E^c a t_c}{2}(t-2t_{fs}-t_c)^2+\frac{E^s a t_{fs}}{2}[(t-t_{fs})^2+(t-3t_{fs}-2t_c)^2] \tag{D.21}$$

where the last term is the contribution of the fiberglass on either side of the spar caps. E^c, the carbon fiber spanwise extensional stiffness modulus, is

$$E^c = E_1^c \tag{D.22}$$

where E_c^1 is the material principal extensional stiffness. Since the glass fibers are oriented ± 45° with respect to the spanwise direction,

$$E^s = 4\left[\frac{2(1-\nu_{12}^s)}{E_1^s} + \frac{1}{G_{12}^s}\right]^{-1} \tag{D.23}$$

where E_1^s, G_{12}^s and ν_{12}^s are the fiberglass principal extensional stiffness, shear stiffness and Poisson's ratio, in material axes.

D.4.4 Torsional Stiffness

The torsional stiffness of a beam is defined as the ratio between an arbitrary applied torque and the resulting twist angle. By compatibility, the twist angle of a multicell beam is the same as that of any of its cells.

$$GJ = \frac{T}{\phi_i} = \frac{2A_i T}{\oint_i \frac{N(s)ds}{G(s)t(s)}} \tag{D.24}$$

or, for the leading edge cell

$$GJ = \frac{2A_L G^s T}{\left[\frac{N_{4T}t}{2t_{fw}} + \frac{N_{2T}l_L}{2t_{fs}}\right]} \tag{D.25}$$

The torsional stiffness is obtained by solving the torsion problem (Eq. D.15) with an arbitrary torque and then using Eq. D.25.

D.5 CALCULATION OF STRESSES

D.5.1 General Procedure

The different fiber reinforced laminated panels constituting the wing torsion box are of symmetric lay-ups. Furthermore, they are assumed to be loaded by in-plane edge loads. Therefore, their deformations entail only in-plane strains. For each laminated panel (laminate) the strains are related to the edge loads by[5]

$$\{\varepsilon\} = [A]^{-1}\{N\}$$

$$\{\varepsilon\}^T = \{\varepsilon_x, \varepsilon_y, \gamma_{xy}\}$$

$$\{N\}^T = \{N_x, N_y, N_{xy}\}$$

$$A_{ij} = \sum_{k=1}^{n_l} Q_{ij}^k t^k; \quad i,j=1,2,6 \qquad (D.26)$$

The strain and load vectors (ε,N) are given in a set of axes called laminate axes (see Fig. 27). The laminate extensional stiffness matrix A is obtained from the

---

[5] The developments of this section belong to the classical lamination theory, they are taken from Ref. 45.

transformed reduced stiffness matrix Q^k and the thickness t^k of the n_l layers constituting the laminate. The transformed reduced stiffness matrix of a layer is dependent on the characteristics of the material making up the layer and on the orientation of the layer material axes with respect to the laminate axes. General expressions for the Q^k matrix may be found in Ref. 45.

The stresses in a layer are given in laminate axes by

$$\{\sigma^k\} = [Q^k]\{\varepsilon\}$$

$$\{\sigma^k\}^T = \{\sigma_x^k, \sigma_y^k, \tau_{xy}^k\} \tag{D.27}$$

Finally, the stresses in the layer material axes are found from

$$\{\sigma'^k\} = [T^k]\{\sigma^k\}$$

$$\{\sigma'^k\}^T = \{\sigma_1^k, \sigma_2^k, \tau_{12}^k\}$$

$$[T] = \begin{bmatrix} c^{k2} & s^{k2} & 2s^k c^k \\ s^{k2} & c^{k2} & -2s^k c^k \\ -s^k c^k & s^k c^k & c^{k2} - s^{k2} \end{bmatrix}$$

$$c^k = \cos\theta^k; \quad s^k = \sin\theta^k \tag{D.28}$$

where the ' symbol is used to identify quantities measured in material axes. The stress analysis for the panels will

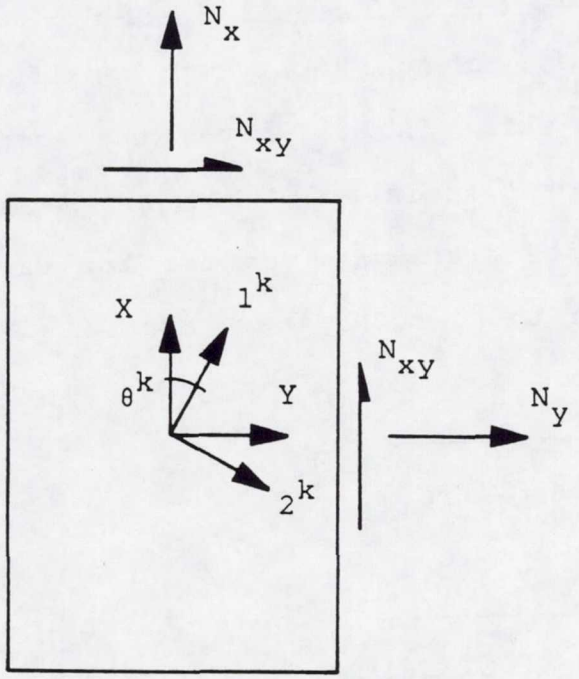

Laminate axes: XY
Material axes for layer k: $1^k 2^k$

Figure 27: Definition of axes system and applied edge loads for an arbitrary laminated panel.

be discussed in the next two subsections. The necessary information is summarized in Table 3.

D.5.2 Stresses in the Spar Caps

The details of the spar cap construction are depicted in Fig. 22, while Table 3 gives the location of the points to be monitored (points 1 through 8). The transformed reduced stiffnesses are now given for the various layers (see Ref. 45). For the carbon fiber material

$$Q^c_{11} = \frac{E^c_1}{(1-\nu^{c2}_{12}E^c_2/E^c_1)}$$

$$Q^c_{12} = \frac{\nu^c_{12}E^c_2}{(1-\nu^{c2}_{12}E^c_2/E^c_1)}$$

$$Q^c_{22} = \frac{E^c_2}{(1-\nu^{c2}_{12}E^c_2/E^c_1)}$$

$$Q^c_{66} = G^c_{12}$$

$$Q^c_{16} = Q^c_{26} = 0 \qquad \text{(D.29)}$$

where E^c_1, E^c_2, ν^c_{12} and G^c_{12} are, respectively, the material extensional stiffness moduli in the fiber

TABLE 3

Summary of information for stress analysis.

Control Point Location	N_x	N_{xy}	Point	Material	θ^k
upper spar cap, front	$-N_1$	$-N_{6f}$	1	carbon fibers	0°
			2	fiberglass	45°
upper spar cap, rear	$-N_1$	$-N_{6r}$	3	carbon fibers	0°
			4	fiberglass	45°
lower spar cap, front	N_1	$-N_{7f}$	5	carbon fibers	0°
			6	fiberglass	45°
lower spar cap, rear	N_1	$-N_{7r}$	7	carbon fibers	0°
			8	fiberglass	45°
leading edge shell		$-N_2$	9	fiberglass	45°
front spar web		N_4	10	fiberglass	45°
rear spar web		$-N_5$	11	fiberglass	45°
trailing edge shell		$-N_3$	12	fiberglass	45°

and across the fiber directions, Poisson's ratio and shear stiffness modulus. For the fiberglass material (thickness $2t_{fs}$)

$$Q^s_{11} = Q^s_{22} = \frac{E^s_1}{2(1-\nu^s_{12})} + G^s_{12}$$

$$Q^s_{12} = \frac{E^s_1}{2(1-\nu^s_{12})} - G^s_{12}$$

$$Q^s_{66} = \frac{E^s_1}{2(1+\nu^s_{12})}$$

$$Q^s_{16} = Q^s_{26} = 0 \qquad \text{(D.30)}$$

where the superscript s refers to the fiberglass material. The stresses in the various layers may be determined from Eqs. D.26-27, together with Eqs. D.29-30. They are in material axes for the carbon fiber layers; for the fiberglass layers, however, transformation D.28 must still be used.

D.5.3 Stresses in the Sandwich Panels

A uniform state of stress exists in the sandwich panels constituting the leading and trailing edge shells, as well as the spar webs (see Fig. 23). Hence, the stresses need only be monitored at the four points mentioned in Table 3

(points 9 through 12). The sandwich core will be assumed non-structural. In this case, the calculations of Subsec. D.5.1 may be carried out quite simply. For the leading and trailing edge shells, we have, in material axes

$$\sigma_1 = -\sigma_2 = \frac{N_{xy}}{2t_{fs}}$$

$$\tau_{12} = 0 \qquad \text{(D.31)}$$

while for the spar webs, t_{fs} in Eq. D.31 should be replaced by t_{fw}.

D.5.4 Failure Criterion

The states of stress described in the two previous subsections are two-dimensional. Therefore, a failure criterion must be used to determine whether a given loading induces failure. Tsai-Wu's criterion reads (Ref. 45)[6]

$$\frac{\sigma_1(\sigma_1+X_C-X_T)}{X_TX_C}+\frac{\sigma_2(\sigma_2+Y_C-Y_T)}{Y_TY_C}-\frac{\sigma_1\sigma_2}{(X_CX_TY_CY_T)^{1/2}}+\frac{\tau_{12}^2}{S^2}-1 \le 0 \qquad \text{(D.32)}$$

where X_C and X_T are the material compressive and tensile strengths along the fibers, Y_C and Y_T the corresponding quantities across the fibers and S the in-plane shear

[6] General formulations for Tsai-Wu's criterion usually involve a strength biaxial tension test. Such a stress is difficult to determine accurately. In the formulation chosen here, the need for that strength is alleviated by specifying that Tsai-Wu's criterion reduces to Von Mise's yield criterion when applied to an isotropic material.

strength. Failure will not occur in the wing section if inequality D.32 is satisfied at all points defined in Table 3; there are twelve such conditions.

D.6 SECTION STABILITY

The stability of the wing box will be ascertained by verifying the stability of each individual component. The leading edge shell, which exhibits a strong curvature, will be replaced by two flat panels. because of the model cross-section symmetry and the nature of the system of induced loads (Fig. 23), only seven panels need be considered; they are numbered as shown on Fig. 28. Two different buckling problems must be solved:

i) Buckling of orthotropic sandwich panels under in-plane shear (panels 1 through 5).

ii) Buckling of orthotropic composite panels under in-plane compression and shear (spar caps, panels 6 and 7).

These problems are discussed in the following subsections.

D.6.1 Sandwich Panels Buckling

The sandwich panels constituting the wing torsion box are primarily loaded in shear. This subsection is concerned with the calculation of the critical load of orthotropic

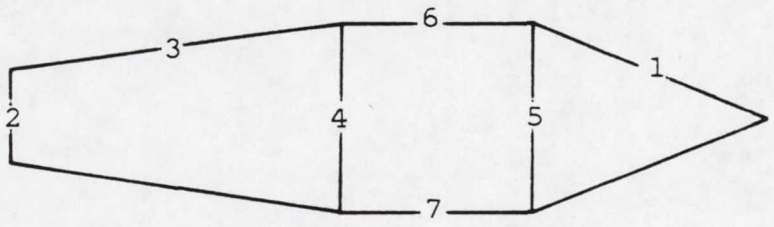

Figure 28: Panel numbering for cross-section stability analysis.

sandwich panels; the developments are adapted from Ref. 46. Figure 29 defines the nomenclature used. Note that the panel edge of length l_α is that which is shorter. The glass fibers are oriented at ± 45° with respect to axes α and β. In this set of axes, the face sheets material properties are

$$E_\alpha = E_\beta = \frac{4}{[2(1-\nu_{12}^s)/E_1^s + 1/G_{12}^s]}$$

$$G_{\alpha\beta} = \frac{E_1^s}{2(1+\nu_{12}^s)}$$

$$\nu_{\alpha\beta} = \frac{[1/G_{12}^s - 2(1-\nu_{12}^s)/E_1^s]}{[1/G_{12}^s + 2(1-\nu_{12}^s)/E_1^s]} \qquad \text{(D.33)}$$

where E_1^s, G_{12}^s and ν_{12}^s are the fiberglass material properties in material axes. Neglecting the contributions of the core material, the panel bending and twisting stiffnesses are

$$D_\alpha = D_\beta = \frac{E_\alpha[t^3 - (t-2t_f)^3]}{12(1-\nu_{\alpha\beta}^2)}$$

$$D_{\alpha\beta} = \frac{G_{\alpha\beta}[t^3 - (t-2t_f)^3]}{12} \qquad \text{(D.34)}$$

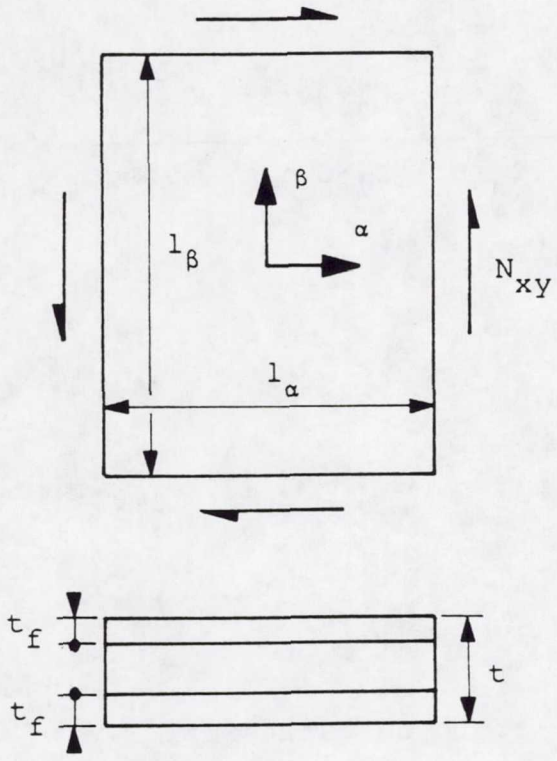

Figure 29: Nomenclature used in sandwich panel buckling analysis.

The critical shear flow is

$$N_{xycr} = \frac{4jD_\alpha}{l_\alpha^2[1+4(K_{MO}/K_M-1)]} \tag{D.35}$$

K_M and K_{MO} are given by

$$K_M = \frac{C_1+2B_2+B_3+AV(1+1/C_4)}{1+V[C_3+B_3+(C_1+B_3)/C_4]+V^2A/C_4}$$

$$K_{MO} = K_M(V=0)$$

$$A = 1-B_2^2+B_3(C_1+2B_2+C_3)$$

$$B_2 = \nu_{\alpha\beta}+2D_{\alpha\beta}/D_\alpha$$

$$B_3 = D_{\alpha\beta}/D_\alpha$$

$$C_1 = C_4 = 1/C_3 = (l_\beta/l_\alpha)^2 \tag{D.36}$$

For an isotropic core material

$$V = \frac{\pi^2 D_\alpha}{l_\alpha^2(t-2t_f)G^f} \tag{D.37}$$

G^f being the core material transverse shear stiffness. Finally, j is a function of B_2 and l_α/l_β; for simply supported panels, it is approximately given by

$$j(l_\alpha/l_\beta, B_2) = 8.2+5.0B_2 +(.7999+9.4748B_2)(l_\alpha/l_\beta)^2$$
$$+(3.1502-8.5488B_2)(l_\alpha/l_\beta)^3$$
$$+(-.4501+5.1740B_2)(l_\alpha/l_\beta)^4 \qquad (D.38)$$

The critical load (Eq. D.35) must be calculated for the five different sandwich panels. The necessary information is summarized in Table 4. For stability, we require for each panel

$$\frac{N_{xy}}{N_{xycr}} - 1 \leq 0 \qquad (D.39)$$

D.6.2 Spar Caps Buckling

The spar caps are loaded in their plane by spanwise normal forces and shear forces. We now calculate their critical loads following developments given Ref. 47. We make the conservative assumption that they are very high aspect ratio simply supported plates. We assume further that the shear force is constant along the edges, taking as applied shear the largest of N_{6f} and N_{6r} (Sec. D.3). The notation used is that of Sec. D.5.

The spar cap bending stiffnesses are

$$D_{ij} = \sum_{k=1}^{n_1} Q_{ij}^k \left(t^k z^{k2} + \frac{t^{k3}}{12}\right) \quad i,j=1,2,6 \qquad (D.40)$$

TABLE 4

Summary of information for sandwich panel buckling analysis.

Panel	N_{xy}	l_α, $l_\beta^{(*)}$	t	t_f
1	N_2	d, $[(.37c-.5a)^2+(.5t)^2]^{1/2}$	t_s	t_{fs}
2	N_3	d, .4t	t_s	t_{fs}
3	N_3	d, $[(.38c-.5a)^2+(.3t)^2]^{1/2}$	t_s	t_{fs}
4	N_5	d, t	t_w	t_{fw}
5	N_4	d, t	t_w	t_{fw}

(*) l_α should be taken as the smallest of the two values given, l_β is the remaining one.

The Q_{ij}^k are the transformed reduced stiffnesses (Subsec. D.5.2) for layer k, t^k is that layer thickness, and z^k the distance between that layer midplane and the laminate midplane.

The critical compressive load is given as

$$N_{xcr} = \frac{2\pi^2 (D_{11}D_{22})^{1/2}}{c^2}\left[1+\frac{D_{12}+2D_{66}}{(D_{11}D_{22})^{1/2}}\right] \qquad (D.41)$$

where c is the length of the edge under the normal loads.

The critical load in shear is given in terms of the parameter

$$\theta = \left(\frac{D_{11}D_{22}}{D_{12}+2D_{66}}\right)^{1/2} \qquad (D.42)$$

Then, for $0 \le \theta \le 1$

$$N_{xycr} = 4\frac{C_a}{c^2}[D_{22}(D_{12}+2D_{66})]^{1/2}$$

$$C_a = 11.71+.095\theta+1.767\theta^2 \qquad (D.43)$$

While, for $1 \le \theta \le \infty$

$$N_{xycr} = 4\frac{C_b}{c^2}(D_{11}D_{22}^3)^{1/4}$$

$$C_b = \frac{5}{\theta}+8.125 \qquad (D.44)$$

For panel stability under combined loading, we require

$$-\frac{N_x}{N_{xcr}} + \left(\frac{N_{xy}}{N_{xycr}}\right)^2 - 1 \leq 0 \qquad \text{(D.45)}$$

This condition must be satisfied for both spar caps, the information necessary to conduct the calculations is summarized in Table 5.

TABLE 5

Summary of information for spar cap buckling analysis.

Spar Cap	N_x	N_{xy}	c
upper	$-N_1$	$\max(N_{6f}, N_{6r})$	a
lower	N_1	$\max(N_{6f}, N_{6r})$	a

Appendix E

NUMERICAL DATA

This appendix gives numerical values for the parameters introduced in Apps. A-D. These values were used when solving the two-level structural design problem or are appropriate for completion of the four-level problem.

E.1 PERFORMANCE SUBPROBLEM

The cross-country speed may be calculated for any of the three thermal models described in Fig. 13; the rate of climb constraint should require a minimum rate of climb value $v_{cmin} = .7$ m/sec, in a weak thermal. An interthermal downdraft of $v_{ith} = .3$ m/sec appears typical. The mass density of air is $\rho = 1.225$ kg/m^3 (standard day, sea level), the acceleration of gravity is $g = 9.81$ m/sec^2.

E.2 AERODYNAMIC SUBPROBLEM

The kinematic viscosity of air is $\nu = 1.4607\ 10^{-5}$ m^2/sec (standard day, sea level). The wing angle of attack is taken as $i_w = .0349$ rad (2^o). The following sailplane parameters were mostly estimated from sketches of the Nimbus II sailplane in the references to App. A. The sailplane fuselage is characterized by a radius $b_f = 0.4$ m, a maximum

height h_f = 0.8 m, a total length l_f = 7.5 m, a maximum cross-sectional area A_c = 0.6 m^2, a wetted area S_{fwet} = 10.0 m^2, a planform area S_f = 3.0 m^2, a distance nose-wing l_{fn} = 2.0 m, a total volume V_f = 1.3 m^3, a distance between wing and horizontal tailplane l_h = 5.0 m, the wing planform area inside the fuselage is S_{fw} = 0.6 m^2. Reference 39 (Chap. IX) recommends a static stability margin $(x_n-x_{cg})/c$ = .05. The horizontal tailplane has a planform area S_h = 1.2 m^2, an average chord c_h = 0.3 m, an aspect ratio A_h = 5.0, a taper ratio λ_h = 0.5, a thickness ratio $(t/c)_h$ = 0.1, a vertical distance between wing and tailplane h_h = 1.2 m. The vertical tailplane has a planform area S_v = 2.4 m^2, an average chord c_v = 0.5 m, a thickness ratio $(t/c)_v$ = 0.1. The two-level subproblem is solved using a fixed total sailplane weight W = 4000. N for the aerodynamic calculations; the wing is assumed untwisted ($\varepsilon_b = \varepsilon_t = 0$), the planform is described by b = 10.0 m, b_b = 5.0 m, c_r = 1.0 m, c_b = 0.7 m, and c_t = 0.3 m. The Fourier series analysis for spanwise distributions of lift and drag is based on n_a = 5 control points; while the aerodynamic parameters transmitted to the global structural subproblem (Subsec. B.5.4) involves 6 control points (n_f = 5).

E.3 GLOBAL STRUCTURAL SUBPROBLEM

In addition to the parameters related to the structural design Requirements and given in Sec. C.3, it is specified that the tip displacement never exceed 0.7 m. The weight for the sailplane without wings is W_{nw} = 2000. N. The discretization of the distributions of weight per unit length and bending and torsional stiffnesses are based on n_s = 5 intervals. The following side constraints are used $1.0 \leq w_j \leq 1.0\ 10^{10}$ (N/m), $1.0\ 10^3 \leq EI_j \leq 1.0\ 10^{10}$ (Nm^2), $1.0\ 10^3 \leq GJ_j \leq 1.0\ 10^{10}$ (Nm^2).

E.4 LOCAL STRUCTURAL SUBPROBLEM

The discretization at the lowest structural level involves n_{el} = 5 elements.

The unidirectional carbon fiber material is a high-strength graphite-epoxy with the following parameters : $E_1^C = 1.47\ 10^{11}$ N/m^2, $E_2^C = 1.09\ 10^{10}$ N/m^2, $G_{12}^C = 6.41\ 10^9$ N/m^2, $\nu_{12}^C = 0.38$, $X_C^C = 1.41\ 10^9$ N/m^2, $X_T^C = 1.46\ 10^9$ N/m^2, $Y_C^C = 1.48\ 10^8$ N/m^2, $Y_T^C = 4.2\ 10^7$ N/m^2, $S = 9.52\ 10^7$ N/m^2, $\rho^C = 1.58\ 10^4$ N/m^3.

The fiberglass material is a bidirectional cloth with fibers running in perpendicular directions and having the following properties: $E_1^S = E_2^S = 1.55\ 10^{10}$ N/m^2, $G_{12}^S = 5.5\ 10^9$ N/m^2, $\nu_{12}^S = .25$, $S^S = 8.0\ 10^7$ N/m^2, $X_C^S = Y_C^S = X_T^S = Y_T^S = 2.4\ 10^8$ N/m^2, $\rho^S = 1.67\ 10^4$ N/m^3.

The foam used as core for the sandwich panels is described by $G^f = 4.0\ 10^6\ N/m^2$, $\rho^f = 5.89\ 10^2\ N/m^3$. The wing ribs are constructed of a 5.0 mm thick foam core with two fiberglass face sheets of 1.0 mm each, for a total weight per unit area $\rho^r = 36.3\ N/m^2$. The ratio between non-structural and structural wing element weight is $\nu = 0.5$.

The design variables are subjected to the following side constraints: (all dimensions are in meters) $5.0\ 10^{-3} \leq a \leq 1.0\ 10^{-1}$, $2.0\ 10^{-4} \leq t_c \leq 5.0\ 10^{-2}$, $2.5\ 10^{-3} \leq t_s \leq 5.0\ 10^{-2}$, $5.0\ 10^{-4} \leq t_{fs} \leq 1.0\ 10^{-2}$, $2.5\ 10^{-3} \leq t_w \leq 5.0\ 10^{-2}$, $5.0\ 10^{-4} \leq t_{fw} \leq 1.0\ 10^{-2}$, $5.0\ 10^{-3} \leq d \leq 5.0\ 10^{-1}$. Furthermore, the following constraints are added to preserve the validity of the analyses: $a \leq 0.1c$, $t_{fs} \leq 0.2t_s$, $t_{fw} \leq 0.2t_w$.

1. Report No.	2. Government Accession No.	3. Recipient's Catalog No.
NASA CR- 172184		

4. Title and Subtitle	5. Report Date
DEVELOPMENT OF A MULTILEVEL OPTIMIZATION APPROACH TO THE DESIGN OF MODERN ENGINEERING SYSTEMS	August 1983
	6. Performing Organization Code

7. Author(s)	8. Performing Organization Report No.
Jean-Francois Marie Barthelemy	
	10. Work Unit No.

9. Performing Organization Name and Address	11. Contract or Grant No.
Virginia Polytechnic Institute and State University Blacksburg, Virginia	NAG1-145
	13. Type of Report and Period Covered
12. Sponsoring Agency Name and Address	Contractor Report
National Aeronautics and Space Administration Washington, D.C.	14. Sponsoring Agency Code 505-33-53-12

15. Supplementary Notes
Langley Technical Monitor: J. Sobieski
Ph.D. dissertation - research performed under Grant NAG-1-145 with VPI&SU.
Principal investigator, Prof. W. L. Hallauer, Jr., VPI&SU.

16. Abstract This report describes an optimization approach to the design of complex engineering systems. The approach assumes a decomposition of the original problem (design of the system) into smaller subproblems (design of subsystems) organized in a multilevel hierarchy.

A general algorithm is proposed which carries out the design process iteratively, starting at the top of the hierarchy and proceeding downward. Each subproblem is optimized separately for fixed controls from higher level subproblems. An optimum sensitivity analysis is then performed which determines the sensitivity of the subproblem design to changes in higher level subproblem controls. The resulting sensitivity derivatives are used to construct constraints which force the controlling subproblems into chosing their own designs so as to improve the lower level subproblem designs while satisfying their own constraints.

The applicability of the proposed algorithm is demonstrated by devising a four-level hierarchy to perform the simultaneous aerodynamic and structural design of a high-performance sailplane wing for maximum cross-country speed. Finally, the concepts discussed are applied to the two-level minimum weight structural design of the sailplane wing. The numerical experiments show that discontinuities in the sensitivity derivatives may delay convergence, but that the algorithm is robust enough to overcome these discontinuities and produce low-weight feasible designs, regardless of whether the optimization is started from the feasible space or the infeasible one.

17. Key Words (Suggested by Author(s))	18. Distribution Statement
Nonlinear programing, decomposition, hierarchy, optimum sensitivity analysis	Unclassified - Unlimited Subject Category 05

19. Security Classif. (of this report)	20. Security Classif. (of this page)	21. No. of Pages	22. Price
Unclassified	Unclassified	238	A11

For sale by the National Technical Information Service, Springfield, Virginia 22161